Développement d'un procédé électrochimique pour le recyclage du néodyme à partir de déchets électroniques

Mickaël Mery

THESE DE DOCTORAT DE L'ETABLISSEMENT UNIVERSITE BOURGOGNE FRANCHE-COMTE

PREPAREE A L'UNIVERSITE DE TECHNOLOGIE DE BELFORT-MONTBELIARD (UTBM)

Ecole doctorale n°37

SPIM (Sciences Pour l'Ingénieur et Microtechniques)

Doctorat de Science des Matériaux

Par

M. MÉRY Mickael

Development of an electrochemical process for the recycling of neodymium from electronic scraps

Thèse présentée et soutenue à Sevenans, le 16 Novembre 2018

Composition du Jury :

M. HIHN Jean-Yves	Professeur des Universités, Université de Franche-Comté	Président
M. SCHWANDT Carsten	Professeur, Université de Nizwa	Rapporteur
M. BUND Andreas	Professeur, Université de Illmenau	Rapporteur
Mme. LEGEAI Sophie	Maître de conférences, Université de Lorraine	Examinatrice
Mme. LANGLADE Cécile	Professeur des Universités, UTBM	Directrice de thèse
M. MASSET Patrick	Professeur, Thermallium sprl	Codirecteur de thèse

Acknowledgment

After four and a half years of literature researching, experiments, solving problems again and again and again, I want to thanks all the persons who supported me during this very special time in my life.

At first I want to thanks my doctoral supervisor Mrs. LANGLADE Cécile. Even if it was not always easy to organise all the administration between Germany and France, it was always a pleasure for me to know that you listen to my problems.

I would particularly like to thanks Patrick Masset, my thesis co-director as well as the leader of the department “new materials” at Fraunhofer UMSICHT. Without your ideas and experience I could not have conducted this research. Thanks for all the hours of meetings and telephone calls, which helped me to carry forward my dissertation.

I would like to thanks the institute Fraunhofer UMSICHT located in Sulzbach-Rosenberg to give me the opportunity to perform my thesis in its laboratory.

Thanks a lot to my colleagues Christoph, Andrea, Eva and Silke. Not only your professional support helped me a lot in the last years. I wouldn’t miss all the time we spend together in the office and the “Biergarten”: talking together about projects, colleagues or family. Especially my private German – Bavarian – language course improved my language skills that much! Your friendship is one big reason why I have never regretted to go through all the ups and downs of this dissertation.

I don’t want to forget to thanks my other colleagues from my department for their support during the dissertation, who helped me to set up my experiments and to analyse my samples.

Additionally I would like to thanks Nicolas Papaiconomou for our constructive discussions and the ICP-OES-analyses.

Additionally I want to thanks my family in law. Thanks to my parents in law, who supported me in the final phase of writing. Thanks for giving us a home while we have started our new life projects. I’m so sorry that I have occupied your living room for nearly nine months. But I’m sure that you always knew that it would worth it.

Moreover, I want to thank all my friends, which I could not meet that regularly because I was sitting all nights for writing and finishing this project.

Je voudrais aussi particulièrement remercier mes parents pour leur support en partie durant ces dernières années. Je sais que ce n'est pas facile de laisser partir son fils à plus de 1000 kilomètres, merci d'avoir accepté mes choix et d'être fiers du travail accompli jusque là.
Depuis le début de ma thèse beaucoup de chose ont changé sur le plan personnel. C'est pour cela que je souhaite enfin remercier ma femme Tina de m'avoir épaulé au quotidien, de m'avoir remis la tête au dessus de l'eau à de nombreuses reprises et de m'avoir poussé ces deux dernières années à achever ces travaux. Enfin je te remercie pour mon plus beau cadeau qui arriva en Août 2016: notre fille Maiva.

…Ich liebe euch…

...Will ich mal wieder mit dem Kopf durch die Wand, legst Du mir Helm und Hammer in die Hand

Nomenclature and Abbreviations

Nomenclature

ΔG^0	standard Gibbs free energy (kJ.mol^{-1})
ΔG^{∞}	standard Gibbs energy of formation at an infinite dilution (kJ.mol^{-1})
ΔG_{sc}^0	Gibbs energy of formation at the supercooled state (kJ.mol^{-1})
ΔE	difference of potential (V)
$\Delta_f H^0$	standard enthalpy of formation (kJ.mol^{-1})
$\Delta_f S^0$	standard entropy of formation (kJ.mol^{-1}.K^{-1})
°	degree
a or α	activity
γ	activity coefficient
φ	density (mg.cm^{-3})
A	electrode surface area (cm^2)
at%	atomic percentage
atm	atmosphere
C	concentration (mol.cm^{-3})
C^0	bulk concentration (mol.cm^{-3})
D	diffusion coefficient (cm^2.s^{-1})
D^0	pre-exponential factor (m.s^{-1})
ε	faradic efficiency
e^-	electron
E	recorded potential (V)
$E_{1/2}$	half wave potential (V)
E_a	activation energy (J.mol^{-1})
E^0	standard potential (V)
E^{0*}	apparent standard potential (V)
E_{eq}	equivalent potential (V)
E_{oc}	open circuit potential (V)
E_{min}	potential correspoonding to the lower intensity of the reduction peak (V)
E_{max}	potential correspoonding to the higher intensity of the roxidation peak (V)
$E_{p,A\ (/B)}$	potential of the cathodic peak (V)
Eq.	equation
eut.	eutectic
F	Faraday constant (C)
i	applied current (A)

I_p	peak current (A)
l	liter
Kg	kilogram
kJ	kilojoule
m	mass (g)
M	molar
MM	molar mass ($g.mol^{-1}$)
mol%	mole percentage
n	mole
Pa	pascal
ppm	part per million
Q	electric charge (C)
R	gas constant ($J.\ K^{-1}.mol^{-1}$)
t	time (s)
τ	transition time (s)
T	temperature (K)
T_f	melting point (K)
v	scan rate ($V.s^{-1}$)
V	volt
wt%	weight percentage
χ	molar fraction
z	number of exchanged electrons

Abbreviations

[A336][NO_3]	tricaprylmethylammonium nitrate
C_8mimNTf_2	1-octyl-3-methylimidazolium bis(trifluoromethylsulfonyl)amide
CP	chronopotentiometry
CV	cyclic voltammetry
D2EHPA	di-(2-ethylhexyl)phosphoric acid
DODGAA	N,N-dioctyldiglycolamid acid
EHEHPA	2-ethylhexylphosphonic acid mono-2-ethyl hexyl ester
EDTA	ethylenediaminetetraacetic acid
EDX	energy-dispersive x-ray spectroscopy
ELV	electric light vehicles
EOL	end-of-life
[Hbet][Tf_2N]	betainium bis(trifluoromethylsulfonyl)imide
HDD	hard disk drive
HEV	hybrid and electric vehicles
Liq.	liquid
ICP-OES	inductively coupled plasma optical emission spectrometry
Ox.	oxidation
Red.	reduction
RE	rare earths
REM	reflection electron microscope
SEM	scanning electron microscopy
SLM	supported liquid membrane
TBP	tributylphosphate
TEHA	tri-2-ethylhexyl amine
TOA	trioctylamine
TODGA	N,N,N',N'-tetraoctyl-3-oxapentanediamide ligand
PC88A	di-2-ethylhexyl phosphonic acid
VIM-HMS	vacuum induction melting follow the hydrolysis and the magnetic separation
WEEE	waste electronic and electrical equipment
XRD	x-ray diffraction

Table of contents

Introduction

This thesis was a part of the research project entitled « Recovery of critical metals from electronic wastes » (original: Rückgewinnung von kritischen Metallen aus Elektronikabfällen) funded by the Bavarian Ministry of Economics Affairs, Energy and Technology and has been proceeded at the Fraunhofer Institute for Environmental, Safety and Energy Technology UMSICHT, which is located in Sulzbach-Rosenberg (Bavaria, Germany)

The aim of this global research topic was the development of reprocessing methods for unrecoverable metals in order to increase yields and selectivity in the recycling of strategic raw materials.
Among other elements, precious metals and rare earths are of highest environmental and economic interest. Moreover some of these elements also present particular geopolitical aspects as they are coming from countries undergoing political instabilities. In order to increase the local sourcing, research projects have been founded to improve both their sorting and recycling.
For example, electronic scraps have been collected separately from other waste fractions for several years. The main reasons for this specific waste sorting are the increase of environmental awareness but also a profitable recovery of the precious metals, which are contained in the electronic scraps. If sorting is an important issue, the feasibility and efficiency of recycling processes are crucial for any further developments.
The work described in this thesis was only dedicated to this last aspect, i.e. the recovery of neodymium (Nd), which is the base of permanent magnets. Due to an increase of the Nd-based magnet production its availability is constantly decreasing. Moreover, due to some geopolitical considerations the raw material price is unstable.

During this thesis a pyrochemical process was developed to recover the metallic neodymium contained in the permanent magnets, which is found in electronic scraps. In order to achieve this recovery, the neodymium properties have been studied in four electrolytes:

- LiCl-KCl
- LiCl-KCl-LiF
- LiF-CaF_2
- LiF-SrF_2

After the study of the previously described electrochemical systems, the possibility of the extraction of neodymium from permanent magnets has been investigated.

This thesis is composed of five chapters:

The first chapter gives an overview of the uses and the economic situation of neodymium. The different possible recycling processes are then presented. Processes which already have been developed in order to recover the neodymium from electronic scraps are explored in detail and their advantages/drawbacks are explained in term of efficiency but also environmental or safety issues. We then propose to have a closer look on the pyrochemical process, which might be an alternative to the existing methods.

The second chapter describes the experimental processes and methods that will be used in this study. The selection of the electrolytes and the electrodes, which depends on the composition of the electrolyte, is explained. Furthermore the electrochemical tests used for the study of the properties of the neodymium in the selected electrolytes are described. Finally this chapter details the analysis methods, which are used to characterise the obtained samples.

The third chapter describes the design of the electrochemical cell, which has been especially developed for this study in order to resist corrosive media and to temperatures up to 1000 °C. The engineering work performed during this thesis represents a very important part of the study. The conception, realisation and validation of the cell design is the key point of the whole study and the base of all further scientific results.

The fourth chapter is dedicated to the determination of the neodymium behaviour in chloride- and fluoride-based electrolytes. The neodymium properties have been determined in different electrolytes in order to find the most appropriate one for the extraction of the neodymium contained in the permanent magnets.

The last chapter is divided into two different parts. The first one is dedicated to the analysis of electronic waste fractions, which have been provided by electronic scraps recycling companies. The aim of this section was to determine the percentage of neodymium contained in electronic scraps. The second part describes the efficiency of the extraction process based on the different results obtained in the previous chapter.

The conclusions of this study will finally be presented as well as recommendations and perspectives for further improvement studies.

Chapter I:

State of the art

Table of contents

Rare earths (RE) elements are becoming very important for current and future industrial products, such as computers, LCD screens and lasers, but also for so-called "green technologies" such as wind turbines, electric cars and bicycles. Due to highly volatile markets, the high environmental impacts and the geopolitical challenges of raw material supply and production, many efforts are made worldwide to develop new recycling processes[1]. Only a few countries have access to neodymium. China dominates the world production with above 90 % of the whole market. According to a recent study of the European Union [2] and the US Department of Energy[3], the RE elements are the most critical raw material resource. Despite extensive research activities in this field, only about 1 % of the RE are currently recycled.[4]

Most of the recycled RE are produced by scraps from permanent magnets manufacturing, the rest is coming from end-of-life (EOL) products. The quantity of recycled EOL products is very low, due to the difficulty to separate scraps containing RE elements from the other materials.[5,6]

This thesis deals with the recovery of neodymium from permanent magnets. Nd-based permanent magnets have better magnetic properties compared to Fe_2O_3 and Al-Ni-Co magnets[7]. In 1960, the first permanent magnet $SmCo_5$ was elaborated. In 1976, the Sm_2Co_{17} permanent magnet was developed, which had a higher magnetic energy density of 260 kJ/m^3 than the $SmCo_5$ magnet 200 kJ/m^3.[8]

In 1984, the NdFeB permanent magnet was discovered by Croat and Sagawa[9,10]. This type of magnet has the strongest magnetic energy density (up to 510 kJ/m^3) so far. The advantage of this type of magnet is the size reduction comparing to other magnets, which allows a mass reduction of the devices.

The Sm-based magnets represent today only 2 % of the global market because of its worse magnetic properties and a higher price for raw material compared to neodymium. The global market is dominated by Fe- and Nd-based magnets.

I. Description of the neodymium-element

In 1885 the Austrian chemist Carl Auer von Welsbach has discovered neodymium. It was extracted from the didymium (Di), which is a mixture of praseodymium (Pr) and neodymium, by a fractional crystallisation in strong nitric acid. His name originates from “neos” which means “new” and “didymos” which means “twin”.[11]

Neodymium is a RE metal and belongs to the lanthanide’s serie with the atomic number 60 (Fig. 1). This compound cannot be found in metallic form. It can be found in the minerals ores Monazite ($(Ce, La, Nd, Th)PO_4$) and Bastnaesite ($(Ce,La,Nd,Pr)CO_3F$).

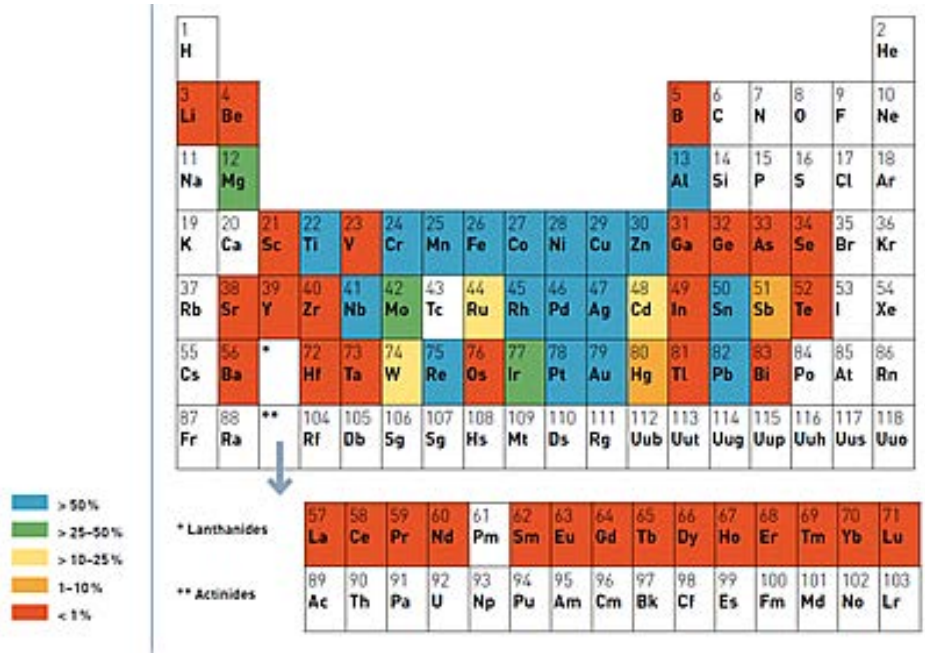

Fig. 1: Period system with indication of the recyclable rates of some elements[12]

In 2008, the annual worldwide consumption of neodymium oxide (Nd_2O_3) represented 23,900 tons. The majority (18,200 tons) of this compound was used for the manufacturing of Nd-based magnets. The repartition of this consumption is summarised in Fig. 2.

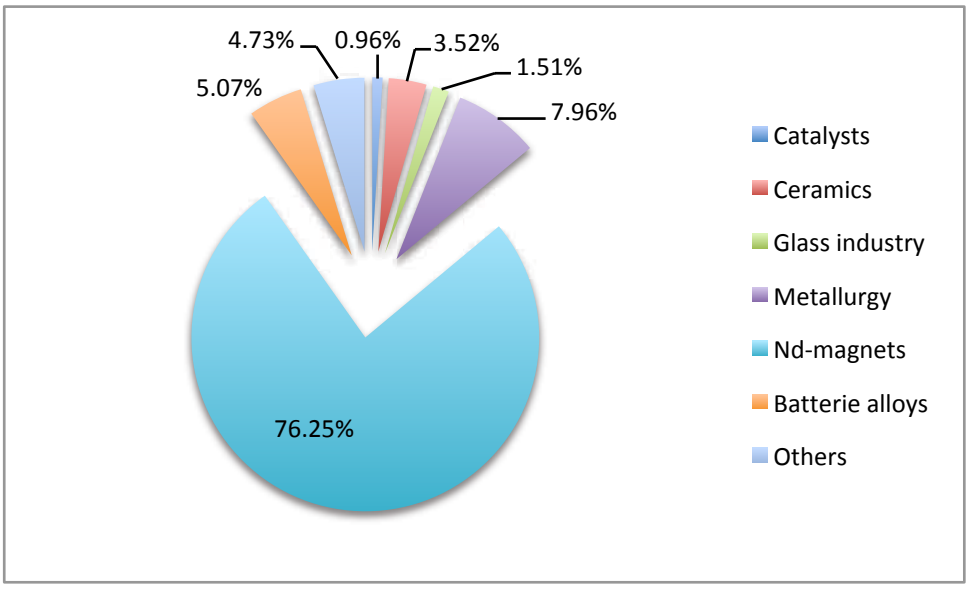

Fig. 2: Consumption (in %) of Nd_2O_3 in 2008[5]

According to the forecast of UNEP, the Emerging Technologies Raw Material Demand (ETMD) for 2030 will represent an amount of 27,900 tons of pure neodymium.[12]

II. Field of applications from NdFeB-magnets

Nd-based magnets are wildely used in different applications from small products like loudspeakers or hard disk drive (HDD) to vehicles and wind turbines. Fig. 3 summarises a repartition of the applications for NdFeB magnets, showing its broad range of utilisations. Two major branches can be observed:

- Neodymium-doped laser-rods (YAG:Nd)
- Permanent magnets

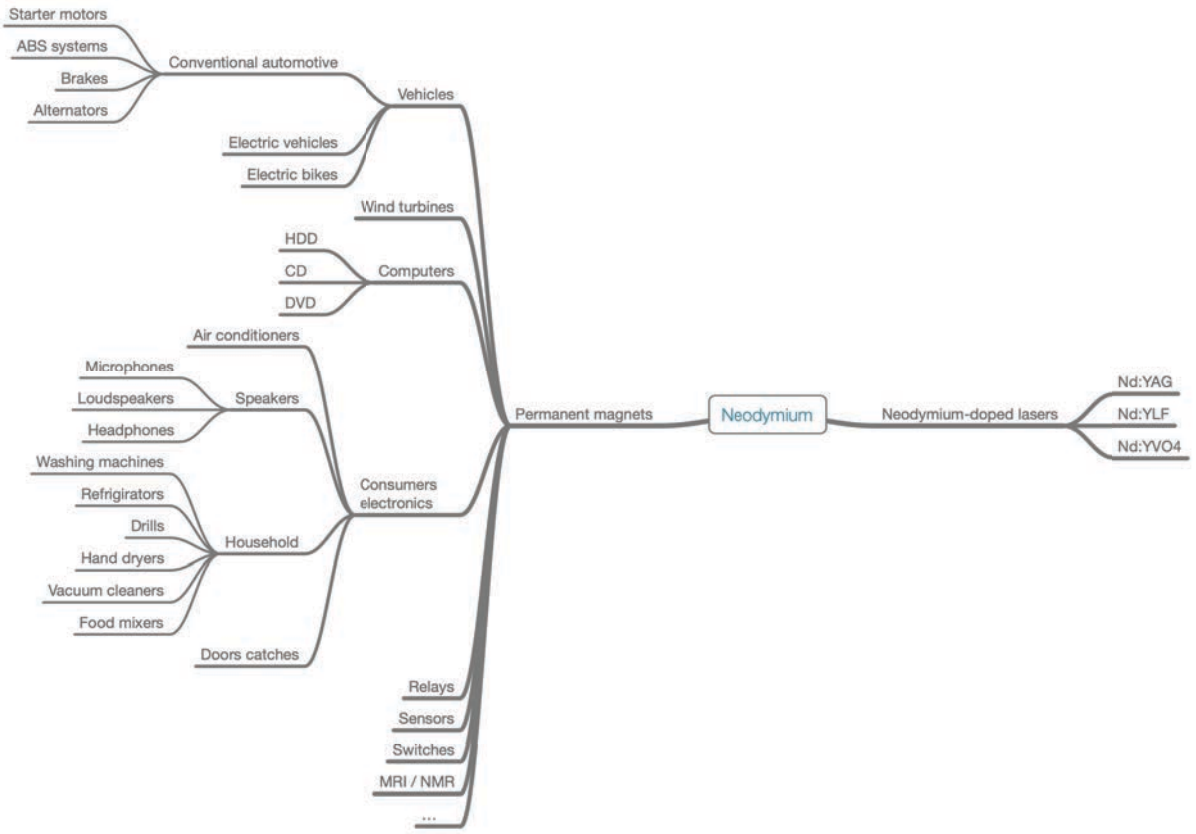

Fig. 3: Overview of the applications for neodymium compounds

Depending on the utilisation, the composition of the NdFeB magnets can be modified. The addition of some percent (1 to 9 %) of dysprosium (Dy) to the magnets increases their temperature stability. The Curie temperature describes the maximal temperature at which the magnet can be used. Above this point the magnet is demagnetised. For a basic NdFeB magnet the Curie temperature is 583 K.

If dysprosium is not used for magnets in HDDs, the magnets used in hybrid or electric cars contain 8.7 % of dysprosium.

III. Availability and threat about the neodymium resources

For a few years the demand of RE in particular for the elements neodymium and dysprosium is drastically increasing, which has a direct consequence on its price. This is due to the development of environmental friendly technologies like wind turbines, hybrid and electric vehicles. Until 2035, the demand of neodymium will drastically increase by 700 %[13].

The RE elements are designated as the most critical raw material group with the highest supply risk by the European Commission.[2]

Neodymium and dysprosium belong to the most critical RE elements described in the medium term critically matrix (Fig. 4) from the U.S. Department of Energy.[3]

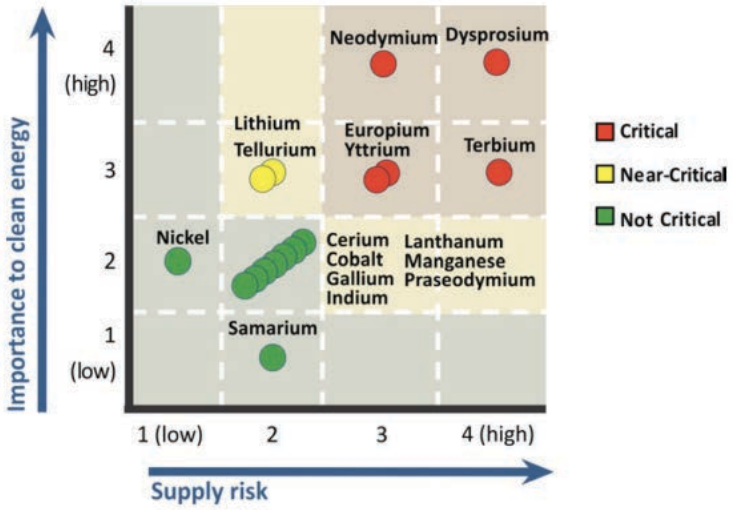

Fig. 4: Description by the U.S. Department of Energy of the most critical RE elements[3]

The low availability of this raw material and the geopolitical considerations of the market lead to sharp fluctuations of the price of neodymium (Fig. 5). These uncertainties create a challenge for the industrial production. Alternatives to minimise these influences are the development of suitable recycling processes.

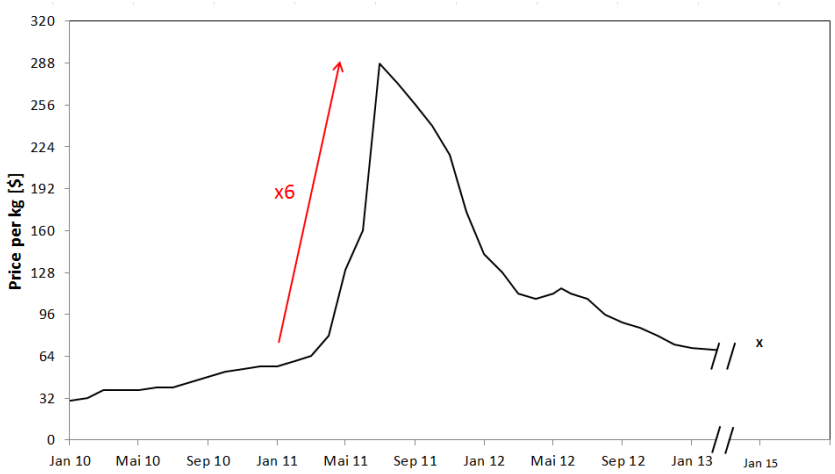

Fig. 5: Fluctuation of price for neodymium ($/kg)[14]

IV. Recycling of permanent magnets

The recycled neodymium field may be sourced from three different flows (Fig. 6). The first material flow is coming from the direct magnet manufacturing. This step creates an amount of Nd-swarfes from 30 % of the starting material resulting from the cutting, grinding or polishing steps. This flow is clearly the easiest to manage and treat. Compositions and contaminations are under control, sorting is easy.

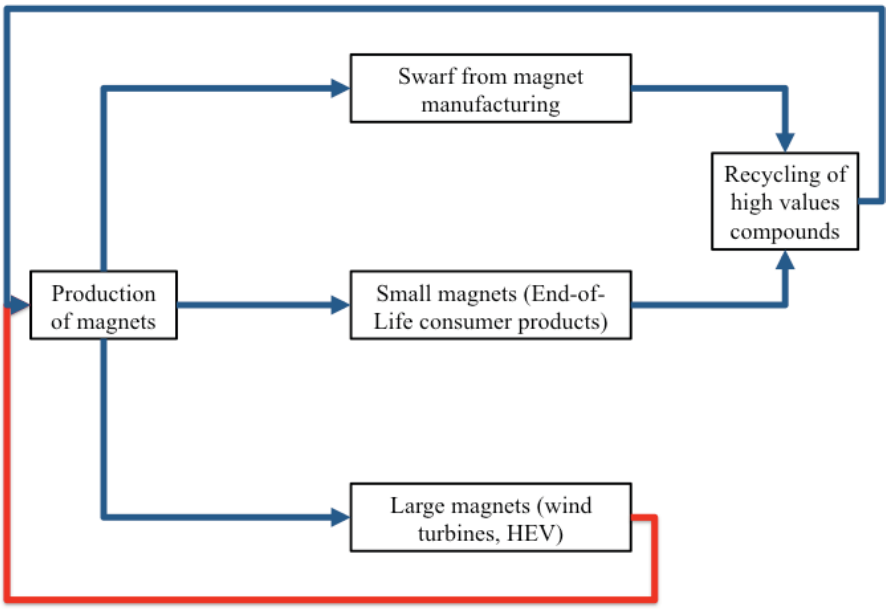

Fig. 6: Recycling sources of NdFeB magnets

The second flow considers all small magnets from the EOL consumer's products. Nowadays, this flow is the most researched project, because of its complexity. The EOL products should be raised in collect centers, where the high value products have to be separated from the rest, which is principally plastic and glass.

The third flow concerns the recycling of large magnets, which are used for wind turbines or hybrid and electric vehicles (HEV). These magnets also represent a very interesting field of potential high value. They can be directly recycled and re-used, because their compositions are almost the same.

The greatest advantage of this last route is that recycling is done at low economic and environmental cost. It has a low energy consumption due to the lack of thermal treatment, and no waste is produced.

There is however one important disadvantage. This process is only suitable for large magnets, which are used in HEV and wind turbines. For all other applications, the magnets cannot be removed easily from the rest of the product and will follow the second path.

Rademaker and co-workers[15] have studied the recycling potential of Nd-based magnets for the three most important applications, which are HDD, wind turbines and automotive industry. Fig. 7 shows the demand of neodymium coming from the raw material and/or the recycled neodymium. This is only a projection until 2030 concerning the three most important applications.

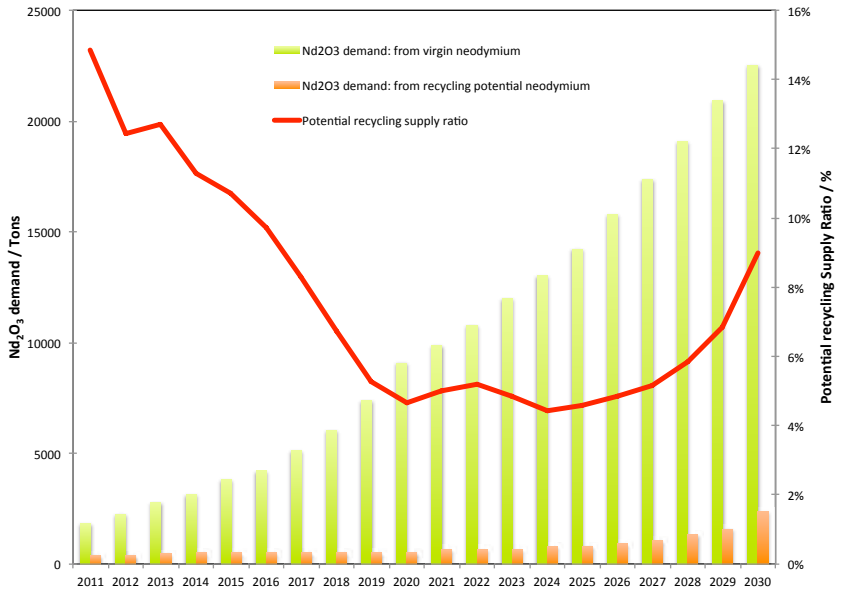

Fig. 7: Estimation of the Nd_2O_3 demand for the manufacturing of NdFeB magnets and the recycling potential of neodymium for the three major applications[16]

To avoid a shortage of neodymium in the near future, it is necessary to find efficient methods of collecting and sorting electronic wastes containing permanent magnets. Afterwards recycling methods have to be developed, which allows to achieve a selective extraction of neodymium in its metallic form. This work will only consider this second aspect of the neodymium recycling question.

IV.1. Shredding process

Nowadays most of the EOL products containing magnets are disposed in shredders. Before the shredding step, hazardous materials are separated from the whole collected waste electronic and electrical equipment (WEEE).

Fig. 8 describes the shredding process. As a first step, EOL products, which are free of toxic components, are shredded. The intermediate product passes through a drum, which separates the materials in two groups: non-ferrous scraps and ferrous scraps, which contain the permanent magnets.

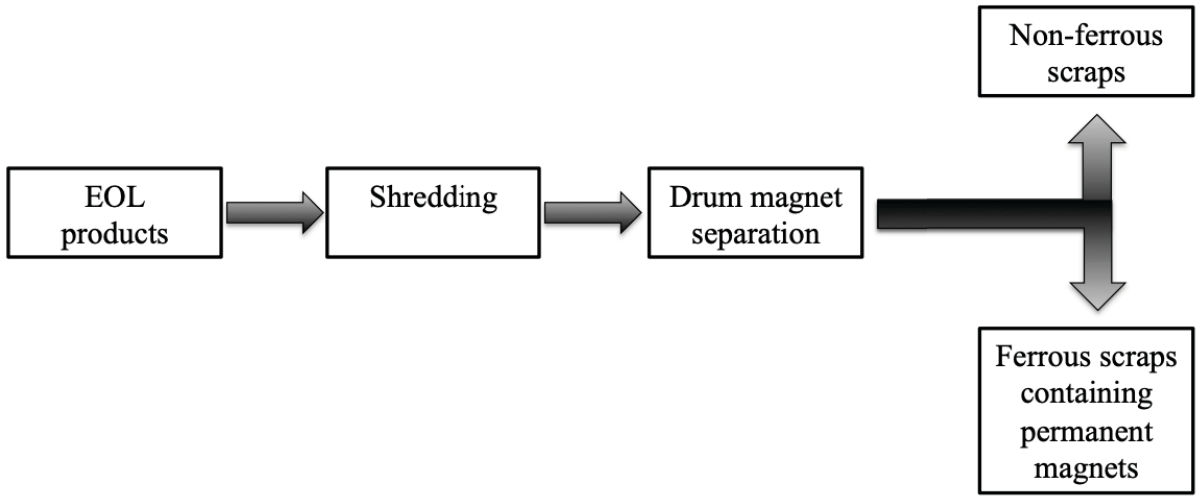

Fig. 8: Shredding process for the EOL products

There is a major drawback for the shredding process of all WEEEs together, i.e. the concentration of the RE elements in the global batch is very low, in particular the concentration for neodymium.

In 2014, Bandara and co-workers[17] studied the concentration of neodymium in shredding products. EOL products from ELVs (Electric Light Vehicles) and house appliances have been used as starting materials. They demonstrated that the quantity of neodymium in the group of ferrous scraps was between 130 and 290 ppm.

In 2015, Habib an co-workers[18] studied an other flow of EOL products: the HDDs. They explained that the presence of neodymium after the shredding process cannot be proved. This effect can be explained by the complexity of the HDDs composition, which contain many by-products.

In order to improve the recovery of neodymium, the permanent magnets should rather be dismantled and separated than using a shredder process. Until 2010 the dismantling was done manually with a rate of 12 units per hour[19].

IV.2. Mechanical separation by Hitachi

Hitachi is now using a special mechanical process to dismantle and to separate RE magnets. A rotational drum allows to recycle NdFeB magnets in HDDs and air conditioners. This machine works by using vibration. The emerging impact of tumbling leads to loosen the screws, which are fixing the components of the HDD. Subsequently the HDDs get broken and its components, e.g. the NdFeB magnets can be separated. Workers can collect the NdFeB magnets by visual screening. This process only needs about 30 min. Comparing to a manual dismantling rate of about 12 HDDs per hour, this innovative machine can deconstruct about 200 HDDs per hour.

A similar machine exists for compressors in air conditioners, which was developed by Hitachi and Mitsubishi Machines. Rotors in the compressor are removed. In order to recycle the NdFeB magnets two different methods can be used. The first method is a non-thermal demagnetisation, which uses resonance-damping demagnetisation at room temperature. The second way to collect the NdFeB magnets is a thermal demagnetisation at 673 to 773 K.

Moreover there are differences between Hitachi and Mitsubishi for the collecting process of magnets. While Hitachi uses the same rotating drum as for HDDs, Mitsubishi utilises drills. Furthermore Mitsubishi tries to use the thermal demagnetisation process to recycle NdFeB magnets in direct drive motors in washing machines.

IV.3. Hydrogen decrepitation of predismantler computer HDDs

The University of Birmingham has developed a new method to separate sintered NdFeB magnets from computer HDDs by using hydrogen at atmospheric pressure at room temperature. During the hydrogen processing $NdH_{2.7}$ is formed at the gain boundaries because of NdFeB absorbing hydrogen. This reaction is exothermic and results in $Nd_2Fe_{14}B$ absorbing hydrogen and forming an interstitial hydride. The volume expansion for this overall reaction is 5 %.

The magnets are brittle so they break down into brittle granules and hydrogenated powder. The hydrogenated material is soft magnetic and is not attracted to ferrous components. This technique is called "Hydrogen Processing of Magnet Scrap". When using this process for HDDs the nickel coating peels away as thin particles from the surface of the nickel coated NdFeB magnets. After the HDD sections went through the hydrogen processing, a porous drum is used to loosen the hydrogenated NdFeB powder from the electronic scraps by rotation. An efficiency of 95 % of recovered neodymium is reported.

At this step, there are still small particles of nickel in the powder. The nickel content can be reduced to less than 325 ppm by using a mechanical sieving technique. The hydrogenated powder is more friable compared to the nickel flakes. That is why it mills faster and while

passing through a 90 µm-sieve, the nickel contamination can be strongly reduced.
This NdFeB-alloy powder can be directly used to produce new NdFeB magnets with either magnetic properties similar to the basic magnet or a cheaper magnet of a lower magnetic performance. These properties depend on the composition of the magnets.
Another way to deal with the obtained powder is the recycling of the RE metals from the extracted material. These powders are vulnerable to chemical influences during the pyro- and hydrometallurgical processing. A much higher input of energy is required for these chemical routes than for direct reprocessing of the alloys. But these routes allow to process mixed scraps, containing different ranged magnets, which cannot be proceed by direct reprocessing.

IV.4. Direct recycling of NdFeB-magnets

The direct recycling process can only be applied for solid, nonoxidised magnets which are originated from HEVs and wind turbines or which are hydrogenated powders resulting from the Hydrogen Processing of Magnets Scraps developed by the University of Birmingham[20]. The direct alloy recycling process has two steps, a re-sintering followed by a melt spinning of the powder or the clean magnets.
This method is similar to the manufacturing of primary magnets. Due to its applications, the alloy compositions have to be adjusted to obtain the requested properties; this leads to a broad range composition of the permanent magnets. Moreover the EOL magnets have a higher oxygen composition. New NdFeB-magnets have an oxygen concentration between 300 and 400 ppm, whereas magnets, which are used in this direct recycling process are included until an oxygen concentration of 5000 ppm[21]. For these reasons some process transformations are necessary because of the high oxygen concentration in EOL magnets. Due to these drawbacks, the direct recycling process is not applied for the production of new magnets. Nevertheless, the main benefit of this process is the presence of a few steps, which means a magnet production cost, which are comparable to other recycling processes.
Zakotnik and Tudor [22] reported the development of a commercial-scale recycling process with a batch production of 120 kg of re-sintered permanent magnets, by using a previous step of scraps separation.
The direct recycling process of Nd-based magnets is only suitable for the large magnets extracted from hybrid and electric vehicles as well as from wind turbines and hydrogenated powders. For the other applications, this method can not be applied, due to the small size of the magnets and their complex integration into the devices, which requires pre-treatments. They also have a wide range of matrix composition. Therefore, a pre-treatment of the WEEE is essential in order to obtain a scrap with a high concentration of permanent magnets. This aim can be achieved by a physical separation, dismantling- and mechanical processes.

After this step a metallurgical extraction can be performed to recover the neodymium contain in the permanent magnets.

Since around 20 years, many research groups developed recycling processes for the recovery of neodymium from NdFeB-magnets. The recycling can be conducted by hydrometallurgical or pyrometallurgical methods. In order to obtain pure neodymium, that means without any contamination of other compounds, a mix of both techniques can be used. At the beginning, researches have been principally focussed on the recycling of scrap and waste (cutting sludge calls “swarf”), which are produced during the manufacturing of permanent magnets. Due to a high scraps production, which contains between 20 and 30 % of the starting material, this flow was preferred to the EOL products[23]. After removing the coating on the scraps, the scraps can be directly reused for the manufacturing of new magnets. On the other side, swarfs have to be recycled by using the metallurgical method.

Today, around 1 % of the neodymium from “small magnets”, which is contained in the EOL products, is recycled.

However, the development of environmental friendly technologies will sharply increase in the next decades, which means the industry will always consume more neodymium (see Fig. 7). Due to the lack of “second hand” materials, the increasing demand on RE clearly leads to a stock decline.

For these reasons, the recovery of the critical materials represents already a big challenge for countries, which have no storage in their lands.

In order to achieve an economical valuable recycling of neodymium, people have to combine a couple of steps. First of all, EOL products have to be collected and they need a pre-treatment: the electronic parts containing the permanent magnets have to be separated from the rest of the waste in order to obtain a high neodymium concentration in the scrap. Afterwards, the neodymium has to be extracted selectively by a metallurgical process in order to be re-used for the manufacturing of new magnets.

IV.5. Hydrometallurgical processes

Hydrometallurgical processes are a traditional way, which is used to recycle permanent magnets. They have been used to recover neodymium from the production line scraps or from easily separable permanent magnets. The magnets waste is dissolved in strong acids like sulphuric acid (H_2SO_4) or hydrochloric acid (HCl) followed by a precipitation of neodymium as oxalate, fluoride or sulphate from the solution.

This process can be hampered by the presence of additional components such as dysprosium or praseodymium, which are also RE element and belong to the lanthanide’s serie.

A protective coating, which is made out of nickel or a mixture of nickel and copper can be found in permanent magnets, which deals as an additional step to remove these compounds.[23,24]

The recovery of neodymium by hydrometallurgical processes is done by several techniques such as:

- a leaching method, which can be a complete or a selective leaching
- a fractional crystallisation method
- a hydrothermal method
- a solvent extraction method
- a separation by ionic liquids

IV.5.1. Complete leaching process

In 1992 Lyman and Palmer developed a hydrometallurgical process to extract the neodymium from the permanent magnets. 1 kg of scraps is first dissolved in approximately 10 L of H_2SO_4. Afterwards, neodymium forms a sulphate salt at pH 2 that has to be converted into NdF_3 by leaching with a hydrofluoric acid (HF) solution for an easier extraction[25].

Another study was done by Lyman and Palmer. They were using H_2SO_4 and a precipitation of a double salt neodymium alkali or ammonium sulphate $Nd_2(SO_4)_3.M_2SO_4.6H_2O$ (M: K, Na;NH_4). For the complete leaching process the iron (Fe) compound is removed from the solution by its precipitation as jarosite ($KFe^{3+}{}_3(OH)_6(SO_4)_2$). The recovery rate of neodymium is 70 % by using ammonium sulfate and it reaches 98 % by using sodium sulfate. With this extraction method for neodymium and iron compounds, boron is not precipitated. Boron can be extracted from the solution by using zinc in order to precipate it as zinc borate hydrate.[26]

Yoon and co-workers[27] explored the recovery of neodymium contained in permanent magnet scraps. The first step was an oxidative roasting followed by a leaching with sulphuric acid. Neodymium is then precipitated as a double salt using sodium sulphate and can be easily extracted with a yield of 99.4 % from the rest of the leached solution. The optimal conditions are:

- for the oxidative roasting: 773 K for sintered scrap and 973 K for bonded scraps
- for the leaching: 2 h by a temperature of 323 K with a pulp density of 15 %
- for the double salt precipitation: 2 equivalent of sodium sulphate and a temperature of 323 K

The yield of the neodymium extraction with the precipitation was over 99.9 %

In 2004 Yoon and co-workers [28] also investigated the extraction of neodymium from permanent magnet scraps and proposed a process including a first oxidative roasting step,

followed by a scrap leaching with acetic acid and a final fractional crystallisation. The optimal condition for the leaching step, consisted of 3 h by 353 K with a pulp density of 35 %, which allows a recovery rate of 90 %. Then the fractional crystallisation allows a neodymium recovery rate of 67.5 %, with the formation of neodymium acetate. The rest of the neodymium, which is presented in the leached solution, can be extracted by using oxalic acid.

Abrahami and co-workers[29] studied the recycling feasibility of neodymium contained in HDDs. During a commercial shredding step, the permanent magnets were collected and demagnetised by a thermal process. Afterward a grinding and screening were done to rise the amount of neodymium in the scraps. They developed two different approaches.

The first started with a molten slag extraction using $CaO\text{-}SiO_2\text{-}Al_2O_3$ and $CaO\text{-}CaF_2$, which allows to remove the neodymium from permanent magnets. This step is followed by a H_2SO_4-leaching. The neodymium is extracted from the leach solution as a double salt $NdNa(SO_4)_2.H_2O$). The yield of this method is 98.4 %

The second route is the direct leaching with H_2SO_4 of the upgraded scraps, which has a recovery rate of 97 %.

Bandara and co-workers[30] investigated the leaching of permanent magnets from shredded electric motors in HCl. This mixture contains permanent magnets, steel and copper. After a demagnetisation step, magnets were dissolved in a stirring solution of 4 M HCl for 24 h. The magnets were totally dissolved, whereas the copper and the steel materials remained in their solid states, which can be extracted by filtration. Oxalic acid was added to the leaching solution to precipitate neodymium as neodymium oxalate, with a yield of 82 % and a purity of 99.8 %.

IV.5.2. Selective leaching

In 1998, Lee and co-workers[31] developed a selective leaching process for the recovery of neodymium from permanent magnet scraps. The scraps are preliminary roasted at an optimum temperature of 973 K in the air and then leached with an optimum concentration of 4 M sulphuric acid. A higher roasting temperature decreases the recovery rate of neodymium during the leaching due to the formation of $NdFeO_3$. 70 % of the neodymium was recovered with the formation of a $Nd_2(SO_4)_3$ precipitate with a leaching time of 3 h at 343 K and a pulp density of 100 kg/m^3.

A special process was discovered by Koyama and co-workers[32] of selective leaching to extract neodymium from EOL permanent magnets. Preliminary, the scraps are roasted at 1173 K for 6 h, and then leached with diluted chloric acid (0.02 M) in an autoclave at 453 K for 2 h. This process allows a recovery rate of 99 % of the neodymium from the leached solution with a residue of 5 % iron.

IV.5.3. Fractional crystallisation method

Wei and co-workers[33] studied the recycling possibility of neodymium by a fractional crystallisation separation process in sulphate solutions. They determined the solubility of $Nd_2(SO_4)_3$ in H_2SO_4-H_2O and $FeSO_4$-H_2O solutions for a temperature between 273 and 353 K. An increase of the temperature creates an increase of the solubility of $FeSO_4$ in H_2O and a fast decrease of the solubility of $Nd_2(SO_4)_3$. Neodymium can be extracted as precipitate $Nd_2(SO_4)_3.8H_2O$ within 273-353 K and $Nd_2(SO_4)_3.5H_2O$ at 353 K.
Sato and co-workers[34] also studied the fractional crystallisation method in sulphate solution to recover neodymium from permanent magnet scraps by the addition of ethanol. Ethanol was added in a solution of sulphuric- and nitric-acid containing neodymium and iron, which has the effect to reduce the solubility of neodymium into the solution. Neodymium was recovered from permanent magnet scraps as $Nd_2(SO_4)_3.xH_2O$ with a yield of 97.1 % and a purity of 96.8 %.

IV.5.4. Hydrothermal method

To recover neodymium from NdFeB sintered magnets, Itakura and co-workers developed a hydrothermal treatment using 3 M of H_2SO_4 and 0.2 M of $(COOH)_2$ for 6 h at 383 K. it has been shown, that more than 99 % of the neodymium as $Nd_2(C_2O_4)_3.xH2O$ with a purity of 99.8 % can be recovered[35].

IV.5.5. Solvent extraction and related techniques

Solvent extraction consists in a separation of ions from a solution, which is based on the formation of a complex between the ions presented in the aqueous phase and ligand molecules contained in the organic phase.
These complexes are immiscible in the organic phase. Several parameters influence the efficiency of a solvent extraction process such as the temperature, the pH from the aqueous solution, the time of contact between both phases and their mixing efficiency. Also the extraction efficiency depends on the properties of the ions and the ligands. Due to their narrow chemical properties, it is relatively difficult to separate different lanthanides contained in a same solution.
The most common ligands used for the extraction of neodymium are organophosphorous based compounds like the di(2-ethylhexyl)-phosphoric acid (D2EHPA).

Mohammadi and co-workers[36] compared two ligands, the D2EHPA and the 2-ethylhexylphosphonic acid mono-2-ethyl hexyl ester (EHEHPA) for the extraction of three RE

ions: yttrium (Y^{3+}), dysprosium (Dy^{3+}) and neodymium (Nd^{3+}). This study showed that both ligands have more affinity with Y^{3+} than with Dy^{3+} and Nd^{3+}.

Kraikaew and co-workers[37] investigated the extraction of RE elements using an isomolar mixtures of tributylphosphate (TBP) and D2EHPA in kerosene at room temperature.

It was shown that the distribution coefficients increase for compounds with higher atomic number. Heavy RE have better distribution coefficients in the 1.0 and 1.5 isomolar mixtures of TBP and D2EHPA in kerosene than in the 50/50 mixture TBP/kerosene.

Liu and co-workers[38] studied the solvent extraction in chloride solution from praseodymium and neodymium using the organophosphorous extractant, bis(2,4,4-trimethylpentyl)phosphinic acid (Cyanex 272) mixed with an amine extractants, such as tri-octyl/decyl amine (Alamine 336), trioctylamine (TOA) and tri-2-ethylhexyl amine (TEHA). The best result was obtained with a mixture of Cyanex 272 and Alamine 336.

Abreu and Morais[39] compared the extraction efficiency of organophosphorous and amine compounds. The organophophorous acids show a better affinity for the RE elements.

Zhu and co-workers[40] showed that amide can also be used as ligand for the extraction of RE elements with a solvent extraction process. They investigated the extraction of RE elements using the N,N,N',N'-tetraoctyl-3-oxapentanediamide ligand (TODGA) from nitric acid into n-dodecane.

Lee and co-workers[41] studied the extraction of neodymium from hydrochloric solution using the cathonic extractant Di-2-ethylhexyl phosphonic acid (PC88A) and soponified PC88A. It was showed that the saponified PC88A has a better extraction efficiency than the PC88A.

Kim and co-workers[42] developed a process to recover RE elements from permanent magnet scraps using a hollow hydrophobic polypropylene fiber membrane. The hollows were filled with a mixture of organic compounds TODGA, Isopar L and TBP (ratio 3:4:3). The RE element were extracted from a nitric acid solution without the extraction of side compounds using a multimembrane configuration. The extraction process was also studied in a hydrochloric acid solution, which showed a co-extraction from RE elements and side compounds such as iron.

IV.5.6. Separation by ionic liquids

Ionic liquids are special solvent, which are only composed of ions, a cation and an anion. They offer an alternative way to recover neodymium from permanent magnets because of their unique properties such as low vapour pressure and intrinsic electric conductivity.

For the extraction of neodymium from permanent magnet scraps, the ionic liquid is mostly combined with an extracting compound such as N,N-dioctyldiglycolamid acid (DODGAA)[43], TODGA[44], D2EHPA[45] or TBP[46].

Baba and co-workers[47] developed a supported liquid membrane (SLM) based on ionic liquids for the selective recovery of neodymium in the presence of iron. They used DODGAA, which is a very soluble extracting agent in 1-octyl-3-methylimidazolium bis(trifluoromethylsulfonyl)amide (C_8mimNTf_2). This process recovers 99 % of neodymium, but also 10 % of iron is co-extracted.

Kikuchi et al.[46] developed an extraction process for neodymium, praseodymium and dysprosium contained in a sodium nitrate solution using tri-n-butylphosphate (TBP) and the ionic liquid tricaprylmethylammonium nitrate ([A336][NO_3]).

Vander Hoogerstraete and co-workers[48] developed a phosphonium ionic liquid (trihexyl(tetradecyl)phosphonium chloride) in order to separate iron and neodymium from the permanent magnet waste. The ionic liquid has a high affinity towards iron and allows its extraction with an efficiency above 99.98 %. Neodymium remains in the solution and can be recovered together with impurities.

In 2014 Vander Hoogerstraete[49] and co-workers developed a procedure to recover neodymium from permanent magnet scraps. The scraps were crushed and milled into powder, which were roasted to obtain metal oxides. Then, the neodymium was selectively leached with nitric- and chloric acid, the iron was left in its solid state. Afterwards the trihexyl(tetradecyl) phosphonium chloride allows the extraction of transition metals (Co, Cu, Mn) from the leached solution. Oxalic acid was added to the solution containing neodymium in order to form a neodymium oxalate precipitate and finally the precipitate was calcinated to recover Nd_2O_3.

In 2015, Dupont and Binnemans [50] investigated a new way to recycle neodymium from roasted permanent magnets using carboxyl-functionalised ionic liquid: betainium bis(trifluoromethylsulfonyl)imide ([Hbet][Tf_2N]). The miscibility of this ionic liquid depends on the temperature. The system [Hbet][Tf_2N]-H_2O is biphasic until 328 K (for a ratio 1:1). Above this temperature the system is monophasic. The leaching is made at 353 K, when all elements are dissolved, the system is cooled down until the formation of the biphasic system is reached. Iron stays in the ionic liquid phase, whereas neodymium moves to the aqueous phase. Afterwards the neodymium was precipitated as neodymium oxalate and calcinated to obtain Nd_2O_3.

Riano and Binnemans[51] demonstrated a recovery process of neodymium based on nitrate ionic liquid. NdFeB magnets were leached in nitric acid. Then transition metals were separated with a liquid-liquid extraction using a nitric acid solution and the ionic liquid trihexyl(tetradecyl)phosphonium nitrate as organic phase. This step is followed by a separation of neodymium and dysprosium through a stripping with ethylenediaminetetraacetic acid (EDTA). The separated neodymium is precipitated using

oxalic acid and calcinated to obtain Nd_2O_3 with a recovery rate of 99.2 % and with a purity of 99.7 %.
The common problem with these processes is the use of large amounts of chemicals; some of them present health hazards and are detrimental to the environment (e.g. HF). This violates current trends and developments towards more environmentally friendly processes. Furthermore, none of the listed processes result in a recovery of metallic neodymium. Either neodymium is obtained as a salt or it is accompanied by substantial amounts of impurities.

Hydrometallurgical extraction methods are also used for the primary processing from bastnaesite and monazite ores for the production of neodymium, which is used for the manufacturing of permanent magnets.

IV.6. Pyrometallurgical process

Pyrometallurgical processes are run at high temperatures and have some advantages over the hydrometallurgical processes:

- less consumption of chemicals
- fewer process steps

IV.6.1. Methods using molten salts

Hua and co-workers[52] demonstrated the feasibility of a neodymium extraction from permanent magnet scraps using the molten chloride salt $MgCl_2$-KCl in a temperature range from 873 to 1473 K. After a grinding step, magnets were added into the salt under an argon atmosphere. 90 % of the neodymium can be extracted from the magnets. Iron, boron and other impurities are left in their solid state.
The research group of Hua also achieved the recovery of neodymium from NdFeB magnet scraps using molten fluoride salts. The neodymium was recovered with a yield of 94.2 % in molten AlF_3-NaF at a temperature between 1073 and 1373 K. As in the chloride-based salt, iron, boron and other impurities are left into their solid state[53].

IV.6.2. Liquid metal extraction

A liquid metal extraction is similar to a liquid-liquid solvent extraction, but at a higher temperature using a liquid metal as solvent. In this process, neodymium is selectively leached from the magnet and forms an alloy with the liquid metal.
In 1995 the AMES Laboratory[54] patent a process dealing with the recovery of neodymium from NdFeB magnet scraps using molten metal M (M: Mg, Ca or Ba). Neodymium was dissolved in the liquid extractant, leaving iron, boron and others residues in their solid state,

to form an M-Nd alloy. Afterwards neodymium was recovered from the alloy through a distillation to evaporate the metal. This process cannot be applied to oxidised scraps.

Xu and co-workers[55] developed a similar process to extract neodymium from permanent magnet scraps using liquid magnesium. In this process, lubricant residues are removed from the magnets using organic solvents. After crushing into fine particles, the magnets are dissolved in liquid magnesium at 1073 K. At this temperature neodymium is soluble in magnesium up to 65 at%[56]. A Nd-Mg alloy is obtained with some residues of iron because 0.035 at% of iron is soluble in magnesium at 1073 K[57]. Neodymium can then be recovered from the alloy by vacuum distillation.

Takeda and co-workers propose an alternative continuous extraction process of neodymium using molten magnesium. A difference of the vapour pressure at 1300 K of magnesium (0.73 atm) and neodymium (10^{-6} atm) and a temperature gradient in the reactor allow the separation of neodymium and magnesium by circulation and vaporisation of magnesium during the extraction[58,59].

The same process is also possible using molten silver at 1235 K, because it selectively dissolves neodymium from the permanent magnets without side reactions with iron or boron. Neodymium forms an alloy with aluminum, which contains up to 55 at% of neodymium. Neodymium is then extracted from the Nd-Al alloy by an oxidation step which leads to Nd_2O_3, which is insoluble in Al[60].

Moore and co-workers[61] explored a similar route using a Cu-based melt at a temperature range between 1723 and 1773 K. Neodymium formed an alloy with copper with a maximal of 25 at% of neodymium.

The process using molten silver could be considered for an industrial upscale because silver is easier to recycle than magnesium. However, silver is more expensive than magnesium, and during the extraction process with silver, a Nd_2O_3 compound is formed. This compound needs to be reduced to the metal form. This high energy-using process produces few wastes for a recovery up to 99 %, but it is not suitable for oxidised magnet scraps and it uses hazardous reagents, especially molten magnesium.

IV.6.3. Glass slag method

The slag process is a broad method to separate and increase the concentration of RE elements, which are found in the shredding residues.

In this process, the waste magnets are treated with a molten medium, e.g. boron trioxide. Neodymium can then be selectively extracted and separated from the other compounds in the resulting solution (e.g. α-Fe and Fe_2B phases) by forming a glass slag with the boron trioxide. The treatment of the glass slag with H_2SO_4 at 423 K for 3 h and Na_2SO_4 at 333 K for

30 min results in a first precipitation of $Nd_2(SO_4)_3xH_2O$. A second precipitate ($Nd(OH)_3$) is formed with the addition of sodium sulphate and sodium hydroxide in the solution.
Saito and co-workers[62] reported the successful extraction of neodymium from NdFeB-magnet scraps using molten boron trioxide. This method produces a Fe-B alloy composed of 2 phases: α-Fe and Fe_2B, which contains less than 0.01 wt% of neodymium. The rest of neodymium was in the slag material.
Saito and co-workers[63] also showed that neodymium can thus be extracted as $Nd(OH)_3$ and $Nd_2(SO_4)_3$. However, the recovery rate is only approximately 57 % and a further process step is necessary to obtain metallic neodymium. This process produces a huge quantity of waste and uses a lot of chemical products without an economic separation between boron oxide and neodymium[64].
Yang and co-workers[19] developed a concept to extract neodymium, which is contained in EOL permanent magnets from HDDs. An enriched scrap was preliminary produced by shredding, crushing and screening of the magnets. Afterwards, they tested two different slags: $CaO\text{-}CaF_2$ and $CaO\text{-}SiO_2\text{-}Al2O_3$ at 1773 K. Both systems allow a recovery rate of more than 99 % of the neodymium contained in the scrap. The Nd-rich slag can be used in a hydrometallurgical extraction process to recover pure neodymium.

IV.6.4. Direct melting

The direct melting of magnet scraps in order to produce new permanent magnets is difficult because of the amounts of oxygen and carbon contained in the scrap. Both elements decrease the recovery rate of neodymium through the formation of a slag rich of Nd_2O_3 and carbon. This results in a loss of neodymium.[64,65]
As a consequence, pre-treatment steps to remove carbon and oxygen are necessary. Decarburisation can be achieved by heating the scrap, which converts carbon to CO_2. Fe_2O_3 can then be reduced by heating in a hydrogen atmosphere, while the reduction of Nd_2O_3 to Nd^0 is done by using calcium metal[66–68].

Bian and co-workers[69] developed a new method called VIM-HMS process (vacuum induction melting follow the hydrolysis and the magnetic separation process) to extract the neodymium, which is contained in clean permanent magnets free of nickel. First, the permanent magnets were melted in a graphite crucible placed in a vacuum furnace with a pressure under 1 Pa. This reaction produces a saturated NdFeBC alloy. The hydrolysis step allows the conversion from neodymium carbides to neodymium hydroxides with iron residues, which are separated by a magnetic separation step. Finally, neodymium hydroxide is converted in Nd_2O_3 by calcination. This method allows an extraction of 93 % of neodymium, which is presented in the permanent magnets with a purity of 99.7 %.

All direct melting processes are environmental friendly methods, because they require no chemicals. But they are only suitable for clean magnets and not for EOL products.

IV.6.5. Gas phase extraction method

Gas phase extraction processes are used to recover neodymium from the magnet scraps while avoiding the oxidation of neodymium. They involve the grinding of magnet scraps into a fine powder followed by chlorination with a chloride reagent in a nitrogen (N_2) stream.

Machida and co-workers[70] showed that neodymium can be selectively recovered from permanent magnet scrap powders using ammonium chloride. The fine magnet powder containing approximately 1 wt% of oxygen is mixed with ammonium chloride and heated to a minimum of 623 K for 3 h under N_2 gas flow. After the chlorination, the powder is soaked in distilled water to leach $NdCl_3$. The recovery rate of $NdCl_3$ is 90 % with some α-Fe and Fe_2B residues. The difference of standard enthalpy formation between $NdCl_3$ and $FeCl_2$ allows a selective chlorination of neodymium.
Uda[71] developed a process to recover neodymium from magnet sludge by using $FeCl_2$. During the reaction, he used activated carbon as a deoxygenising agent, which converts Nd_2O_3 to $NdCl_3$. After the reaction, a mixture of $NdCl_3$, $FeCl_2$ and Fe-alloy is obtained with a recovery rate of $NdCl_3$ of 96 % after 12 h at 1023 K. The neodymium chloride is extracted from this mixture with a yield of 76 % by vacuum distillation.
Itoh and co-workers[72] demonstrated the selective extraction of neodymium from permanent magnet scraps through a chlorination step by using ammonium chloride (NH_4Cl) at 573 K for 3 h. The neodymium of the NdFeB-magnets was converted to $NdCl_3$ and extracted with a yield of 90 % with some α-Fe and Fe-B residues.
Murase and co-workers[73] suggested a neodymium recovery from permanent magnets by a chemical vapour transport along a temperature gradient. As a chlorination agent, they used pure chlorine gas and aluminium chloride. $NdCl_3$ is deposited in a high temperature zone (1023 - 1173 K) while the other chlorides MCl_n (M: Ni, Co, Fe, Zr, Al, Cu) are deposited at lower temperatures (623 - 973 K). The recovery rate of neodymium is more than 99 % after 6 h of reaction.

The recovery of neodymium from permanent magnet scraps can also be done by using sulfation roasting and was demonstrated by Önal and co-workers[74]. First of all, the compounds from the scraps are converted to sulfate by a digestion in H_2SO_{4conc}. Afterwards the mixture is roasted until the decomposition from iron sulphate to iron oxide is reached, which is insoluble in water, whereas the neodymium sulphates stay stable.

After the sulfation roasting, a water leaching allows the recovery of 95 % of the neodymium in the leaching solution with a purity of 98 %. Iron is separated from by the formation of hematite (Fe_2O_3).

IV.7. Alternative process: the pyrochemical process

Hydrometallurgical and pyrometallurgical processes allow the recovery of neodymium from permanent magnet scraps. The recovery rate of almost each method is higher than 90 %. Unfortunately, these processes have many drawbacks.
The direct re-use process is the most economical way; it needs neither energy nor chemical products. It also generates no waste, but it is only applicable to the large magnets coming from wind turbines or HEVs.
Hydrometallurgical processes are generally appropriate to all types of magnets. But these methods need many steps before the recovering of pure neodymium. They also consume large amounts of chemicals and produce much waste.
Finally pyrometallurgical processes can be generally used for almost all magnet composition, and they require fewer steps than the hydrometallurgical processes. The liquid method extraction allows the recovery of neodymium under its metallic state. But theses processes require a lot of energy and some methods produce large amounts of solid waste.This is the case of the electroslag refining and the glass slag method.

IV.7.1. Electrochemical process

The electrochemical process to recover neodymium from permanent magnet scraps is a special issue, which was not extensively explored until today. A few studies have shown that there is the possibility to recover this element from scraps. From the thermodynamic side, neodymium can be selectively dissolved from the magnet scraps due to its more reactive properties in molten salts compared to iron.

Oishi and co-workers[75] developed a process to recover neodymium from magnet scraps by using a rare-earth-iron-group metal alloy diaphragm as bipolar electrode in molten chloride salts. First the neodymium of the magnet scrap is dissolved at the anode and reduced on the anode side of the diaphragm. Then neodymium atoms diffuse through the diaphragm until the cathode side of the diaphragm and are oxidised as Nd^{3+} in order to be reduced on the cathode as pure metal or as an alloy with nickel.
The same process was studied in molten fluoride salts by Kobayashi and co-workers[76]. They extracted neodymium at 1123 K from the electrolyte LiF-CaF_2-NdF_3 (0.30 mol%) as a neodymium-nickel alloy by using a bipolar electrode and a nickel plate as cathode.

Martinez and co-workers [77] studied the extraction of neodymium from permanent magnet scraps based on an electrolysis process in the eutectic LiCl-KCl and equimolar NaCl-KCl mixtures. The electrochemical behaviour of neodymium has been investigated with an inert electrode (tungsten) and with a reactive electrode (iron). They also demonstrated the feasibility of the neodymium recovery with a very slow kinetic dissolution of the anode made of NdFeB.

This last process can be an alternative to all previous described process. This pyrochemical process is used for the reprocessing of nuclear spent fuel.
Pyrochemical processes allow a selective separation and recovery of lanthanides and actinides. They are widely used in the nuclear field since some decades and still in development. They are mainly based on chloride or fluoride salts.

IV.7.2. Electrochemical behaviour in chloride-based salts

In molten LiCl-KCl two oxidation states Nd^{3+} and Nd^{2+} are stable[78]. The electrochemical reduction process of Nd^{3+} in chloride molten salts was identified to be a two-step process via Nd^{2+} cations:

$$Nd^{3+} + e^- \leftrightarrow Nd^{2+}$$
$$Nd^{2+} + 2e^- \leftrightarrow Nd^0$$

The standard redox potential of the Nd^{3+}/Nd^0 couple was calculated from $E^0_{3/2}(Nd^{3+}/Nd^{2+})$ and $E^0_{2/0}$ (Nd^{2+}/Nd^0) using Eq. (1).

$$E^0_{3/0} = \frac{E^0_{3/2} + 2 * E^0_{2/0}}{3} \quad (1)$$

The standard redox potential $E^0_{3/0}$ of the Nd^{3+}/Nd^0 couple can also be calculated from the apparent standard potential $E^{0*}_{3/0}$ with the following equations (Eq. (2) and (3)):

$$E^0_{3/0} = E^{0*}_{3/0} - \frac{RT}{zF} * ln(\alpha_{MCl_x}) \quad (2)$$

$$\alpha_{MCl_x} = \gamma_{MCl_x} * \mathrm{X}_{MCl_x} \quad (3)$$

where α_{MCl_x} represents the activity of the metal, γ_{MCl_x} the activity coefficient and X_{MCl_x} the molar fraction.

For dilute solution $\gamma_{MCl_x} = 1$, Eq. (3) can be simplified as follows (Eq. (4)):

$$\alpha_{MCl_x} = \mathrm{X}_{MCl_x} \quad (4)$$

Then the standard potential $E^0_{3/0}$ of the Nd^{3+}/Nd^0 couple can be calculated with Eq. (5).

$$E_{3/0}^{0} = E_{3/0}^{0*} - \frac{RT}{zF} * ln(\mathrm{X}_{MCl_x}) \quad (5)$$

Fig. 9 describes the relationship between the Nernst equation and the Gibbs free energy of formation.

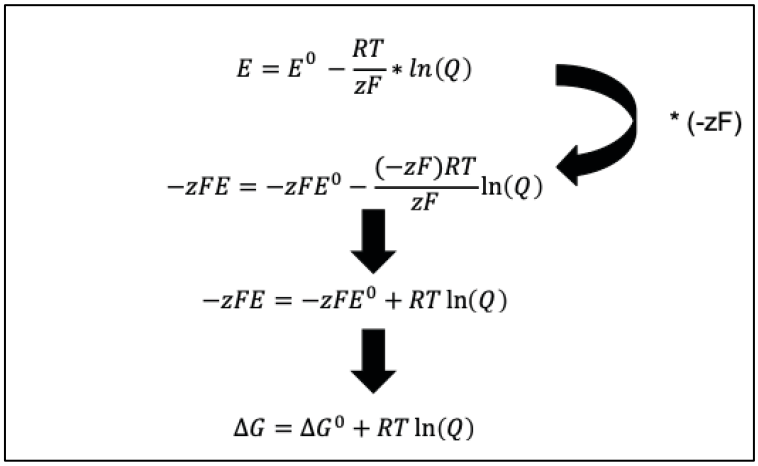

Fig. 9: Relationship between Nernst equation and the Gibbs free energy of formation

From the electrochemical measurements and by using the relationship described in Fig. 9, the standard Gibbs free energy change of $NdCl_3$ formation can be calculated with the following equation (Eq. (6)):

$$\Delta G_{3/0}^{0} = -zFE_{3/0}^{0} \quad (6)$$

where $\Delta G_{3/0}^{0}$ corresponds to the following reaction:

$$Nd(s) + \frac{3}{2}Cl_2(g) + 3Cl^-(sol.) \leftrightarrow NdCl_6^{3-}$$

Fig. 10a represents the evolution of $\Delta G_{3/0}^{0}$ in LiCl and LiCl-MCl melts (M = Na, K, Rb, Cs) as a function of LiCl content at 923 K, whereas Fig. 10b represents its evolution versus the polarising power of the solvent cations. The addition of LiCl in LiCl-MCl melts (M = Na, K, Rb, Cs) tends to decrease significantly the value of $\Delta G_{3/0}^{0}$, which in turn suggests a change in the solvation of the metallic cation. The standard Gibbs free energy decreases also with the increase of alkali cation radius (Li^+, Na^+, K^+, Rb^+, Cs^+) and inversely with its polarising ability. This is an indication that smaller cations interact strongly with Cl^- and that the formation of complexes such as $NdCl_6^{3-}$ is favoured in the presence of larger averaged cationic.

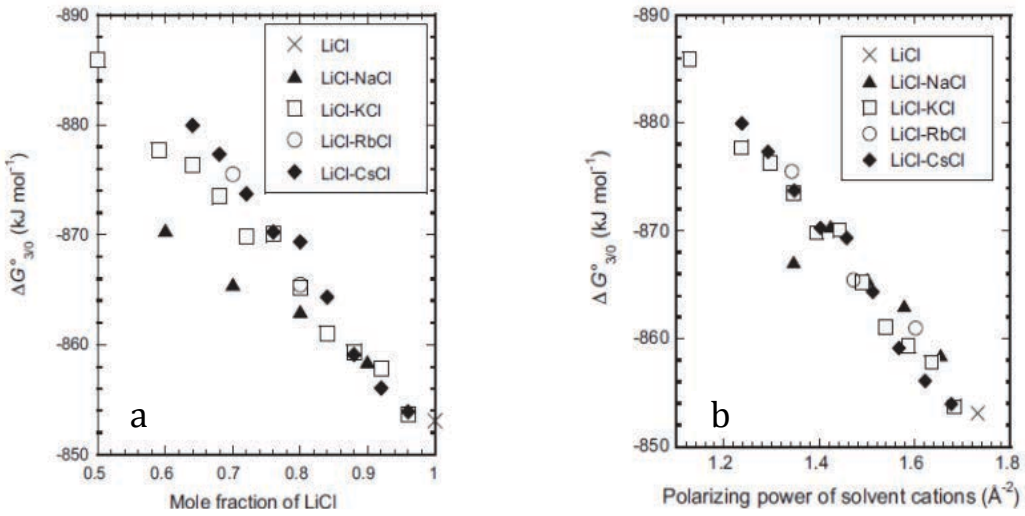

Fig. 10: (a): Dependence of the standard Gibbs free energy as a function of the LiCl amount in LiCl-MCl melts (M = Na, K, Rb, Cs). (b): Dependence of the standard Gibbs free energy as a function of the polarising power of the solvent cations in LiCl-MCl melts (M = Na, K, Rb, Cs).[79]

Fukasawa and co-workers[80,81] studied the electrochemical behaviour of neodymium in LiCl-$CaCl_2$ and determined standard redox potentials which are summarised in Tab. 1.

	LiCl-KCl$_{eut.}$	**equimolar CaCl$_2$-NaCl**	**LiCl-CaCl$_{2eut.}$**
T / K	**E^0 (V vs. Cl$_2$/Cl$^-$)**	**E^0 (V vs. Cl$_2$/Cl$^-$)**	**E^0 (V vs. Cl$_2$/Cl$^-$)**
673	-3.1518		
723	-3.105[75] / -3.135[76]		
733	-3.0867		
773	-3.0798		
823	-3.0558	-3.0068	-3.0238
873		-2.9728	
913			-2.9648
923		-2.9238	

Tab. 1: Standard redox potential of Nd^{3+}/Nd^0 system vs. Cl$_2$/Cl$^-$

They have also studied the dependence of the standard Gibbs free energy depending to the melting composition in LiCl, LiCl-$CaCl_2$, LiCl-$BaCl_2$ and LiCl-$SrCl_2$ (Fig. 11).

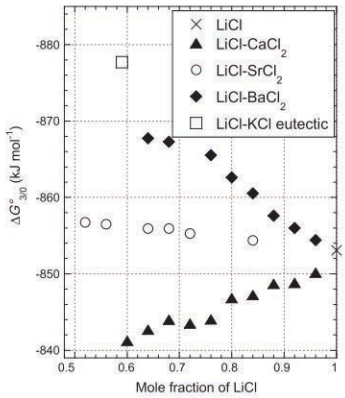

Fig. 11: Dependence of standard Gibbs free energy of Nd^{3+} [82]

For the melt LiCl-$CaCl_2$ and LiCl-$SrCl_2$, the absolute values of the standard Gibbs free energy decrease with the increase of the mole fraction of LiCl, which suggests that the stability of $NdCl_6^{3-}$ decreases. On the other side, concerning the melt LiCl-$BaCl_2$, the neodymium complex will be more stable with the increase of the mole fraction of LiCl. These facts suggest that an increase of the cation radius increases the stability of $NdCl_6^{3-}$ [82]. They have shown that the reduction process of Nd^{3+} consists of two steps.

Novoselova and co-workers[83] studied the electrochemical and spectrophotometric behaviour of neodymium in the eutectic salt LiCl-KCl-CsCl at a temperature range from 573 to 943 K. They determine that $NdCl_2$ is not stable above 810 K, due to its disproportion reaction:

$$3NdCl_2 \leftrightarrow 2NdCl_3 + Nd$$

Vandarkuzhali and co-workers[84] studied the electrochemical behaviour of NdO^+ ions in $MgCl_2$-NaCl-$KCl_{eut.}$. They show that the reduction of these ions is reversible for a scan speed between 25 $mV.s^{-1}$ and 75 $mV.s^{-1}$.

Sridharan[85] studied the thermal properties of LiCl-$KCl_{eut.}$ for the nuclear waste separation and the electrochemical properties of neodymium in this salt at 773 K.

Masset and co-workers[78] have studied the electrochemical reduction of $NdCl_3$ on a tungsten-working electrode in LiCl-$KCl_{eut.}$ at 733 K by using cyclic voltammetry and chronopotentiometry, the values are summarised in Tab. 1.

Yamana and co-workers[86] produced divalent neodymium in LiCl-$KCl_{eut.}$ at 773 K. During the electrolysis a precipitate of neodymium was formed, which is attributed to the disproportion reaction of Nd^{2+}. Yamamura and co-workers[87] studied the electrochemical behaviour of the chlorides of lanthanum, cerium, neodymium, samarium and dysprosium in LiCl-KCl and NaCl-KCl media.

Smolenski and co-workers[88] studied the electrochemical behaviour of $NdCl_3$ in LiCl–$KCl_{eut.}$ by using a liquid working electrode, which is composed of a gallium-indium eutectic alloy at the

temperature range of 723 – 823 K. They calculated the activity, solubility and activity coefficients. These parameters have been used to determine the separation factor of uranium from neodymium on gallium-indium eutectic alloy for the treatment of nuclear wastes.

Tang and Pesic[89] investigated the electrochemical behaviour of $NdCl_3$, the mechanisms of nucleation and the growth of neodymium during the reduction process in LiCl–$KCl_{eut.}$ with a molybdenum electrode. At a low concentration, the neodymium nucleates and grows progressively on the electrode surface. At a higher concentration, above 2 wt%, the nucleation mechanism is instantaneous. The augmentation of the concentration increases the density of the deposition.

Vandarkuzhali and co-workers[90] investigated the electrochemical behaviour of $NdCl_3$ in LiCl-$KCl_{eut.}$ with an inert electrode of tungsten at two reactive electrodes of aluminium and cadmium. They calculated the standard redox potential of the Nd^{3+}/Nd^0 system on three different working electrodes depending from the salt temperature (Tab. 2).

	W electrode	Al electrode	Cd electrode
T / K	**E^0 (V vs. Cl_2/Cl^-)**	**E^0 (V vs. Cl_2/Cl^-)**	**E^0 (V vs. Cl_2/Cl^-)**
698		-2,640	-2.733
723	-3.093	-2.623	-2.726
733			-2.723
748	-3.079	-2.606	
758			-2.716
773	-3.065		-2.711
798	-3.050	-2.573	

Tab. 2: Standard redox potential of the couple Nd^{3+}/Nd^0 depending of the nature of the electrode [89]

They also determined the diffusion coefficient $D_{Nd^{3+}/Nd^{2+}}$ and D_{Nd^{2+}/Nd^0} which are summarised in Tab. 3.

T (K)	$D_{Nd3+/Nd2+}$ ($cm^2.s^{-1}$) x 10^5	$D_{Nd2+/Nd0}$ ($cm^2.s^{-1}$) x 10^5
723	0.28	0.98
748	0.45	1.38
773	0.54	1.69
798	0.76	2.03

Tab. 3: Diffusion coefficient of Nd^{3+} and Nd^{2+} [89]

De Yan and co-workers[91] investigated the electrochemical behaviour of neodymium by a co-reduction with aluminium in LiCl-KCl-$AlCl_3$-$NdCl_3$ at 873 K. They proved the feasibility of the co-reduction of aluminium and neodymium to form an Al_yNd_x-alloy. After an electrolysis of 30 h, 99.25 % of the neodymium, which was contained in the melt was recovered with the

formation of two phases: Al_2Nd and Al_3Nd at a potential of -1.32 and -1.43 V. During the electrolysis, a depolarisation of the reduction potential to a more anodic potential was observed.

Yasuda and co-workers[92] investigated the electrochemical formation of a Nd-Ni alloy in NaCl-$KCl_{eut.}$ (50.6-49.4 mol%) with 0.5 mol% of $NdCl_3$ at 973 K. They found a formation of four different alloys ($NdNi_2$, $NdNi_3$, $Nd2Ni_7$ and $NdNi_5$) by using an open-circuit potentiogram for a Ni plate electrode after the electrolysis at −0.03 $A.cm^{-2}$.

De Córdaba and co-workers[93] determined the activity coefficient of neodymium in $Al_{liq.}$ at a temperature between 973 and 1073 K, which can be calculated with the Eq. (7).

$$log\gamma_{Nd(Al)} = 9.81 - 17134/T(K) \quad (7)$$

They have shown that Nd^{3+} can be reduced to Nd^0 in two steps (Nd^{3+}/Nd^{2+}, Nd^{2+}/Nd^0) in $CaCl_2$-$NaCl_{eut}$, and that the oxidation step Nd^{2+} is stable in this melt.

Kvam and co-workers[94] investigated the solubility of metallic neodymium in LiCl-$NdCl_3$ and LiCl-KCl-$NdCl_3$ systems. The solubility is maximal 11 wt% in pure LiCl and decreases with the addition of KCl to reach only 4 wt% with 60 % of KCl. Moreover the solubility is constant in the temperature range 1023 – 1173 K and follows the reaction, which is written below.

$$Nd_{(s)} + NdCl_{3(l)} = NdCl_{2(l)}$$

With the addition of $NdCl_3$ in the system the solubility of metallic neodymium increases. This information is important to determine how much metallic neodymium can be diluated in each melt for its extraction process, which is described in chapter 5 of this thesis.

IV.7.3. Electrochemical behaviour in fluoride-based salts

In order to raise the efficiency fluoride-based molten salts can be an alternative to chloride salts. The efficiency is higher because only one reduction step of neodymium ions is involved. Tab. 4 summarises the standard potentials calculated from the Gibbs energy database[95,96]. The most appropriate salts for the electrochemical study of neodymium ions are LiF and LiF-CaF_2, due to their more cathodic potential compared to the reduction potential of the neodymium ions.

	NdF_3	**LiF**	**LiF-CaF_2**	**LiF-NaF**	**LiF-KF**
mol%	100	100	79.2/20.8	60/40	51/49
E_{red}	-4.88	-5.31	-5.29	-4.88	-4.81

Tab. 4: Calculated reduction potential in V vs (F_2/F^-) of solvent cations and neodymium ions at 1100 K.[97]

IV.7.3.1 LiF-electrolyte

The electrochemical behaviour of LiF-NdF_3, LiF-Nd_2O_3 and LiF-NdF_3-Nd_2O_3 was investigated by Stefanidaki and co-workers[98]. The solubility of Nd_2O_3 in LiF is very low and produces the formation of neodymium oxyfluorides $[NdOF_5]^{4-}$ in the electrolyte. They have detected by Raman spectroscopy that the structure of neodymium fluoride in the molten salt is an octahedral complex anion $[NdF_6]^{3-}$.
The following reaction shows the reduction mechanism for obtaining metallic neodymium from the complex.

$$2[NdF_6]^{3-} + 6e^- = 2Nd_{(s)} + 12F^-$$

The solubility of Nd_2O_3 in LiF-NdF_3 is 0.13 mol% at 1023 K and can reach 0.22 mol% at 1173 K[99].
Thudum and co-workers[100] found out that metallic neodymium can be produced by the reduction of $[NdF_6]^{3-}$or $[NdOF_5]^{4-}$depending of the OF/F molar ratio. At low molar ratio, neodymium is produced by the reduction of $[NdF_6]^{3-}$. Above a critical concentration of Nd_2O_3, the reduction of $[NdOF_5]^{4-}$ turns out neodymium.
Dysinger and Murphy[101] also studied the reduction of neodymium from the salt LiF-CaF_2-NdF_3-Nd_2O_3 at a temperature between 1303 and 1333 K on a tungsten electrode.

IV.7.3.2. LiF-CaF_2-electrolyte

Taxil and co-workers[102] investigated the extraction processes of neodymium, gallium and samarium in LiF-CaF_2 for the reprocessing of nuclear spent fuel. By using a square wave voltammogram they have shown that the addition of Li_2O in the melt decreases the intensity of the peak of NdF_3, due to the reaction with O^{2-} ions. This reaction leads to the production of neodymium oxyfluorides species, which was confirmed by Stefanidaki[98].
Hamel and co-workers[97] studied the electrochemical behaviour of neodymium in LiF-$CaF_{2eut.}$ at 1083 K on a molybdenum electrode. The reduction process of Nd^{3+} to Nd^0 takes place in only one step, and the diffusion coefficient of Nd^{3+} ions is 1.3×10^{-5} $cm^2.s^{-1}$. They also extracted metallic neodymium from the melt by using an electrolysis process.

Deposition of neodymium on a reactive electrode

The electrodeposition of Nd^{3+} on a reactive electrode such as copper or nickel takes place to more anodic potentials compared to an electrodeposition on an inert electrode. This shift is called “depolarisation” and is between some mV and few hundreds mV[103]. The depolarisation reduces the risk of the co-deposition of lithium. The reaction of Nd^{3+} and the electrode leads to the formation of an intermetallic compound as described in the following reaction:

$$Nd^{3+} + 3e^{-} + xM = Nd_xM$$

where M represents the metal of the electrode

x is the number of M atoms

The electrodeposition of Nd^{3+} on a reactive electrode of nickel was demonstrated [103–107]. The depolarisation of the reduction peak of Nd^{3+}/Nd^{0} is 400 mV with the use of a nickel electrode compared to the reduction on an inert electrode of molybdenum or tantalum. Different phases can be found in the formed alloy: $NdNi_2$, $NdNi_3$, Nd_2Ni_7 and $NdNi_5$[105,106].
The electrodeposition of Nd^{3+} was also investigated on an electrode of copper[102,105,107,108]. In this case, the depolarisation of the reduction peak of Nd^{3+}/Nd^{0} is around 250 mV with the use of a reactive electrode compared to the reduction on an inert electrode of molybdenum. The intermetallic alloy is formed in the following phases: CuNd, Cu_2Nd, Cu_4Nd, Cu_6Nd.

Co-reduction of neodymium and aluminium ions

The co-reduction process consists of a simultaneous reduction of two different ions to create an alloy during the electrolysis on an inert electrode. This technique can be compared to the previous method, which consists of a deposition on a reactive cathode. The advantages of this method are that the cathode is not consumed during the reaction and the deposition process is faster. During the co-reduction a depolarisation can be noticed. The reduction potential is shifted to a more anodic potential than during the reduction of pure neodymium on an inert electrode, which is nearby the solvent reduction. This depolarisation allows a complete extraction of neodymium.
The co-reduction process of neodymium and aluminium in LiF-$CaF_{2eut.}$ was investigated by Gibilaro and co-workers[102,109,110], which follows the mechanism:

$$xNd^{3+} + yAl^{3+} \rightarrow Nd_xAl_y$$

The phases of the formed alloy can be controlled by the application of a fix potential during the electrolysis (Tab. 5).

Phase	$AlNd_3$	$AlNd_2$	Al_3Nd	$Al_{11}Nd_3$
E (V vs. Pt)	-1.88	-1.69	-1.49	-1.33

Tab. 5: Composition of the Al_yNd_x-alloy depending of the standard potential applied during the electrolysis[102]

IV.7.3.3. FLINAK-salt

Shim and co-workers[111] investigated the reduction process of Nd^{3+} in the molten salt LiF-NaF-$KF_{eut.}$, which is called FLINAK, on a tungsten electrode. They identified a reduction

process of Nd^{3+} in two steps, starting with the reduction of Nd^{3+} in Nd^{2+} followed by the reduction of Nd^{2+} in neodymium metal. They also developed the galvanostatic reduction of Nd^{3+} by using a liquid bismuth electrode.

Zvejskova and co-workers[112] studied the FLINAK mixture, which has a melting point of 727 K, on a platinum electrode. Their results are similar to the results of Shim. The reduction of Nd^{3+} follows a two-step reduction. They also found a peak corresponding to the reduction of platinum ions at the counter electrode.

V. Conclusion of the chapter

Due to the strong development of environmental friendly technologies and the increase of the use of electronic devices, the demand on neodymium will be even larger during the next decades. This means that the neodymium feedstock will be drastically reduced.

Moreover the price of pure neodymium is unstable due to geopolitical consideration.

This chapter gives an overview of the different recycling processes to recover neodymium from electronic scraps. Nowdays there is no process, which is used at an industrial scale, due to the complex composition of the electronic scraps and many disanvantages of the previous described recycling processes, like a high consumption of chemicals or energy.

As previously described, the pyrochemical process can be an alternative to the existing neodymium recycling processes. This method is already widely used in the nuclear field for the treatment of nuclear fuel waste. It allows a selective separation of actinides and lathanides. This technique could be a solution for the recycling of the permanent magnets and the selective recovery of the neodymium. That’s why we have decided to study the electrochemical behaviour of the neodymium in molten salts.

The following chapters will describe the experimental setup to determine the behaviour of neodymium in different electrolytes, which is followed by the analysis of the neodymium’s recovery in some selected electrolytes.

Chapter II:

Material and Methods

Table of contents

As shown in the previous chapter, several studies deal with the research of efficient processes for the recovery of neodymium from electronic scraps. Most of these processes are very laborious due to high consumption of energy and chemical products as well as multiple steps before reaching the recovery of pure compounds. The use of the pyrochemical process can be a solution to extract pure neodymium from scraps in fewer steps. For the successful execution of this thesis, the development and the utilisation of particular material and methods have a primary importance.
This chapter is divided into two parts, the first part describes the experimental device that has been developed. The second one is devoted to the characterisation methods that have been used to control and evaluate the result of this new device.

To present the new experimental setup, different elements have to be detailed and justified. Among them the crucibles, electrolytes, electrodes and glove-box will be presented as well as the dedicated data acquisition system which has been developed to control the complete process.

The second part deals with the description of the various techniques that have been used to qualify and quantify the results obtained during this work. The electrochemical measurements that have been used during this study (cyclic voltammetry, chronopotentiometry, chronoamperometry, electrolysis) will be presented. Physical analyses (EDX/REM, optical microscope, SEM) and chemical analysis (ICP-OES) have also been performed for the analysis of the solute and products during the basic electrochemical experiments and the electrolysis.

I. Material

I.1. The crucibles

Due to their resistance against the fluoride-based salts, the graphite crucible was favoured to the Al_2O_3 crucible.
For the basic experiments with a chloride and a fluoride mixture, the salt was placed in a cylindrical graphite crucible (Fig. 12) with a height of 60 mm and an internal diameter of 50 mm with a 3 mm thick wall, which represents a volume of 112 cm^2 (Fig. 13). The amount of used salts was approximately 65 g, which represents a height between 13 and 18 mm depending of the salt mixture.

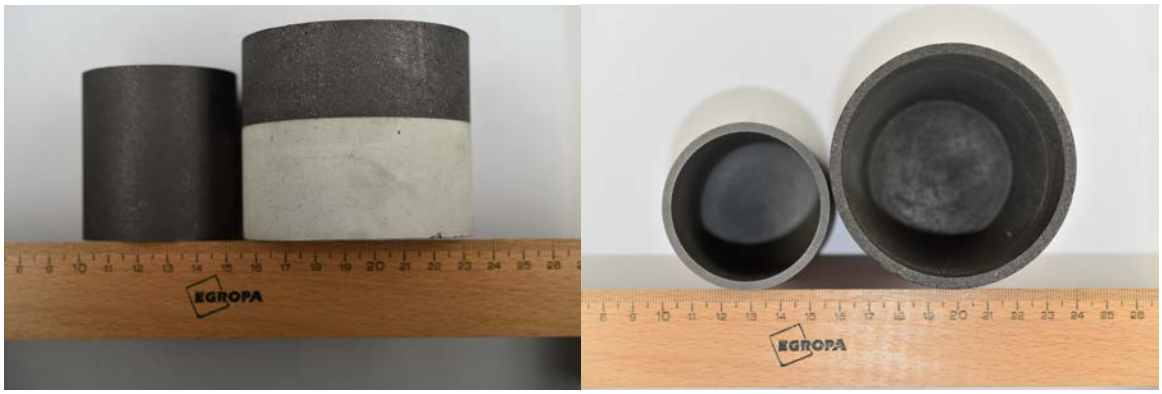

Fig. 12: Graphite crucibles used during the study of the behaviour of neodymium in different electrolytes and the electrolysis processes

A bigger crucible (230.5 cm^2) was required for the electrolysis to increase the amount of salt and the surface of the electrode immerged in the electrolyte.

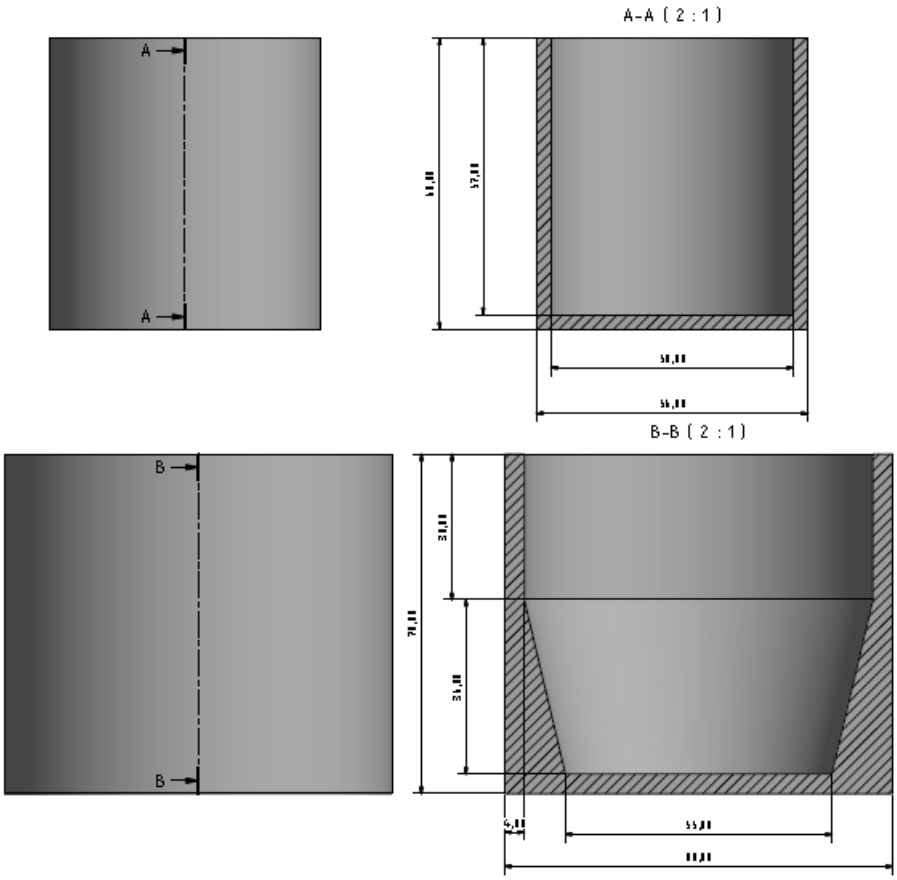

Fig. 13: Diagram of graphite crucibles

In order to remove the residual humidity, which is contained in the graphite crucible, each crucible has to be completely dried before the first utilisation. In the glove box, the crucibles are placed in a flushed reactor with argon and then heat up to 473 K.

I.2. The electrolytes

This research focused on different types of electrolytes, in order to demonstrate the behaviour of neodymium and to observe the salt influence. Based on the previous literature survey, the following salts were selected and will be used during this work.

- Chloride-based salt (LiCl-KCl)
- Mixtures of chloride and fluoride salts (LiCl-KCl-LiF)
- Fluoride-based salts (LiF-CaF_2, LiF-SrF_2)

These electrolytes have been choosen after the study of their properties. The eutectic LiCl-KCl mixture was selected due to its low melting point (626 K). Moreover these electrolytes are well described in the literature, which allows a comparison to validate the electrochemical process.

After the study of the neodymium behaviour in the eutectic mixture LiCl-KCl, it was demonstrated that its reduction process is composed of two reduction steps, which influence the efficiency during the electrolysis process due to a disproportion mechanism.

The fluoride-based mixtures can be an alternative to the chloride-based mixtures. The possible compositions are:

- LiF
- LiF-NaF
- LiF-KF
- LiF-CaF_2
- LiF-MgF_2
- LiF-SrF_2

The LiF-NaF and LiF-KF mixtures cannot be used to study the behaviour of neodymium because sodium and potassium are reduced before neodymium that prevents its reduction.

The LiF-MgF_2 mixture, with a melting point of 1015 K has been used without success. After each experience, it was noticed that the bottom part of the reference electrode, which was deeped in the electrolyte was dissolved. An explanation for this result could be a reaction between platinum and magnesium.

From the comparison of the three remaining compositions, which have been left only the LiF-CaF_2 and LiF-SrF_2 mixtures have been selected. They contain only elements with a more anodic reduction potential than the redox potential of the neodymium. Moreover they have a melting point approximately 353 K lower than the melting point of LiF that will represent a great energy saving when the process will be update to an industrial scale.

I.2.1. LiCl-KCl salt

The first used salt was an eutectic LiCl-KCl mixture. LiCl and KCl were obtained from VWR Germany with a purity of 99 % (respectively 99.5 %). After receiving the salts, they were directly stored in the glove box to avoid the formation of LiCl-xH_2O with the humidity which is contained in the air.

The composition of the salt was 59.2 mol% of LiCl and 40.8 mol% of KCl with a melting point of 626 K (Fig. 14[113]). The salt was directly prepared in the crucible with the help of a precision balance. After mixing the salt was strongly stirred in order to obtain a homogenised mixture.

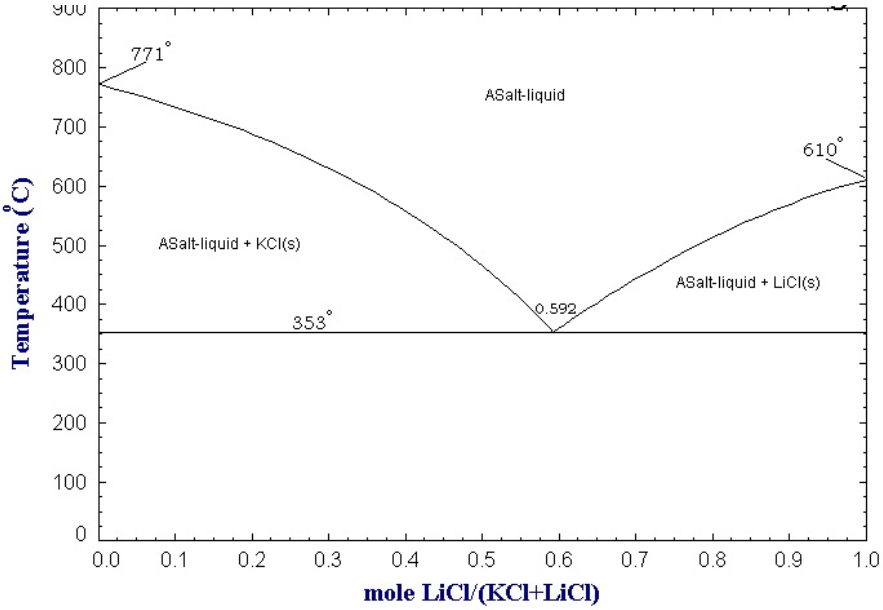

Fig. 14: LiCl-KCl phase diagram[113]

The density of the salt LiCl-$KCl_{eut.}$ is calculated by Eq. (8).

$$\rho = 2.0286 - (5.2676 * 10^{-4})T \qquad (8)^{85}$$

I.2.2. LiCl-KCl-LiF salt

The LiF salt was purchased at VWR Germany and had a purity above 98.5 %. The mixture of the eutectic was determined by the Fig. 15 and is composed of 58 mol% of LiCl, 38 mol% of KCl and 4 mol% of LiF.

The ternary composition has a melting point of 618 K.

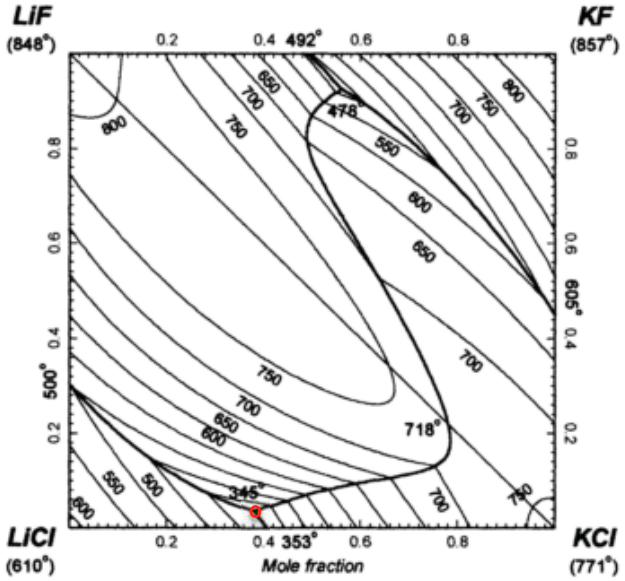

Fig. 15: Li, K//F, Cl phase diagram[114]

I.2.3. LiF-CaF_2 salt

The binary mixture is composed of 79.2 mol% of LiF and 20.8 mol% of CaF_2 and has a melting point of 1040 K (Fig. 16). The calcium fluoride was purchased by VWR Germany and has a purity of 99.5 %. The density of this eutectic salt is determined by the Eq. (9)[110].

$$\rho = 2.45 - (3.7 * 10^{-4})T \quad (9)$$

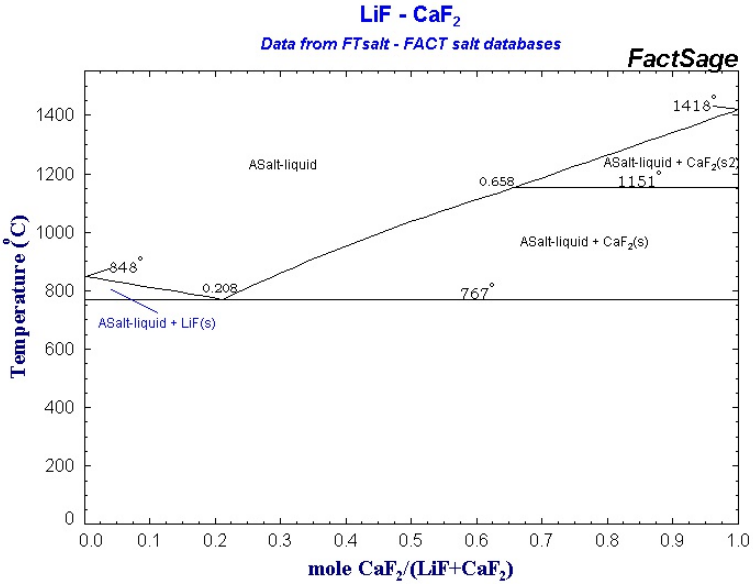

Fig. 16: LiF-CaF_2 phase diagram[115]

I.2.4. LiF-SrF_2 salt

The composition of this binary mixture is 81.5 mol% of LiF and 18.5 mol% of SrF_2 and it has a melting point of 1044 K (Fig. 17). The strontium fluoride was purchased from VWR Germany and has a purity of 99 %.

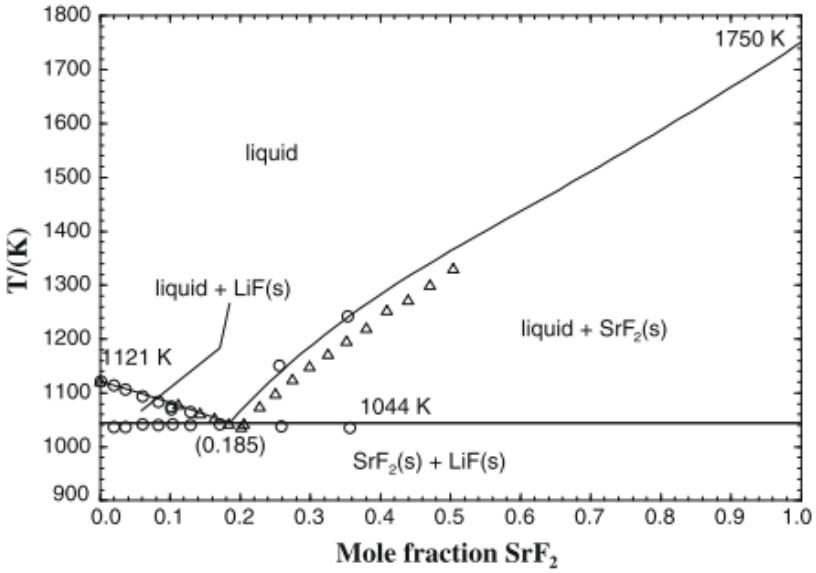

Fig. 17: LiF-SrF_2 phase diagram[116]

I.3. The electrodes

The arrangement of the electrode was controlled by an 8 mm Inconel 625 tube. In this tube an Al_2O_3 tube was placed to avoid any electrical contact between the Inconel and the electrode. This system was sealed with silicon based glue (3), which resists high temperatures (Fig. 18).

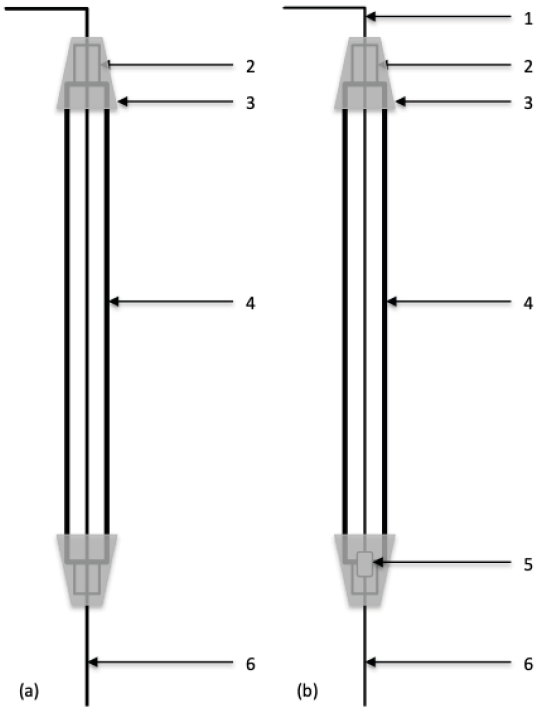

Fig. 18: Assembly of current supply and electrodes
(1): wire for current supply; (2): alumina tube; (3): high temperature silicon; (4): Inconel 625 rod; (5): connection between wire and electrode; (6): electrode. (a): normal configuration for working electrode, (b): configuration for the counter and reference electrode made of respectively glassy carbon and platinum.

I.3.1. Reference electrode

A special Pyrex® tube, with a very thin bottom wall was used for testing the chloride salt. The reference electrode was a 1 mm silver wire dipped in a mixture of LiCl-KCl and 0.75 mol/kg of AgCl (Fig. 19).

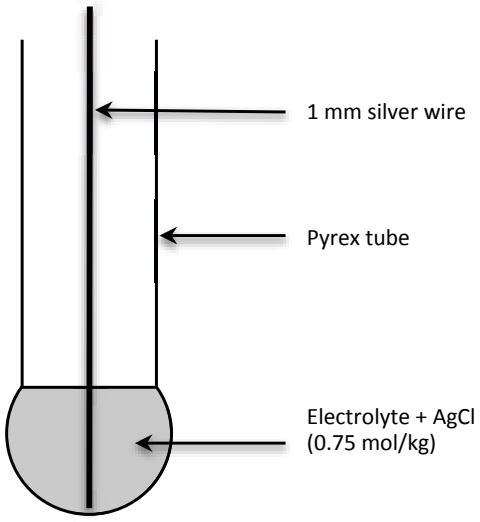

Fig. 19: Illustration of the reference electrode for chloride salts

The literature shows that the majority of electrochemical potential in chloride salts are expressed versus the reference couple Cl_2/Cl^-. Therefore in this experiment the standard potential was converted from the couple $Ag^+/AgCl$ to the reference couple Cl_2/Cl^-.
Eq. (10) expresses the relationship between Ag/AgCl to Cl_2/Cl^- reference electrode at a low concentration of AgCl in LiCl-$KCl_{eut.}$.[117]

$$E^0_{AgCl} = -1.0910 + 2.924 * 10^{-4} * T(K) \quad (10)$$

This equation is based on the extrapolation of infinite dilution, which was extracted from the published work of Yang und Hudson. [118]

The potential of the couple Ag/AgCl (1 wt% or X_{AgCl} = 0.0039) depending from E^0_{AgCl} is defined in the Eq.(11).[119]

$$E_{AgCl} = E^0_{AgCl} + \frac{RT}{nF} * \ln(X_{AgCl}) \quad (11)$$

Eq. (12) is the result of the insertion of Eq. (10) and Eq. (11) and allows the estimation of the potential shift, which corresponds to the change of the reference electrode from Ag/AgCl to Cl_2/Cl^-.

$$E_{AgCl} = -1.0910 + 2.924 * 10^{-4} * T + \frac{RT}{zF} * \ln(X_{AgCl}) \quad (12)$$

By applying Eq. (12) at different temperatures the following values of E_{AgCl} vs Cl_2/Cl^- (Tab. 6) were obtained

T / K	E_{AgCl} (V vs. Cl_2/Cl^-)
723	-1.2252
773	-1.2344
823	-1.2437
873	-1.2530
923	-1.2623

Tab. 6: Potential of AgCl vs. Cl_2/Cl^-

For fluoride salt, a 0.5 mm platinum wire was used as reference electrode, which was dipped in the electrolyte. The electrical contact was set up with a tantalum wire. The platinum wire is considered as a quasi reference electrode. Then the values of the apparent standard potential will be refered versus F_2/F^-. The determination of the reference system in fluoride-based electrolytes is described in section II.2.2. of chapter IV.

I.3.2. Counter electrode

For the experiment in chloride salts, the counter electrode was a molybdenum wire with a diameter of 1 mm.
However in fluoride salts, the counter electrode was a glassy carbon rod (Goodfellow) with a diameter of 2 mm. A tantalum wire, which was rolled to an extremity of the glassy carbon rod managed the electrical contact.

I.3.3. Working electrode

For the investigations of the neodymium properties in molten salts, various materials were used as working electrode: aluminium wire (1.5 mm, Alfa Aesar, purity 99.99 %), tungsten wire (1 mm, VWR, purity 99.95 %) and molybdenum wire (1 mm, Goodfellow, purity 99.95 %). Tungsten und molybdenum do not react with the chloride and fluoride-based molten-salts [120]. Furthermore both materials have no interaction with neodymium. Thus these inert electrodes inhibit the production of an alloy during the electrolysis.

I.3.4. Electrode for the extraction

The anode consists of a 1 mm tantalum wire basket on which four permanent magnets are maintained (Fig. 20).

Fig. 20: Configuration of the anode

The basket containing the magnets was totally immersed in the molten salts.

I.4. The glove box

The glove box (Fig. 21) allows the control of the atmosphere with a nitrogen gas flow. The quantity of O_2 and H_2O was kept lower than 15 ppm during all this work in order to avoid the contamination of the salt.

Each salt, crucible and all other components such as electrodes, magnets, which were used for the execution of the electrochemical experiments, were stored in the glove box.

After the preparation of the crucibles and the fixation of the electrodes in the salt, the reactor was hermetically closed, removed from the glove box and placed in the furnace.

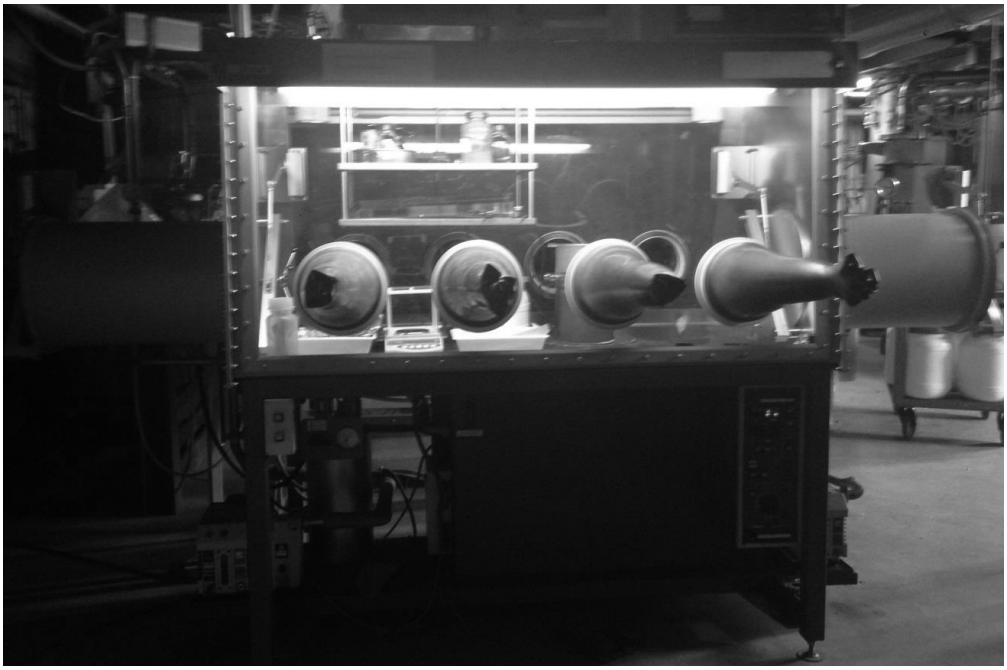

Fig. 21: Glove box for the preparation of the experiments and storage of materials

I.5. Data acquisition system

All electrochemical studies carried out in the different salts and electrolysis experiments were performed using a BioLogic Science Instrument SP 300 potentiostat/galvanostat. The potentiostat was controlled by a computer using the EC-Lab-software version 11.

All analyses of the experiments were performed using Microsoft office softwares.

II. Methods

II.1. Electrochemical techniques

II.1.1. Cyclic voltammetry (CV)

Cyclic voltammetry is one of the most widely used electrochemical techniques.
This method consists of a linearly potential variation (Fig. 22) applied to the working electrode between two limits (E_{max} and E_{min}) according to a simultaneous measurement of the resulting current arising from the corresponding electrochemical reaction.
The linear variation is described by Eq. (13).

$$E = E_i \pm vt \quad (13)$$

E_i represents the initial potential in volt. v is the scanning speed of the potential in volt per second and it is kept constant during the process. t is the duration of the process in seconds.

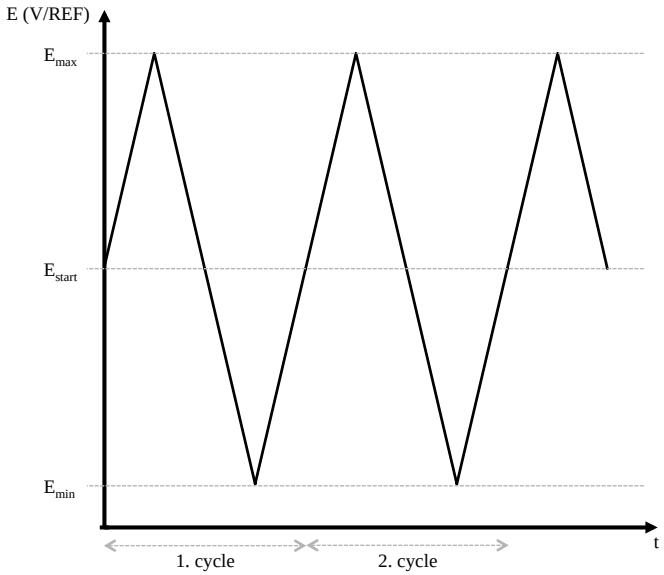

Fig. 22: Potential fluctuation for the cyclic voltammetry

The return scanning provides information about:

- the nature of the formed products
- number of reduced compounds
- the reversibility of the system

The obtained voltammograms show the evolution of the current density as a function of potential. They usually have one or more peaks corresponding to reduction or oxidation reactions at the electrodes. Conventionally, reduction phenomena are associated to negative currents and oxidation to positive currents.

The shape of the obtained intensity-potential curves (Fig. 23) allows to distinguish the different redox systems according to whether they are reversible, quasi-reversible or irreversible. [121–123]

This graph (Fig. 23) points out information about the studied system. Due to the Berzins-Delahay relationship [124], it is possible:

- to check the kinetic limitation of the reaction (activation or diffusion)
- to calculate the diffusion coefficient, if the reaction is controlled by the mass transport of matter
- to determine the concentration of the studied species

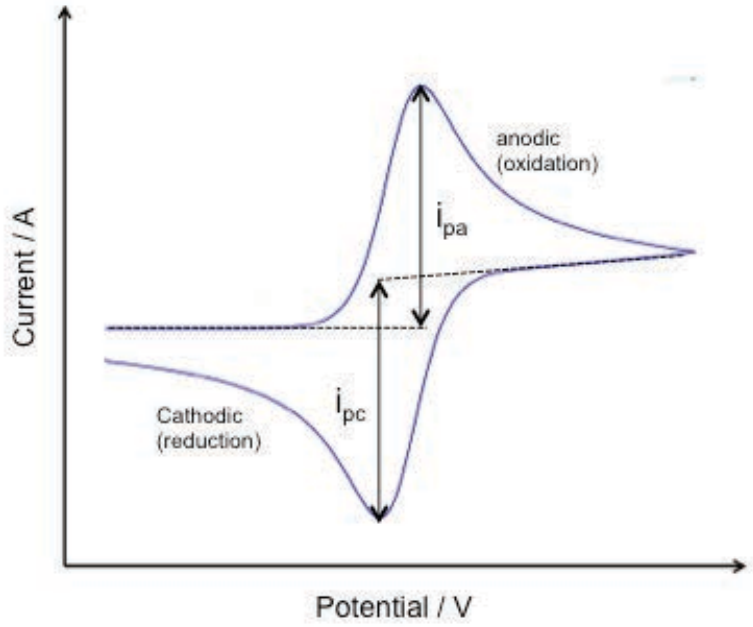

Fig. 23: Typical cyclic voltammogram

In the case of a quasi-reversible electron transfer and a limitation of the reaction by the diffusion of ions in solution, where the oxidant or the reductant is insoluble, the intensity of the reduction peak (Ip) is then proportional to the square root of the scan rate (v) (relationship Berzins Delahay [124]) according to Eq. (14).

$$\mathrm{I_p} = -0.61\mathrm{zFA}C^0\sqrt{\frac{\mathrm{zF}}{\mathrm{RT}}\mathrm{Dv}} \qquad (14)$$

where

I_p: peak current (A)

z: number of exchanged electrons

F: Faraday constant

A: electrode surface Area (cm^2)

C^0: bulk concentration (mol.cm^{-3})

R: gas constant (J. K^{-1} .mol^{-1})

T: temperature (K)

D: diffusion coefficient (cm^2.s^{-1})

v : scan rate (V.s^{-1})

If the product of the electrochemical reaction is soluble, the relation between Ip and $v^{1/2}$ is given by the Randles Sevcik relationship (Eq. (15)).

$$\mathrm{I_p} = -0.446\mathrm{zFA}C^0\sqrt{\frac{\mathrm{zF}}{\mathrm{RT}}\mathrm{Dv}} \quad (15)$$

The diffusion coefficient is calculated by the Eq. (14) and (15). D depends on the variation of the temperature according to the Arrhenius relation (Eq. (16)):

$$D = D^0 exp\left(-\frac{E_a}{RT}\right) \quad (16)$$

where

D: diffusion coefficient (cm^2.s^{-1})

D^0: pre-exponential factor (cm^2.s^{-1})

E_a: activation energy (J.mol^{-1})

T: temperature (K)

R: gas constant (J. K^{-1} .mol^{-1})

II.1.2. Chronopotentiometry (CP)

This test is performed under a controlled current and the electrode potential measured, as a function of time.

A potential variation is related to a change of the species concentration at the surface of the electrode. The transition time τ is equal to the time necessary for the concentration of electroactive species to reach zero at the surface electrode.

This technique is used to evaluate the number of reactions occurring to the working electrode and to investigate electrode kinetics. The curve E = f(t) contains plateaus corresponding to the redox potential of electroactive species as shown on Fig. 24.

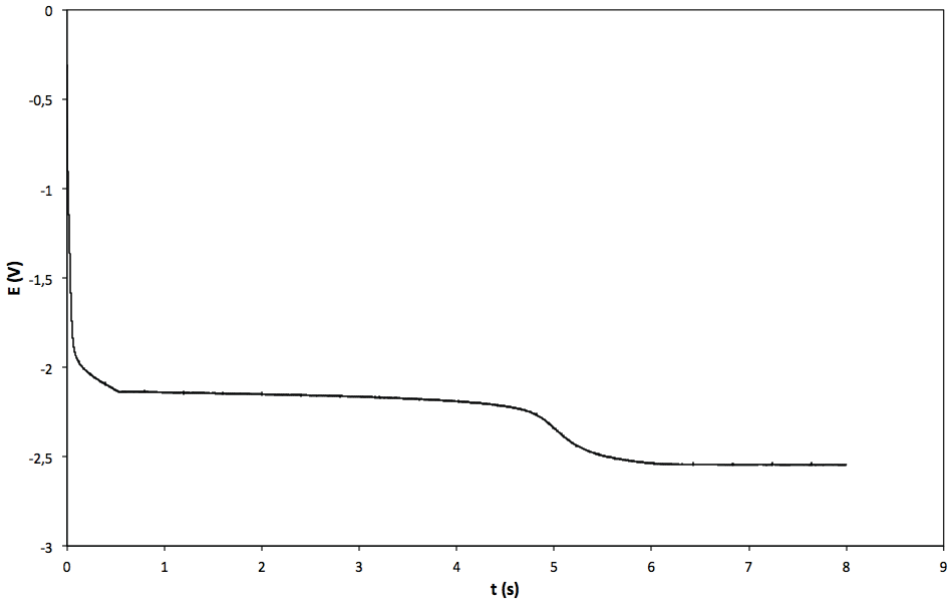

Fig. 24: Typical chronopotentiogram of 0.5 mol% of $NdCl_3$ obtained in the eutectic LiCl-KCl

If the diffusion of ions is linear and the experimental time is short enough to ignore the diffusion of the ions from the electrolyte to the diffusion layer, the transition time is related to the current density by the Sand's law [125] (Eq. (17)):

$$i\tau^{1/2} = \frac{zFAC\pi^{1/2}D^{1/2}}{2} \quad (17)$$

where

i: applied current (A)

τ: transition time (s)

z: number of exchanged electrons

F: Faraday constant

A: surface area of the electrode (cm^2)

C: bulk concentration ($mol.cm^{-3}$)

D: diffusion coefficient ($cm^2.s^{-1}$)

II.1.3. Chronoamperometry (CA)

The chronoamperometry is a transient electrochemical technique, where a potential (anodic or cathodic) is applied at the working electrode and the corresponding current at the working electrode resulting from an electrochemical reaction is measured versus time. This technique involves a stepping potential of the working electrode from an initial potential (E_{oc}) to a potential at which the faradic reaction occurs. It is used for measuring the diffusion coefficient of the electroactive species, which are contained in the electrolyte, or on the surface area on the working electrode.

The Cottrell's equation, Eq. (18), is used to determine the current-time dependency:

$$i = \frac{zFAC\sqrt{D}}{\sqrt{\pi t}} \quad (18)$$

where

i: current (A)

t: time (s)

z: number of exchanged electrons

F: Faraday constant

A: surface area of the electrode (cm^2)

C: bulk concentration ($mol.cm^{-3}$)

D: diffusion coefficient ($cm^2.s^{-1}$)

II.2. Electrolysis – Faraday's law

The electrolysis may be controlled by a fixed current, which is called chronopotentiometry or a fixed potential called chronoamperometry.

If the electrolysis is controlled with a constant current, the variation of the potential of the anode and the cathode as a function of the time was recorded. The advantage of this method is the possibility to work at the limit current in order to obtain a higher kinetic. The only threat is the unwanted side reaction as soon as the current is above the limit current.

On the other side, electrolysis with a constant potential imposes to fix a potential on an electrode versus a reference or a potential difference between an anode and a cathode. The result is the measured current, which explains the reactions taking place at the anode. If the faraday yield is closed to one then the transferred charged can be expressed by Eq. (19).

$$Q = it = nFz \quad (19)$$

where,

Q : charge number (C)

i : current intensity (A)

t : reaction time (s)

n : theoritical amount of transformed species (mol)

z: exchanged electrons

Faraday's law (Eq. (19)) allows estimating the quantity of reduced or oxidised species. If all the electrons are used to carry out an oxidation or reduction phenomenon, the faradic yield is equal to 100 %.

II.3. Characterisation of the samples

After the electrolysis process, the electrodes have to be removed from the electrolyte. They are fixed a few centimeters above the crucible, which contains the electrolyte. The temperature in the electrochemical cell is maintained for one hour to allow the removal of the electrolyte, which is stocked on the electrodes by droping down in the crucible. By using this process, it is possible to recover an almost clean electrode, which can be analysed later.

II.3.1. Optical microscope

The optical microscope allows a global overview of the sample, which have been obtained during the electrolysis process. The microscope « EPIPHOT NIKON » with a reverse lock was equipped with a camera CCD from Sony and the software « Archimed » allow the record and the analysis of pictures from each sample.

II.3.2. Scanning electron microscope (SEM)

The Scanning Electron Microscope, which employs an electron beam permits a qualitative analysis of the deposition on the anode obtained during the electrolysis. The used SEM « FEG JOEL 7800F » was coupled to Energy-Dispersive X-ray spectrometer with a Xflash detector.
The analysis method allows the detection of each element, which is contained in the deposit.

II.3.3. Characterisation of the electrolyte and the electrode

In order to confirm the efficiency of the electrolysis step, it is necessary to determine the quantity of each element contained in the electrolyte and in the Nd-based magnets fixed at the anode.

II.3.3.1. ICP-OES (Inductively Coupled Plasma – Optical Emission Spectroscopy) analysis

Before the start of the analysis, the samples have to be completely dissolved according to the process described in section II.3.3.2. of this chapter.
After this preparation step the solution is ionised by argon plasma in a temperature range between 6000 and 8000 K, which is generated and maintained by a magnetic field induced by a coil.
The Optical Emission Spectrometer allows the analysis of the light produced by the elements, which are contained in the solution. Each element has a specific wave length i.e. 406.1 nm for neodymium.

II.3.3.2. Preparation of the samples for the ICP-OES analysis

For the ICP-OES analysis, the samples have to be dissolved in a solution of 6 M of hydrochloric acid. Afterwards the obtained solution has to be diluted to reach the range of the compounds concentration, which can be detected by ICP-OES without overload.

It is also necessary to prepare reference samples with a specific concentration of the tested required elements. For the neodymium, five reference samples have ben prepared with the following concentrations of neodymium: 0.2, 5, 10, 20, 40 ppm.

III. Conclusion of the chapter

The present chapter described materials, electrochemical and characterisation techniques allow the determination of the behaviour of neodymium in different chloride and fluoride electrolytes.

The characterisation of the samples should enable us to describe the quality and quantity of the extracted compound.

Before starting the electrochemical experiment, it was necessary to develop a specific electrochemical cell, which could resist to aggressive environment conditions like corrosion and high temperatures.

Chapter III:
Design and elaboration of the electrochemical cell

Table of contents

Before starting the electrochemical study of the neodymium behaviour in molten salts, it was necessary to develop a specific electrochemical cell. In this thesis, chloride- and fluoride-based salts were used, that's why the material which is in contact with the salts has to be resistent against their aggressive character and high temperatures.
This chapter explains the description of the electrochemical cell elaboration, the different constrains which have to be considered and choices that have been done.
First of all, we will define the requirements of such a reactor. Then, we will described each element, which forms the electrochemical cell. Moreover, the used furnace and the gas system which is needed to maintain an inert atmosphere, will be explained.

I. Requirements of the electrochemical cell

The first challenge was the modification of an existing glove-box to incorporate a furnace, which has to be fixed on the bottom of the glove-box. This solution would have permitted to use a fixed reaction chamber and a removable elevator, on which the electrode and the crucible containing the electrolyte would have been fixed.
These modifications include a complete reorganisation of the glove-box. In its initial configuration it was not possible to implement such a solution.
Then, it was necessary to create a reactor, which had to be portable and airtight in order to be extracted from the glove box through the introducing chamber which has a diameter of 400 mm.
The second important requirement is the resistance against aggressive media like molten salt and the resistance against high temperatures which can reach approximately 1273 K. These operating conditions strongly limited the potential materials for the cell construction.
A key issue was the necessity to reduce drastically the temperature between the bottom and the top of the reactor, where the seal is fixed in order to keep the tightness. This temperature difference can reach 1123 K. The temperature of the lid has to be maintained under 423 K over the whole experiment duration which can reach three or four days, in order to avoid the degradation of the sealing. A degradation of the sealing can create some leaks, which threaten the health and safety of the user.

The last challenge concerned the fixation of six entrances (or exit) on the lid for:

- a reference electrode
- a counter electrode
- a working electrode
- a thermocouple to control the salt's temperature
- a gas inlet
- a gas outlet

II. Basic design of the electrochemical cell

As previously described in the introduction of this chapter, the electrochemical cell has to fit inside the introduction chamber of a glove box. Fig. 25 shows the first possible design of the electrochemical cell. With 200 mm as external diameter, the high of the chamber can reach 348 mm.

Fig. 25: First schematic description of the introduction chamber of the glove box

As mentioned before, the electrochemical cell needs cooling elements to maintain the temperature of the lid under 423 K. Fig. 26 describes the design of the cell. The lid is composed of 3 parts:

- 1: the top of the lid, which is made of aluminium is the first cooling chamber
- 2: this part made of Inconel 625 provides the connection between the cooling chambers and closes the reaction chamber
- 3: the second cooling chamber, which is made of Inconel 625 makes the connection between the reaction chamber and the lid.

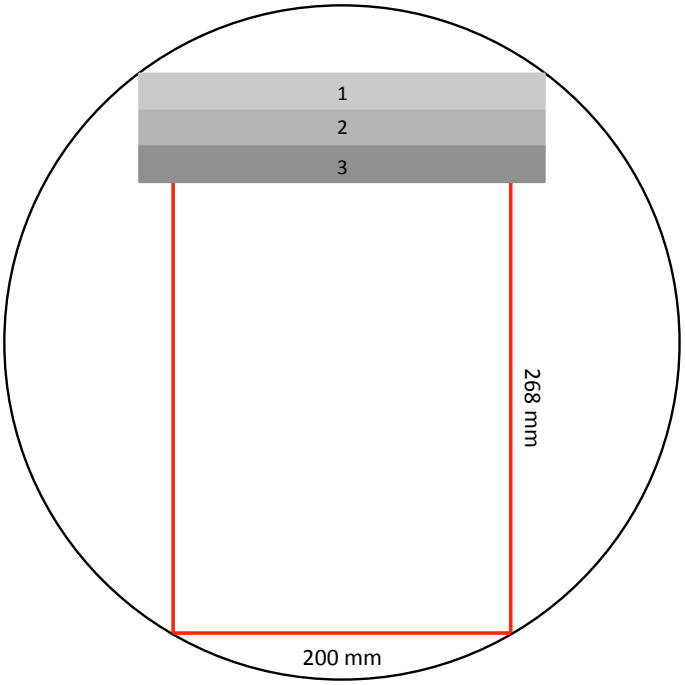

Fig. 26: Second schematic description of the introduction chamber of the glove box. (1): top of the lid, second cooling chamber; (2): separator between both cooling chambers, closing part of the reactor chamber; (3): Flange ring: first cooling chamber fixed on the reactor chamber

The whole electrochemical cell is composed of two principal parts:

- a reaction chamber
- an elevator, on which the electrodes are fixed, gas inlet and outlet and the thermocouple

III. Design of the electrochemical cell

Molten salts are very aggressive media and particularly the fluoride-based salts. During this thesis some salts based on chlorides, fluorides and a chloride/fluoride mixture were tested. The choice of the reactor material is therefore limited by the high dissolving power of these salts. Thus, oxide materials, such as alumina, silica or glass are suitable only for chloride-based salts, whereas fluoride-based salts would destroy such materials which are not oxide-saturated. The use of oxide-based materials in direct contact with salt can contaminate it and disturb the results of the electrochemical experiments. A standard electrochemical cell was therefore not suitable for our planned experiments and a new cell had to be developed especially for electrochemical experiments in this type of molten media.

Some fluoride salts have a melting point as high as 1173 – 1223 K, that's why the reactor shall resist to a constant temperature of minimum 1273 K. Inconel 625 raw material (a nickel-based alloy) was selected for the construction of the reactor as this material exhibits a high corrosion resistance against every molten media and has a melting temperature in the range of 1563 – 1623 K[126].

The complete electrochemical cell was developed using the software “Autodesk Inventor Professional”.

III.1. Reaction chamber

The reaction chamber (Fig. 27) is composed of:

- a bottom with a diameter of 200 mm and a thickness of 3 mm (3),
- a 235 mm tube with a 3 mm thick wall as reaction chamber (2),
- and a flange ring containing the first cooling chamber (1).

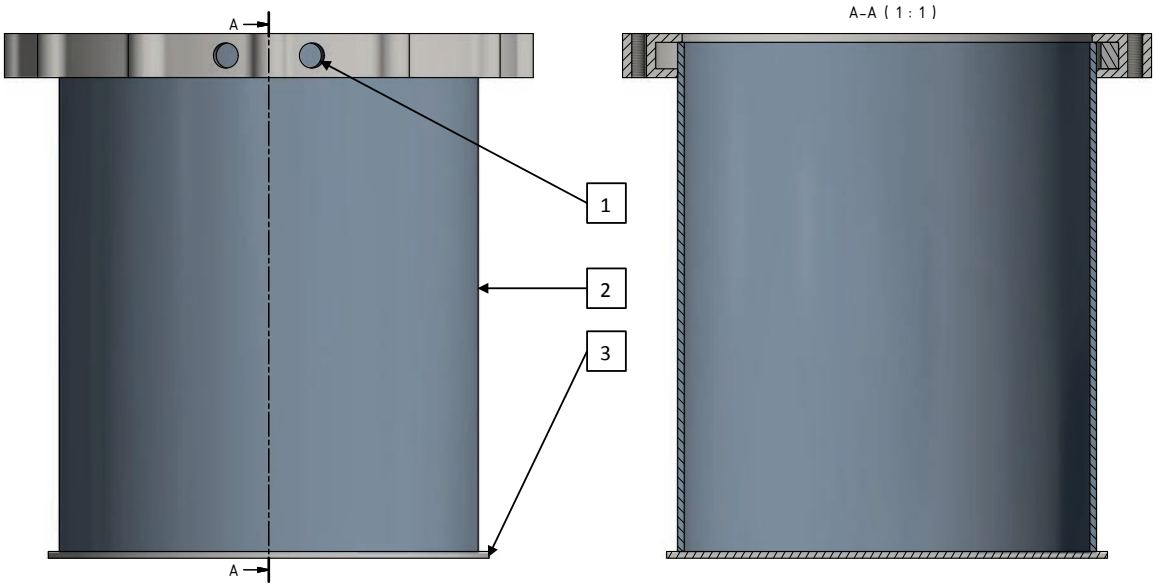

Fig. 27: Reaction chamber of the electrochemical cell.
(1): flange ring inclusive cooling chamber; (2): tube of the reaction chamber; (3): bottom of the reaction chamber

The high diameter, which is 184 mm inside the chamber has been selected in the perspective of an upscaling after the laboratory experiments. The chamber’s height of 235 mm has been chosen for two reasons. First, the crucible which contains the electrolyte can be placed in the middle of the furnace. And second, enough space between the crucible and the lid of the electrochemical cell is necessary to place thermal barriers to reduce the temperature gradient.

III.1.1. Flange ring

Fig. 28 shows a CAD-representation of the flange ring. This part is the connection between the reaction chamber and the elevator part.

Fig. 28: Flange ring

The flange ring is welded to the tube of the reaction chamber by using an Inconel 625 wire. The advantage of using the same material for the part of the electrochemical cell and the welding is to obtain a stable construction with the same expansion factor.
In this part a water input and output (1) were positioned to create a loop for the cooling cycle. This loop was directly connected to the cooling circuit which is included in the cooling ceiling system as described in section III.2.5.

III.2. Elevator part

The elevator, which is represented on Fig. 29 is the most important part of the electrochemical cell. It contains the following fixations:

- the crucible, which contains the electrolyte, with its centering ring to be maintain in the middle of the electrochemical cell
- the thermal barrier
- the holding rods
- the cooling ceiling system. This piece is made of aluminium to limit the weight of the electrochemical cell. Aluminium can be used here because this part has no direct contact with the corrosive environment of the reaction chamber.
- the elevator lid: it closes the reaction chamber and connects the flange ring, which is fixed on the reaction chamber, to the cooling ceilings system. The holding rods are fixed on this piece.
- the electrode introduction system which allows the fixation of the three electrodes, the thermocouple and the gas inlet and outlet.

To obtain an airtight sealing, two O-rings are fixed on the electrode introduction system: the first one between the flange ring and elevator ring and the second one between the elevator ring and the cooling ceiling system.

In order to protect the top of the reactor, in particular the fixation of the electrodes and the sealing of the cell with an O-ring, ten isolation shields in Inconel 625 were interposed between the bottom and the lid. Moreover the flange and the lid were cooled down using a double water circulation.

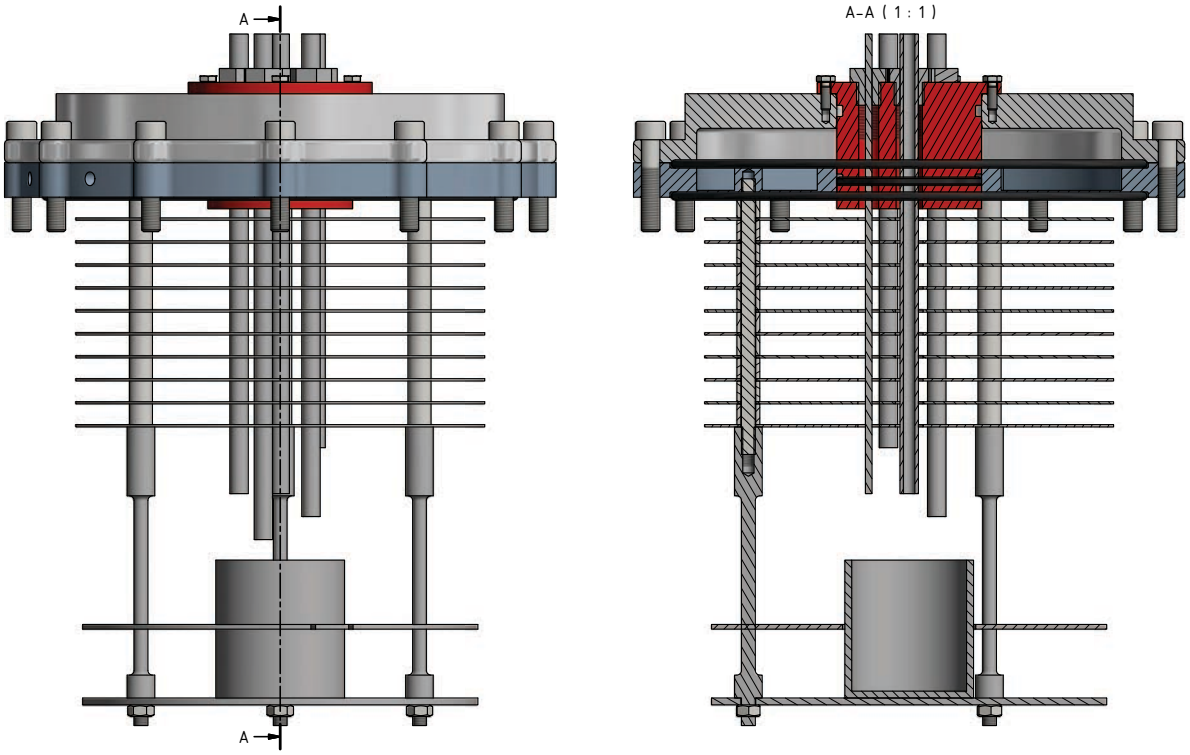

Fig. 29: CAD-representation of the elevator part

III.2.1. Crucible and centering ring

As described in the section I.1. of chapter II, a crucible with an external diameter of 56 mm (± 1 mm) was used. In order to maintain the crucible in the middle of the reaction chamber, a centering ring was designed.

Fig. 30 shows the configuration of the centering ring. The 58 mm diameter of the middle hole allows a perfect centering of the small crucible in the chamber. Additionally, three slots in the ring allow the fixation of the holding rods.

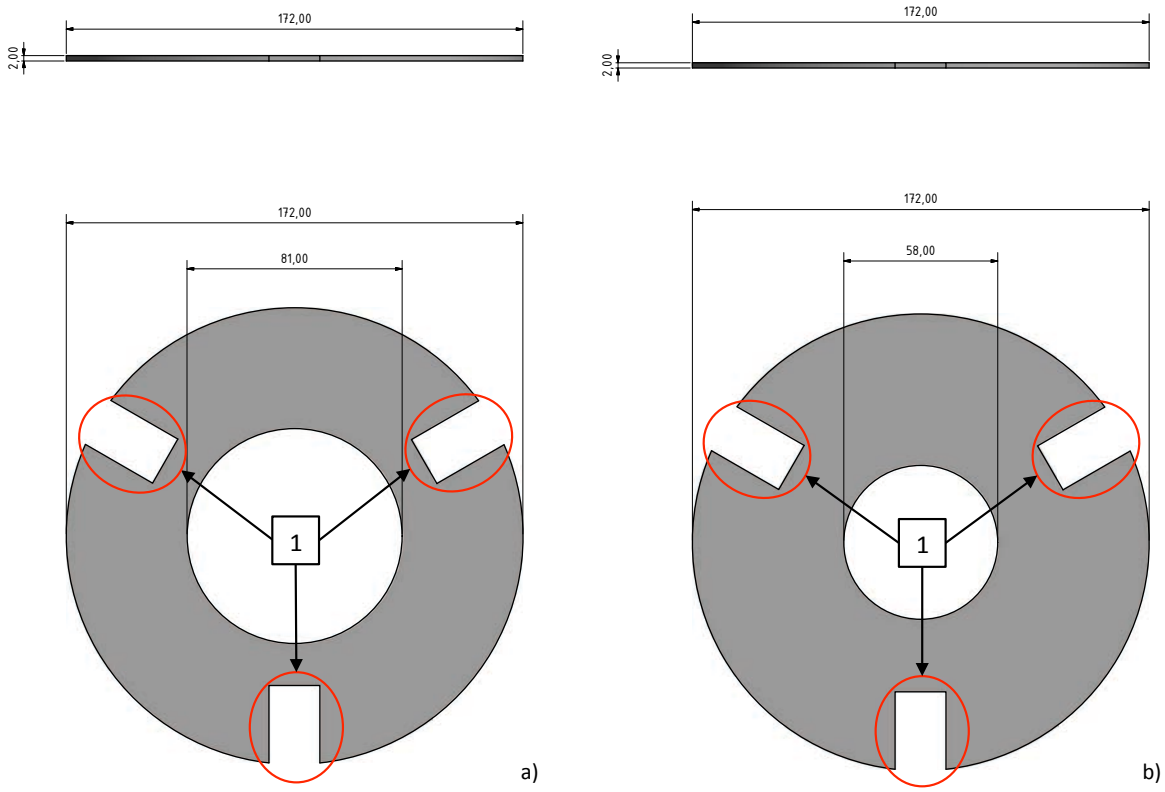

Fig. 30: Centering ring

(1): slots for the passage of the holding rods. a): configuration for bigger crucibles, b): configuration for small crucibles as described in section I.1. of chapter II

III.2.2. Elevator lid

The elevator lid is one of the most important parts of the electrochemical cell. It generates the airtight sealing between the reaction chamber and the top of the cell. Fig. 31 shows the detailed representation of the elevator lid.

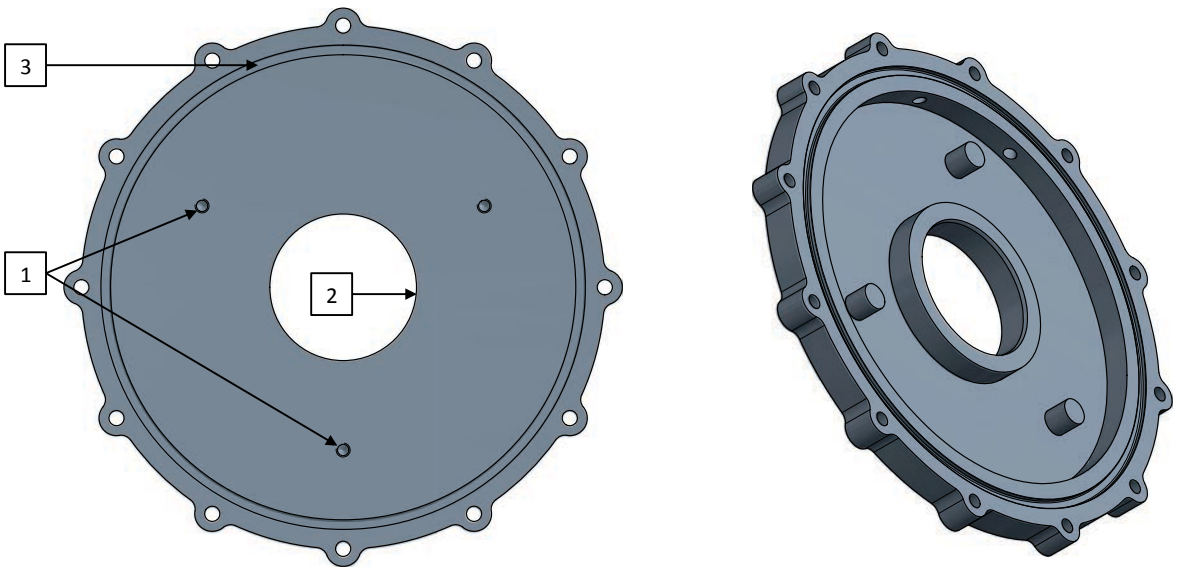

Fig. 31: elevator lid

The figure above shows three screw threads (1) which are incorporated for the fixation of the holding rods. The opening in the middle of the piece (2) allows the passage of the electrode introduction system. Moreover, the ditch allows the fixation of an O-ring (3), which is essential for the sealing.

III.2.3. Holding rods

Fig. 32 describes the configuration of the holding rods. They consist of two parts, which can be fixed together by the screw thread located at the end of each part.
The three holding rods have two main functions. The first is the stabilisation of the whole elevator part. The three rods are fixed to the elevator lid with an angle of 120° between each rod. This configuration allows a high stability of the piece.

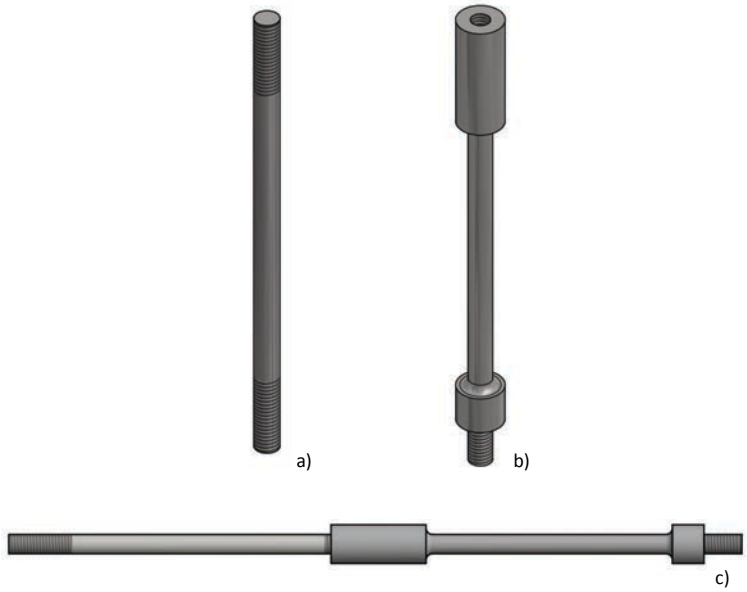

Fig. 32: Holding rods a): upper part; b) bottom part; c) complete holding rod

The second function is the fixation of the thermal shielding system, in order to reduce the temperature gradient between the bottom and the top of the electrochemical cell.

III.2.4. Thermal shielding system

As described in section I of this chapter, the temperature has to be reduced drastically between the top of the crucible and the bottom of the lid. To achieve this precondition, ten thermal shields were interposed in this part of the electrochemical cell.
Fig. 33 shows the configuration of a thermal shield. The barrier has a diameter of 178 mm and a thickness of 1 mm. Three holes (1) with an angle of 120° allow the passage of the upper part of the holding rods. The six others holes in the middle of the piece permit the introduction of the electrodes, the thermocouple and the gas supply. Each thermal barrier is separated by a 10 mm spacer.

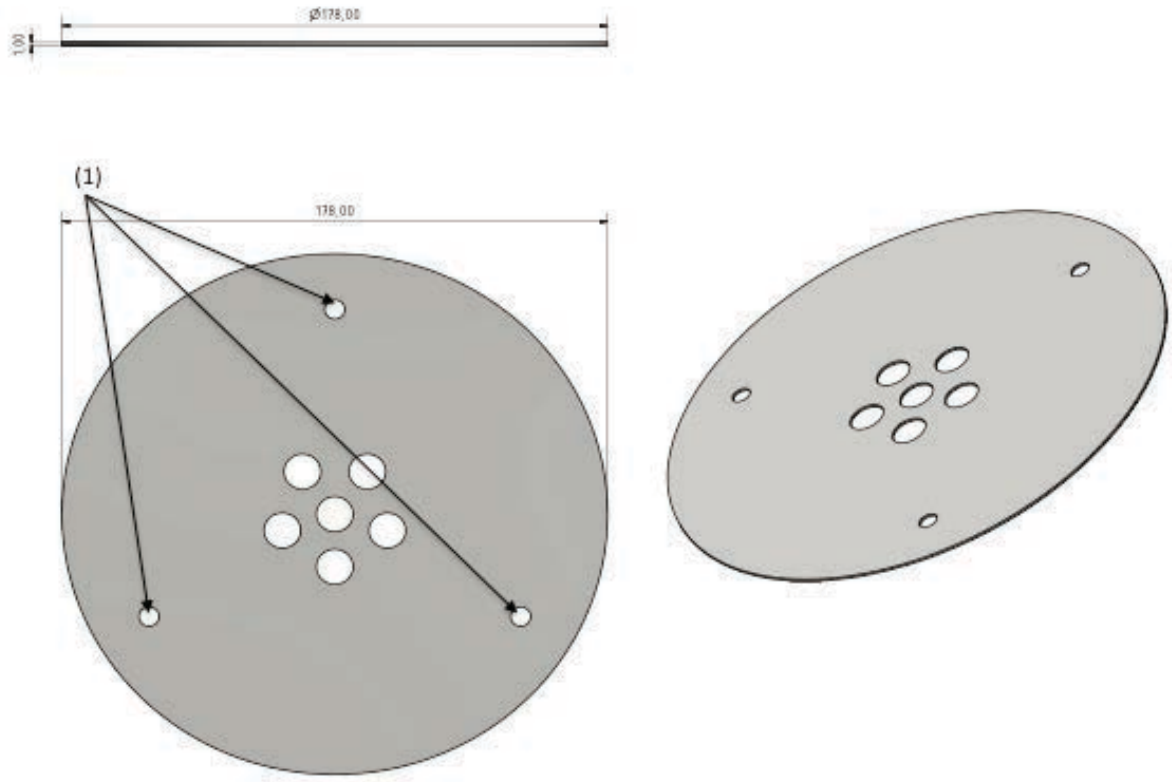

Fig. 33: Isolation shield and spacer

III.2.5. Cooling ceiling system

The cooling ceiling system is placed on the top of the electrochemical cell. This part is made of aluminum to reduce the weight of the reactor. There is neither a contact to the electrolyte or to the vapour in the reaction chamber. The aluminum cooling ceiling system is a good thermal conductor and helps to reduce the temperature of the lid.

Fig. 34 shows the configuration of the cooling ceiling system. This part is fixed on the elevator lid by using of twelve screws, which are located on the external diameter with an angle of 30° between each screw. Between the elevator lid and the ceiling system an O-ring is placed as described in the section III.2.2. of this chapter.

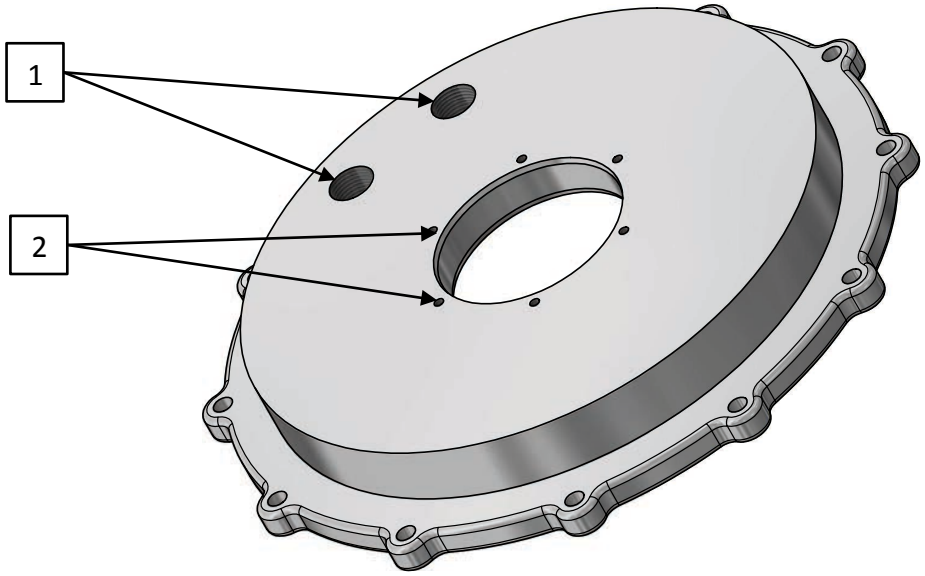

Fig. 34: Design of the cooling ceiling system

A water input and output are placed on the top of the ceiling system to produce a cooling cycle. This loop is directly connected to the cooling circuit, which is included in the flange ring. The airtight fixation of the electrode introduction system is created by the six screw threats, which are localised in the middle of this piece.

III.2.6. Electrode introduction system

The electrode introduction system was the most complicated part to be designed. It was challenging to place six holes (three for the electrodes, two for the gas system and one for a thermocouple) in a diameter of 50 mm. The diameter corresponds to the internal diameter of the crucible described in chapter 2.
In each hole, a guide pipe was placed as described in chapter 2. These pipes were fixed with a “316 SS Tube fitting male connector” from the company Fitok, which allows an airtight sealing.

Fig. 35 shows a CAD-design of the electrode introduction system. In the bottom section two O-rings are placed in order to create the sealing with the cooling ceiling system and the elevator lid. Six holes have been designed in the central part in order to place the above-mentioned elements. In the external part six screws have been placed for the fixation of the electrode introduction system on the cooling ceiling system.

Fig. 35: CAD-design of the electrode introduction system

Fig. 36 shows the arrangement of the electrode introduction system. In the middle (1) the thermocouple type K is placed. It is the only element which has not to be removed after each experiment. Holes #2 and #3 are provided for the gas input and output with an one-way valve.

Fig. 36: Arrangement of the electrode introduction system

The reference electrode was placed on position #4. Finally the counter and the working electrodes are placed on position #5 and #6. Each configuration of the electrodes is described in section I.3. of chapter II.

The setting of the electrode introduction system allows a precise control of the gap between each component.

IV. Overview of the connection of the electrochemical cell

Fig. 37 shows an overview of the different connections on the top of the electrochemical cell. This figure summarises all of the above-mentioned connections.

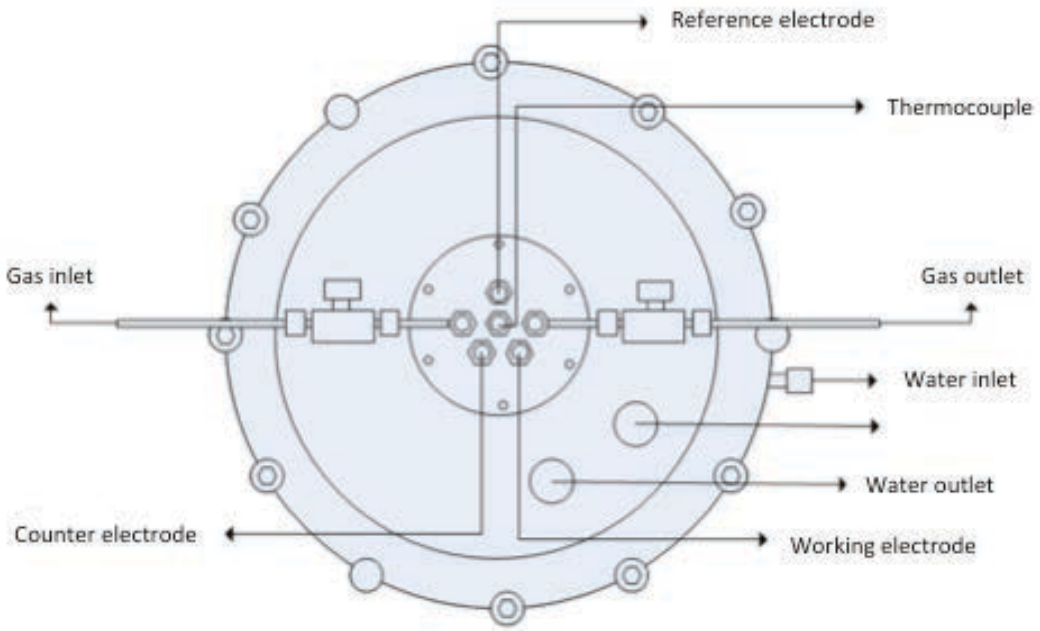

Fig. 37: Overview of the connections on the top of the reactor

As described on the above-mentioned figure, one-way valves have been installed between entry (or exit) from the electrode introduction system and the supplying pipe to avoid a gas reflux.

V. Furnace and gas system

V.1. Furnace

After the development of the electrochemical cell, the next challenge was the elaboration of a furnace to heat only the required part of the reactor, which means the 1/3 bottom part. The furnace was the tube oven Modell ROM 230/250/11-VS and was developed in collaboration with the company ibf. It was controlled by the software “Control Software Eurotherm iTools”, version 7.60.

V.2. Gas system

The inert atmosphere inside the electrochemical cell is maintained using a constant flow of argon. The electrochemical cell is removed from the glove box and placed in the furnace. Afterwards the gas inlet and outlet are screwed on the one-way valves. Before the heating start, the reaction chamber is flushed during one hour with a 10 l/h flow of argon.

When the electrochemical cell starts to be heated, the flow of argon is reduced to 2 l/h. This flow is maintained during the whole experiment process and also the cooling phase of the furnace.

The outgoing gas passes through a security bottle. This is required to avoid that the liquid, which is contained in the washing bottle, arrives inside the reactor due to depression. Then the outgoing gas passes through a washing bottle in order to clean this gas before its rejection in the atmosphere.

The lid is maintained at room temperature by a flow of cold water during the heating of the furnace and the execution of the experiment until the cooling down of the furnace. Fig. 38 shows an overview of the experimental setup.

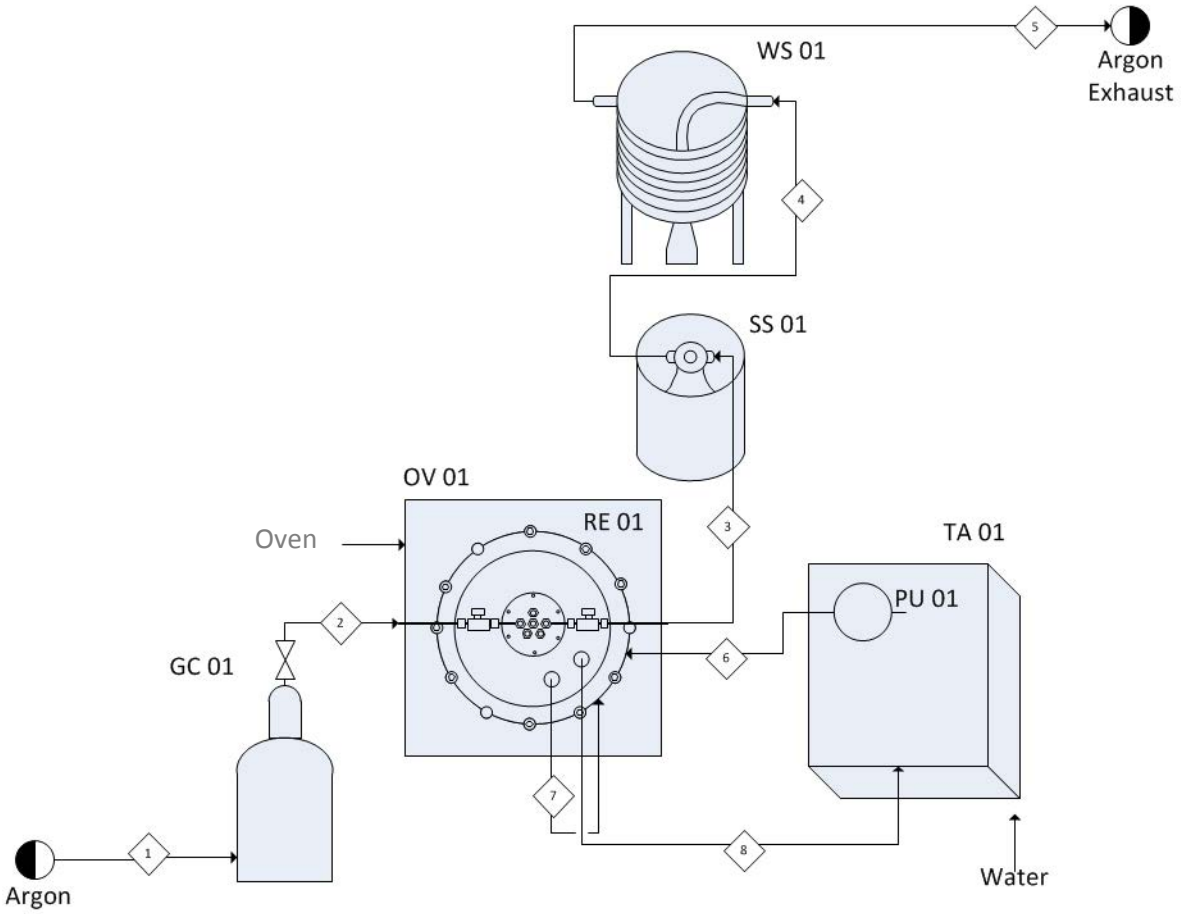

Fig. 38: Configuration of the furnace, gas and cooling system. The Inconel reactor was flushed with an argon flow of 2 l/h in order to obtain an inert atmosphere. The outgoing gas passes through a security bottle (SS 01), which has the function to avoid the entrance of liquid in the reactor in case of under pressure. Then, the outgoing gas goes through a washing bottle (WS 01) before leaving the system. The top of the reactor has to be cooled down under 423 K in order to protect the sealing gasket. The cooling water was pumped from a 600 l water tank (TA 01) to the reactor in a closed system, which limits the water consumption.

VI. Validation of the electrochemical cell

After its conception, the electrochemical cell had to be tested under specific conditions in order to validate its design and the correct working of the different components.

VI.1. Cold test

At first, the gas tightness had to be tested. A flow of 10 l/h of argon was set. If the reactor is airtight after five minutes, gas bubbles should be visible in the cleaning bottle placed just before the gas exit.

This first gas bubbles test is not sufficient to proof the validation of the cold test. Some small leaks can be found at each connection point for example on the electrode and the

thermocouple. A leak test is therefore essential for each connection point before each experiment.

The second cold test is a waterproof test for the cooling system. The cold water is pumped from the water tank to the electrochemical cell in order to cool down the top of the electrochemical cell, which is sensitive to high temperatures due to the sealing system. This test shows no leak in the cooling circuit.

VI.2. Hot tests

These first tests were followed by tests at high temperature to check the system reaction and integrity. The electrochemical cell was then heated up to 1223 K with a heating rate of 5 K/min. Every 373 K the temperature stayed constant for 15 min. Then the furnace was heated up to 1223 K and maintained constant during 45 min.

Fig. 39 represents the evolution of the temperature inside the electrochemical cell in comparison to the furnace temperature up to a maximum temperature of 1223 K. The set temperature of 1223 K in the furnace is reached after 365 min, whereas the temperature inside the reactor is reached 30 min later.
The calibration shows that the set temperature is exactly the same as the temperature in the electrochemical cell.

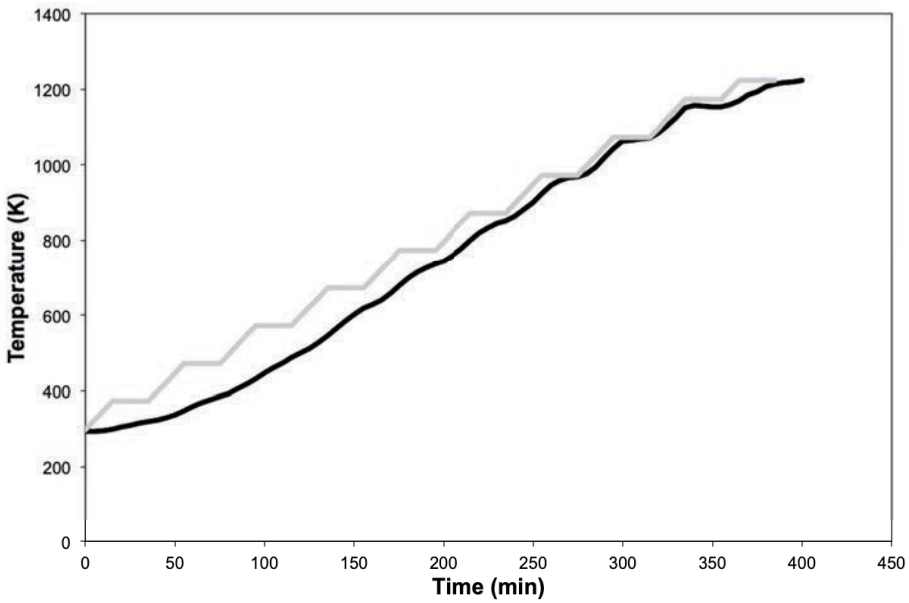

Fig. 39: Calibration of the furnace and the electrochemical cell (grey curve: furnace setting, black curve: thermocouple inside the electrochemical cell)

VI.3. Comparison with the literature

After the cold and hot tests, it is necessary to validate the complete setting by comparing the results obtained in our new test rig to the literature. A standard electrochemical experiment was performed for this purpose. As the eutectic LiCl-KCl electrolyte has been widely investigated with numerous results presented in the literature, we have chosen to make the validation. The electrolyte was LiCl-KCl_{eut} (59.2 - 40.8 mol%) salt as described in section I.2.1. of chapter II.

The experiment was conducted at 723 K with a three-electrode-system:

- a tungsten wire with a diameter of 1 mm as working electrode,
- a molybdenum wire with a diameter of 1 mm as counter electrode
- an Ag/AgCl reference electrode as described in section I.3.1. of chapter 2

Fig. 40 shows a typical cyclic voltammogram of a LiCl-$KCl_{eut.}$ salt on a tungsten electrode as working electrode at 723 K. The electrochemical window goes from – 2.5 V, which corresponds to the reduction of the ions Li^+ in Li^0, up to +1.2 V, which corresponds to the oxidation of Cl^- in Cl_2. This result is in accordance with the literature.[127]

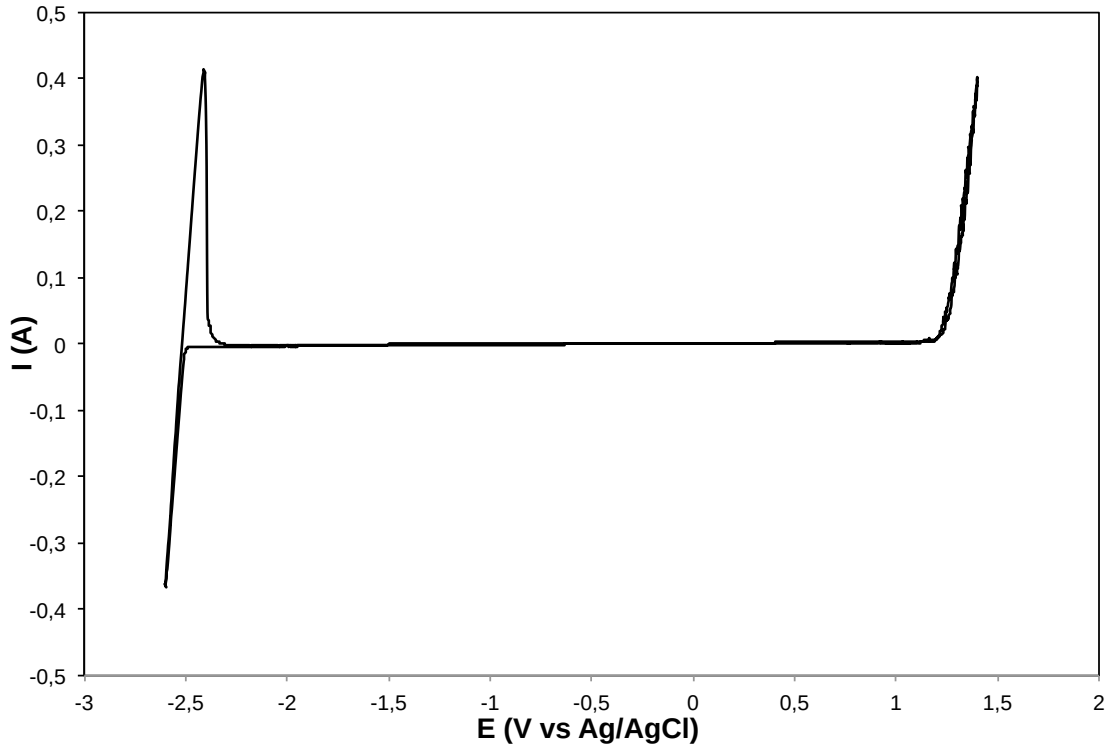

Fig. 40: Cyclic voltammogram of LiCl-KCl eutectic salt on a tungsten electrode at 723 K, counter electrode: molybdenum, reference electrode: Ag/AgCl (1wt%), A = 0.2 cm^2, v = 0.1 V s^{-1}

Moreover this blank experiment without any dissolved neodymium salt shows no significant peak between the reduction of lithium and the oxidation of chlorine which means that no oxide is presented in the electrolyte as dissolved O^{2-}. The blank experiment confirms the right conception and the correct setup of the electrochemical cell.

Chapter IV:
Experimental Part – Properties of neodymium in molten salts

Table of contents

This chapter deals with the electrochemical properties of neodymium dissolved in molten salt electrolytes. The reduction mechanism was studied by using transient electrochemical technique like cyclic voltammetry or chronopotentiometry.
The reduction scheme provides information, which are required for an efficient electrolysis process. Different salts were tested to verify if they could respond to all requirements, which are needed for the extraction of pure neodymium from permanent magnet scraps.

The behaviour of neodymium ions was studied at different temperatures in the following molten salts:

- $LiCl\text{-}KCl_{eut.}$
- $LiF\text{-}CaF_2$
- LiCl-KCl-LiF
- $LiF\text{-}SrF_2$

The reasons for this choice of electrolytes are described in detail in section I.2 of chapter II.

The study of the reduction mechanism of neodymium ions needs different setup due to the specific properties of the chosen molten electrolytes. Some materials are not suitable for all electrolytes. The first part of this chapter deals with the configuration of the electrochemical cell.

The second section deals with the electrochemical properties of the neodymium compounds in selected electrolytes, with the determination of the reduction potential of each neodymium ion contained in the electrolyte, the stability of these products and the diffusion coefficients.

I. Configuration of the electrochemical cell

Molten salts might be very aggressive media. The most important disadvantage is their power to dissolve. This constraint reduces the choice of the material for the design of the experimental setup. One example can underline this requirement i.e. if the electrolyte is composed of molten fluoride salts, all other materials containing oxides like glass or alumine are attacked by molten salts.
Beside the properties of molten salts, high temperatures favour the alloy formation, that can influence the signal, which is measured by the electrodes. Then, it is necessary to prevent the introduction of oxide into the electrochemical cell.

Materials	Max. Temperature (K)	Electrolyte
Pyrex	773	Cl^-
quartz	973	Cl^-
molybdenum	1873	F^-, Cl^-
Platinum	1673	F^-, Cl^-
Alumina	1773	Cl^-
Graphite	2273	F^-, Cl^-
Glassy carbon	1773	F^-, Cl^-
Tantalum	1873	F^-, Cl^-

Tab. 7: Overview of properties of material, which can be used in molten salts

According to Tab. 7 and the analysis of the state of the art, the following electrode configuration was chosen:

The setup for the chloride-based salt consists of:

- a 1 mm of diameter molybdenum wire as working electrode
- a 1 mm of diameter tungsten wire as counter electrode
- a Pyrex® tube, with a very thin bottom wall containing a 1.5 mm of diameter silver wire dipped in a mixture of the same composition as the electrolyte + 0.75 mol/kg of AgCl as reference electrode. The detailed description of the configuration of this type of electrode is described in section I.3.1 of chapter II.

For salts containing fluorides, the following setup is constructed using:

- a 1 mm of diameter molybdenum wire as working electrode
- a 2 mm of diameter glassy carbon rod as counter electrode
- a 0.5 mm of diameter platinum wire as reference electrode.

In order to determine the electrochemical properties of neodymium salt, it is necessary to know as precisely as possible the concentration of neodymium ions contained in the electrolyte and the surface of the working electrode, which is dipped in the same electrolyte.

In order to calculate these values for each experiment, the following experimental parameters have to be known:

- the dimension (radius, high, wall thickness, volume) of the used crucible
- the radius of the working electrode
- the density of each component in the electrolyte. Depending on the working temperature, the variation of the density has also to be taken into account.

By using the density and the quantity of each component presented in the electrolyte, it is possible to calculate, which volume is needed individually for each component at each temperature.
It is possible to calculate the height in the crucible, which represents the electrolyte by knowing the volume of the crucible and the volume of the melted electrolyte.

If the distance between the bottom of the crucible and the extremity of the electrode was the same for each experiment, the density of the salt changes, depending on the temperature. A temperature increase decreases the density of the salt that results into an augmentation of the volume of the electrolyte.
The increase of the electrolyte's volume leads to an increase of the electrolde surface, which is dipped in the melt and to a decrease of the neodymium concentration, which is expressed in mol per cubic centimeter of electrolyte.

Tab. 8 summarise the neodymium concentration and the surface of the working electrode depending on the temperature. These values are used to carry out the calculations to define the neodymium properties in each electrolyte.

Electrolyte	T (K)	C_{Nd} (mol/m^3)	$A_{electrode}$ (cm^2)
LiCl-KCl	723	1.477E-4	0.473
	773	1.453E-4	0.484
	823	1.430E-4	0.495
	873	1.406E-4	0.506
LiF-CaF_2	800	2.790E-4	0.343
	825	2.770E-4	0.346
	848	2.760E-4	0.349
	872	2.740E-4	0.351
LiCl-KCl-LiF	725	1.516E-4	0.481
	776	1.492E-4	0.491
	823	1.470E-4	0.501
	872	1.447E-4	0.512

Tab. 8: Summary of the neodymium concentration and the surface area of the working electrode which is dipped in each electrolyte at the experimental temperatures.

II. Electrochemical properties of neodymium in molten salts

II.1. Electrochemical behaviour of neodymium in LiCl-$KCl_{eut.}$

The first investigated electrolyte was the eutectic mixture between LiCl- and KCl- salt with the respective mol% proportion 59.2 and 40.8.

In order to study the behaviour of the neodymium ions, a temperature range from 723 to 873 K was used.

Fig. 41 shows a comparison of two cyclic voltammograms. The black curve represents the electrolyte LiCl-KCl_{eut}, whereas the grey curve represents the same electrolyte containing 0.5 mol% of $NdCl_3$. The addition of $NdCl_3$ in the pure electrolyte leads to the appearance of two cathodic peaks at potential closed to -2.1 V vs. Ag/AgCl and -1.9 V vs Ag/AgCl corresponding to the reduction steps of Nd^{3+} and Nd^{2+} as described above.

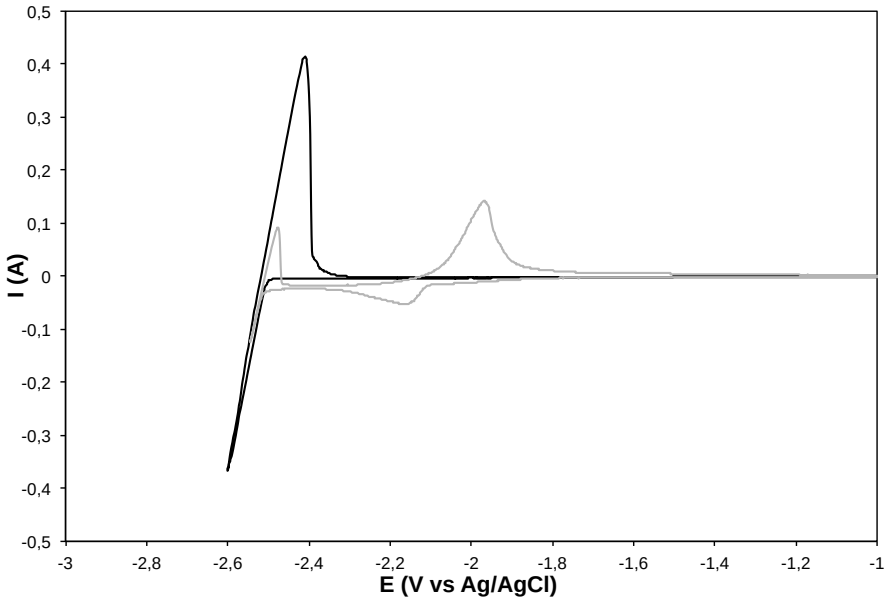

Fig. 41: Cyclic voltammograms of LiCl-KCl (black curve) and LiCl-KCl-$NdCl_3$ (0.5 mol%), (grey curve), at 723 K, scan rate: 0.1V.s^{-1}. Working electrode: tungsten, counter electrode: molybdenum, reference electrode: Ag/AgCl

In the eutectic LiCl-KCl, the neodymium ions can be found in the complex form $NdCl_6^{3-}$ *and* $NdCl_4^{2-}$, which correspond to the Nd^{3+} and Nd^{2+} ions. It has been proved that the stability of the neodymium complex is linked to the polarisation power of the electrolyte. That means that the electrolyte which contains larger cations helps the stabilisation of the complex $NdCl_6^{3-}$.[82] [79]

II.1.1. Study of the neodymium properties using the cyclic voltammetry

Fig. 42 shows a cyclic voltammogram, which represents the redox process of neodymium ions in the eutectic LiCl-KCl electrolyte. In the LiCl-KCl electrolyte the neodymium ion are reduced to neodymium metal in two steps. The peaks A and A' correspond to the soluble-soluble transition Nd^{3+}/Nd^{2+} whereas the peaks B and B' correspond to the soluble-insoluble transition Nd^{2+}/Nd^{0}.[90]

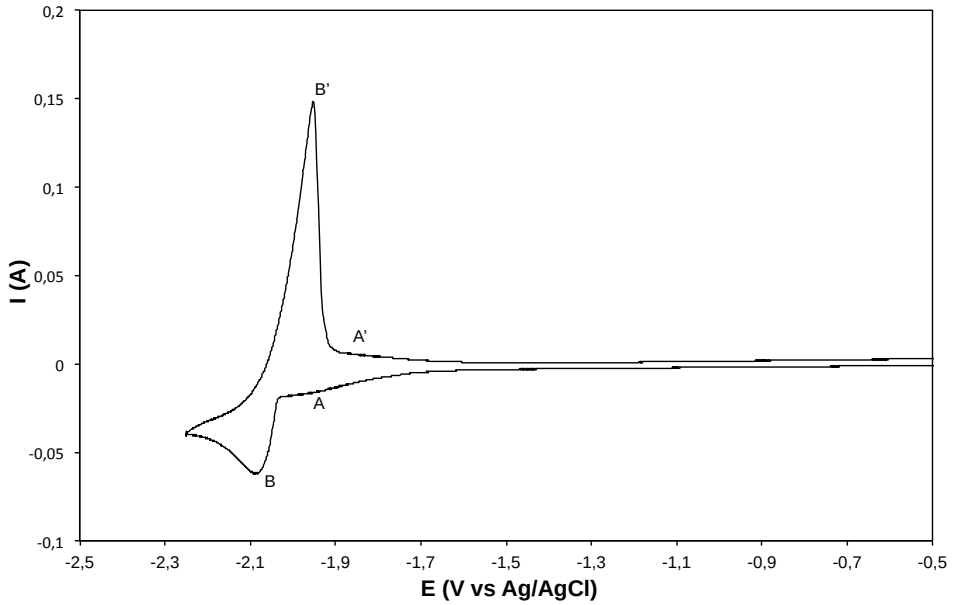

Fig. 42: Cyclic voltammogram of neodymium ions in the eutectic LiCl-KCl at 823 K scan rate: 0.1 $V.s^{-1}$. Working electrode: tungsten, counter electrode: molybdenum, reference electrode: Ag/AgCl.

The electrochemical reduction of Nd^{3+} is achieved in two steps:

$$Nd^{3+} + e^{-} \leftrightarrow Nd^{2+}$$

$$Nd^{2+} + 2e^{-} \leftrightarrow Nd^{0}$$

The first reaction is a soluble-soluble transition whereas the second refers to a soluble-insoluble transition.

The Nd^{2+} is considered as an unstable cation and disproportionate into Nd^{3+} and Nd^{0}. After the first reduction step the Nd^{2+} ions undergo a disproportion reaction as follows:

$$3Nd(II) \leftrightarrow 2Nd(III) + Nd(0)$$

In the first step Nd^{2+} ions are formed from the Nd^{3+} ions. That's why it is considered that $C_{Nd^{3+}} = C_{Nd^{2+}}$.[128,90,129]

Fig. 43 shows the cyclic voltammograms from the eutectic LiCl-KCl containing 0.5 mol% of $NdCl_3$ at 823 K. Fig. 43(a) represents the whole voltammogram containing both reduction steps of the neodymium ions, whereas Fig. 43(b) focuses only on the reduction step from

Nd^{3+} to Nd^{2+}. The Nd^{3+}/Nd^{2+} and Nd^{2+}/Nd^{0} systems can be considered as reversible at a scan rate from 20 $mV.s^{-1}$ up to 500 $mV.s^{-1}$ between 723 and 873 K.

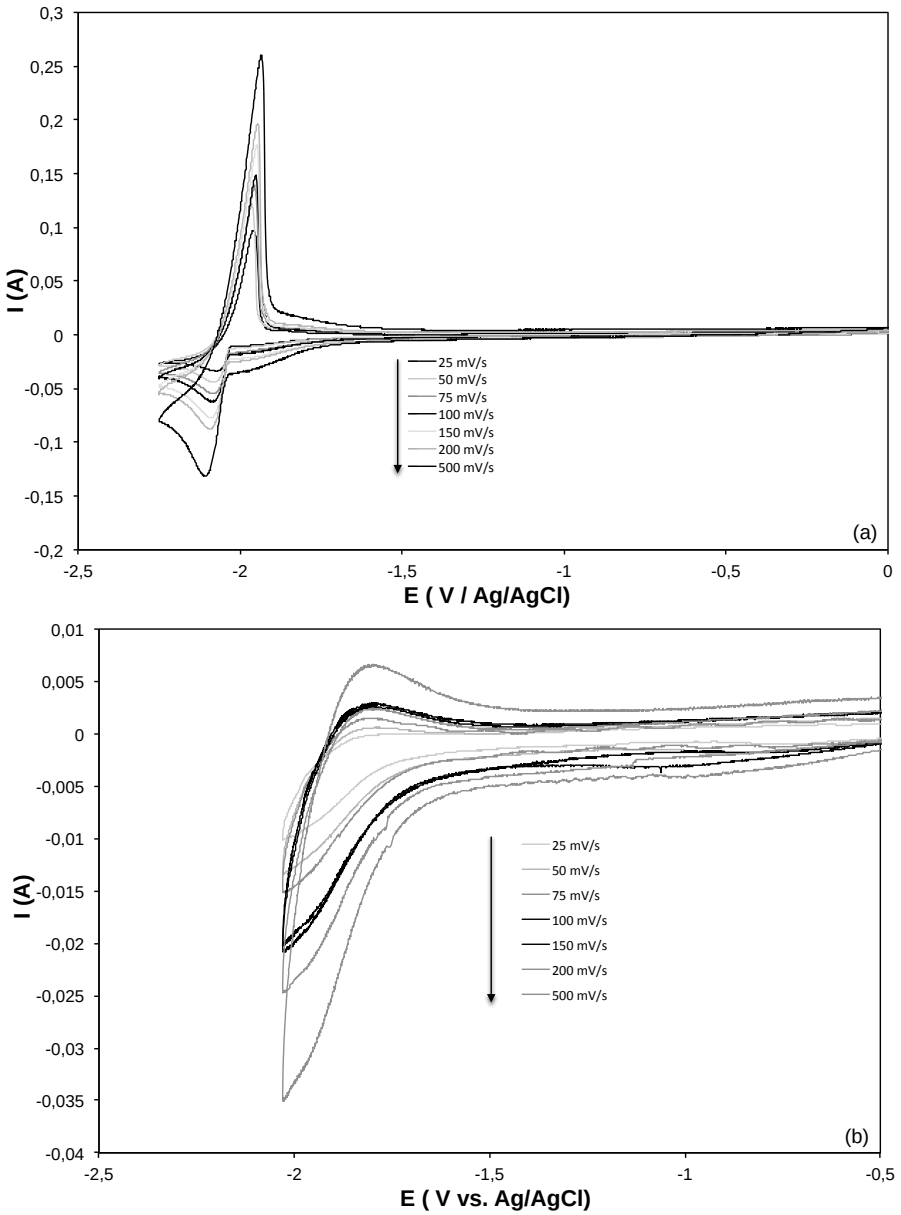

Fig. 43: Representation of cyclic voltammograms for the reduction of Nd^{3+} to Nd^{0} (a) and for the reduction of Nd^{3+} to Nd^{2+} (b) in the eutectic LiCl-KCl containing 0.5 mol% of $NdCl_3$ at 823 K. Working electrode: tungsten, counter electrode: molybdenum, reference electrode: Ag/AgCl

Fig. 44 shows that the increase of the scan rates leads to a shift of the cathodic peak potential towards more negative potentials, whereas the anodic peak potential is shifted towards more positive potentials. This information shows that the neodymium reduction of Nd^{2+} into Nd^{0} is quasi-reversible.

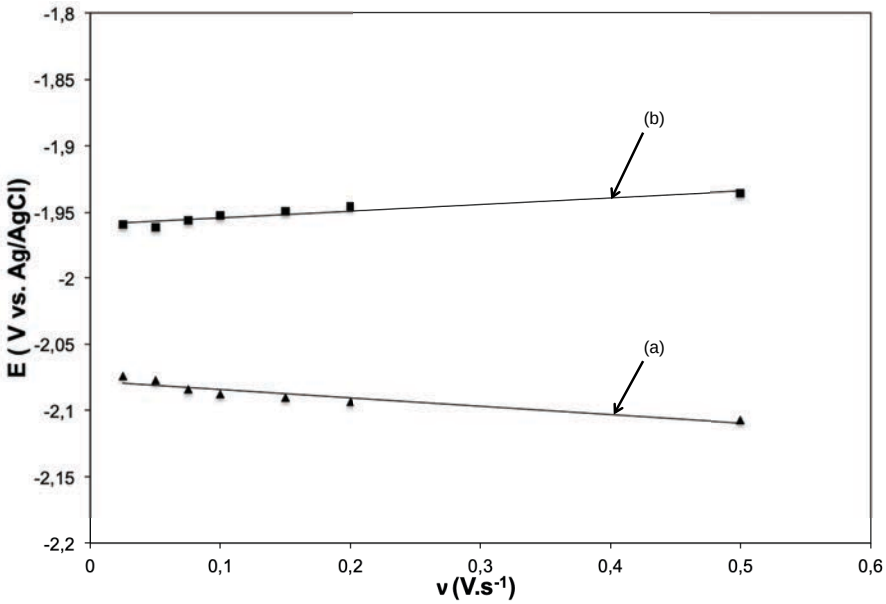

Fig. 44: Evolution of the cathodic (a) and anodic (b) peak potential corresponding to the Nd^{2+}/Nd^{0} redox system with the increase of the scan rate at 823 K

II.1.1.1. Determination of the apparent standard potential

Study of the soluble-soluble transition Nd^{3+}/Nd^{2+}

In theory, both reduction steps have to be considered as independent reactions. In the eutectic LiCl-KCl electrolyte, this hypothesis is not correct, due to the close values of the standard potential of the both redox systems (Eq. (20))

$$E_{p,A} = E_{1/2} + 1.11\frac{RT}{zF} \quad (20)^{90}$$

where $E_{1/2}$ represents the half wave potential and $E_{p,A}$ represents the potential of the cathodic peak. The half-wave potential is defined by Eq. (21):

$$E_{1/2} = E^{0}_{Nd^{3+}/Nd^{2+}} + \frac{RT}{zF}\ln\left(\frac{\gamma_{Nd^{3+}}}{\gamma_{Nd^{2+}}}\right) + \frac{RT}{zF}\ln\left(\frac{\sqrt{D_{Nd^{2+}}}}{\sqrt{D_{Nd^{3+}}}}\right) \quad (21)$$

where $E^{0}_{Nd^{3+}/Nd^{2+}} + \frac{RT}{zF}\ln\left(\frac{\gamma_{Nd^{3+}}}{\gamma_{Nd^{2+}}}\right)$ represents the apparent standard potential $E^{0*}_{Nd^{3+}/Nd^{2+}}$.

The apparent standard potential is estimated by a reunification of Eq. (20) and (21), which leads to Eq. (22). The apparent standard potential $E^{0*}_{Nd^{3+}/Nd^{2+}}$ is calculated with Eq. (22).[130,131]

$$E^{0*}_{Nd^{3+}/Nd^{2+}} = E_{p,A} - 1.11\frac{RT}{zF} - \frac{RT}{zF}\ln\left(\frac{\sqrt{D_{Nd^{2+}}}}{\sqrt{D_{Nd^{3+}}}}\right) \quad (22)$$

The values of the apparent standard potential $E^{0*}_{Nd^{3+}/Nd^{2+}}$ of the soluble-soluble system are summarised in Tab. 9. The values of this potential increase linearly with the increase of the temperature.

T (K)	$E^{0*}_{Nd3+/Nd2+}$ (V vs. Cl_2/Cl^-)
723	-3.050
773	-3.016
823	-2.981

Tab. 9: Apparent standard potential for the soluble-soluble system Nd^{3+}/Nd^{2+} at 723, 773 and 823 K

The evolution of the apparent standard potential is described on Fig. 45. The values of $E^{0*}_{Nd^{3+}/Nd^{2+}}$ fall along the line of equation:

$$E^{0*}_{Nd^{3+}/Nd^{2+}} = -3.548 + (6.89 * 10^{-4}) * T \text{ in V vs. } Cl_2/Cl^- \quad (23)$$

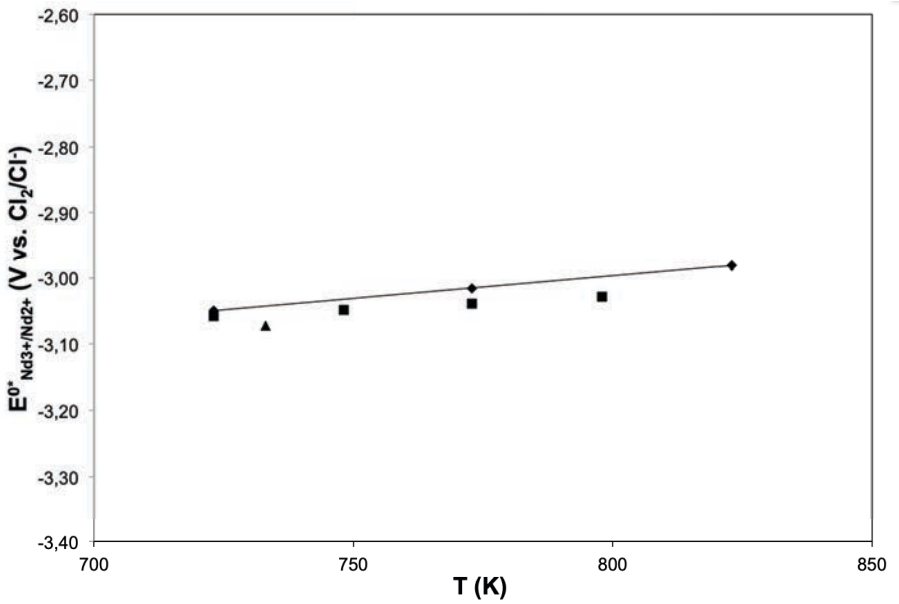

Fig. 45: Evolution of the apparent standard potential $E^{0*}_{Nd^{3+}/Nd^{2+}}$ depending on the absolut temperature. (◆): this study; (■)[90] ;(▲)[78]

The values of the apparent standard potential found in this study are in good agreement with the literature. The difference between two potentials (literature – this study) at the same temperature is lower than 1 %.[78,90]

Study of the soluble insoluble transition Nd^{2+}/Nd^0

The standard potential of the soluble-insoluble system Nd^{2+}/Nd^0 is calculated from the value of the cathodic potential peak $E_{p,B}$ using Eq. (24). [78,129]

$$E_{p,B} = E^0_{Nd^{2+}/Nd^0} + \frac{RT}{zF} ln\left(\frac{a_{Nd^{2+}}}{a_{Nd^0}}\right) - (0{,}9241)^2 * \frac{RT}{zF} \quad (24)$$

where $E^{0}_{Nd^{2+}/Nd^{0}}$ is the standard potential, $a_{Nd^{2+}}$ and $a_{Nd^{0}}$ the activities of Nd^{2+} and the neodymium metal in the electrolyte, respectively.

The activity is expressed by Eq. (25):

$$a_{Nd^{2+}} = \gamma_{Nd^{2+}} * X_{Nd^{2+}} \quad (25)$$

where $\gamma_{Nd^{2+}}$ represents the activity coefficient of Nd^{2+} and $X_{Nd^{2+}}$ the molar fraction of Nd^{2+} in the electrolyte in mol.cm^{-3}.

The standard potential $E^{0}_{Nd^{2+}/Nd^{0}}$ is directly related to the apparent standard potential $E^{0*}_{Nd^{2+}/Nd^{0}}$ by Eq. (26).

$$E^{0*}_{Nd^{2+}/Nd^{0}} = E^{0}_{Nd^{2+}/Nd^{0}} + \frac{RT}{zF}\ln(\gamma_{Nd^{2+}}) \quad (26)$$

Assuming that the activity of the pure neodymium metal is equal to one and according to the combination of Eq. (24) to (26), the expression of the potential can be rearranged as follows (Eq. (27)):

$$E_{p,B} = E^{0*}_{Nd^{2+}/Nd^{0}} + \frac{RT}{zF} ln(X_{Nd^{2+}}) - (0{,}9241)^2 * \frac{RT}{zF} \quad (27)$$

The values of the apparent standard potential $E^{0*}_{Nd^{2+}/Nd^{0}}$ are summarised in Tab. 10.

T (K)	$E^{0*}_{Nd2+/Nd0}$ (V vs Cl_2/Cl^-)
723	-3.078
773	-3.052
823	-3.011

Tab. 10: Apparent standard potential $E^{0*}_{Nd^{2+}/Nd^{0}}$

The values of this potential increase linearly with the increase of the temperature. The evolution of the apparent standard potential is described on Fig. 46. The values of $E^{0*}_{Nd^{2+}/Nd^{0}}$ fall along the line of equation (Eq. (28)):

$$E^{0*}_{Nd^{2+}/Nd^{0}} = -3.556 + (6.62 * 10^{-4}) * T \text{ in V vs. } Cl_2/Cl^- \quad (28)$$

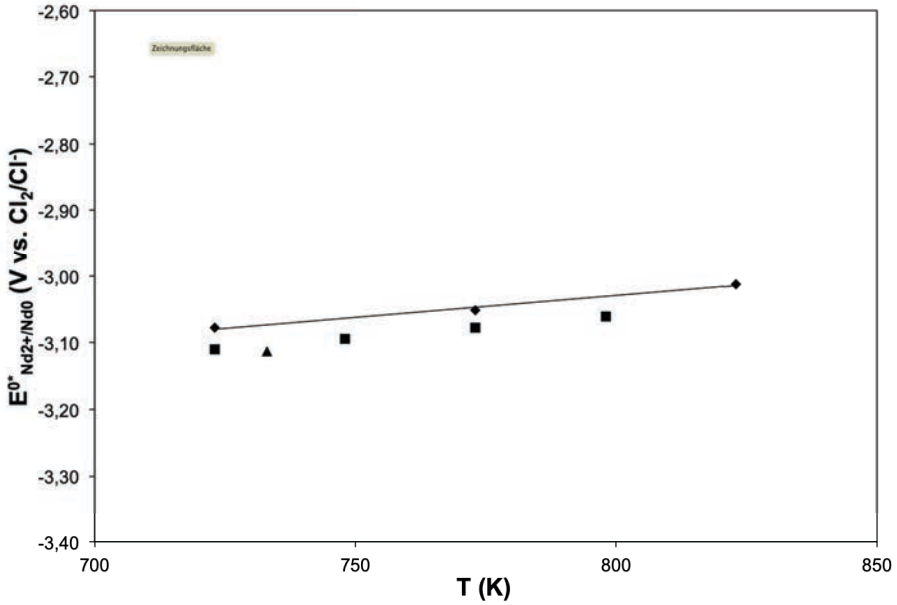

Fig. 46: Evolution of the apparent standard potential $E^{0*}_{Nd^{2+}/Nd^0}$ depending of the absolut temperature. (◆): this study; (■)[90] ;(▲)[78]

The apparent standard potential of the system Nd^{3+}/Nd^0 can be calculated from the values of the apparent standard potentials $E^{0*}_{Nd^{2+}/Nd^0}$ and $E^{0*}_{Nd^{2+}/Nd^0}$ by using Eq. (29).

$$E^{0*}_{Nd^{3+}/Nd^0} = \frac{E^{0*}_{Nd^{3+}/Nd^{2+}} + 2 * E^{0*}_{Nd^{2+}/Nd^0}}{3} \quad (29)$$

The values of the apparent standard potential $E^{0*}_{Nd^{3+}/Nd^0}$ are summarised in Tab. 11.

T (K)	$E^{0*}_{Nd3+/Nd0}$ (V vs Cl_2/Cl^-)
723	-3.068(*) / -3,0927[90]
733	-3.0997[78]
748	-3.0790[90]
773	-3.040(*) / -3.065[90]
798	-3.0503[90]
823	-3.001(*)

Tab. 11: Apparent standard potential $E^{0*}_{Nd^{3+}/Nd^0}$

The values of the standard potential, which have been measured in this study are close to the values that can been found in the literature. [78,90] The difference between the potential values at a fixed temperature is less than 1 %. This variation can be due to systematic errors, which occurs during the preparation and the accomplishment of the experiments and the analysis of the results.

II.1.1.2. Determination of the diffusion coefficient

Determination of the diffusion coefficient $D_{Nd^{3+}/Nd^{2+}}$

From the cyclic voltammogram the diffusion coefficient $D_{Nd^{3+}/Nd^{2+}}$ from the soluble-soluble transition is described by the Randles-Sevcik equation, Eq. (30):

$$\frac{I_{p,Ac}}{\nu^{1/2}} = -0.446 * (zF)^{3/2} * (RT)^{-1/2} * A * C_{Nd^{3+}} \sqrt{D_{Nd^{3+}}} \quad (30)$$

Fig. 47 shows the linear relationship between the cathodic peak current and the square root of the potential scan rate.

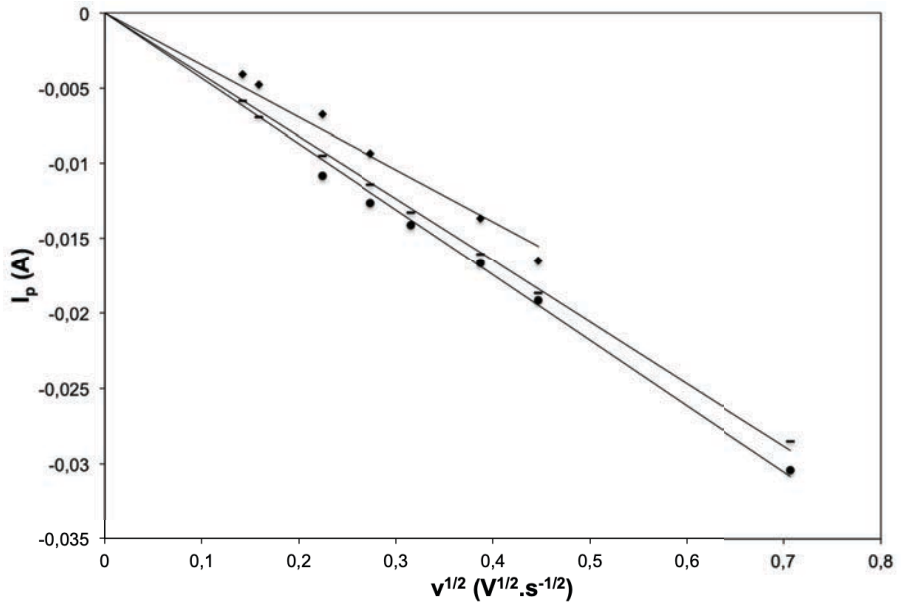

Fig. 47: Dependence of the cathodic current of the peak A versus $\nu^{1/2}$ for different temperatures. Working electrode: tungsten, counter electrode: molybdenum, reference electrode: Ag/AgCl, (◆) 723 K, (-) 823 K, (●) 873 K

The slope of the presented curve (Fig. 47) enables us to estimate the diffusion coefficient using Eq. (31).

$$D_{Nd^{3+}} = \left[\frac{I_p}{\nu^{1/2}} * \frac{1}{-0.446 * (zF)^{3/2} * (RT)^{-1/2} * A * C_{Nd^{3+}}}\right]^2 \quad (31)$$

In the range of 723 to 873 K the diffusion coefficient values of $D_{Nd^{3+}/Nd^{2+}}$ are between 1.12x10^{-5} and 1.57x10^{-5} cm^2.s^{-1} (Tab. 12).

T (K)	$D_{Nd3+/Nd2+}$ ($cm^2.s^{-1}$) x 10^5
723	1.12
823	1.30
873	1.57

Tab. 12: Diffusion coefficient $D_{Nd^{3+}/Nd^{2+}}$ depending on the absolute temperature, which has been determined by cyclic voltammetry analysis

The linear relationship, which is shown on Fig. 48, proves that the variation of the diffusion coefficient depending on the absolute temperature is compatible to the Arrhenius law (Eq. (16)).

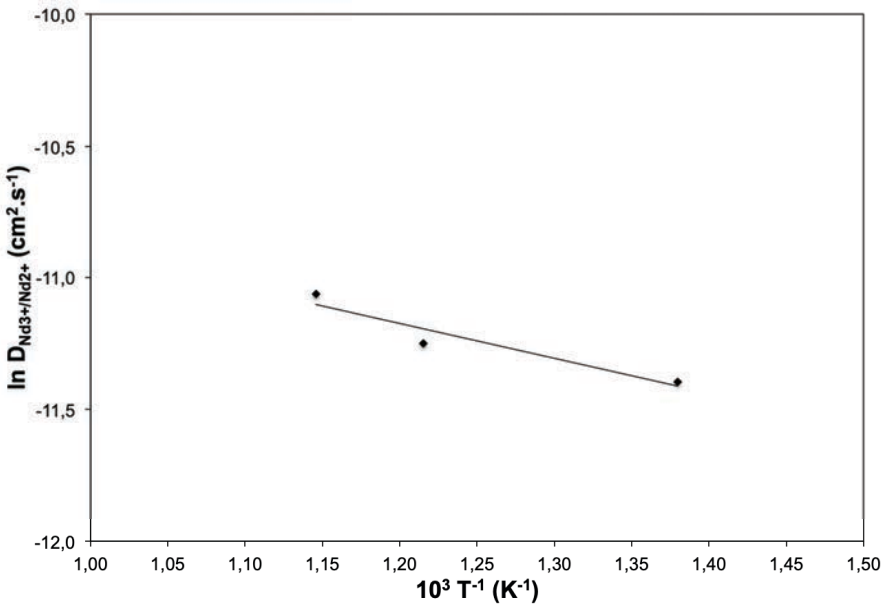

Fig. 48: Linear relationship between the logarithm of Nd^{3+} diffusion coefficient and the inverse of the absolute temperature

Determination of the diffusion coefficient D_{Nd^{2+}/Nd^0}

From the cyclic voltammogram the diffusion coefficient D_{Nd^{2+}/Nd^0} from the soluble-insoluble transition is described by the Berzins-Delahay equation, Eq. (32):

$$\frac{I_{p,B}}{\nu^{1/2}} = -0.61 * (zF)^{3/2} * (RT)^{-1/2} * A * C_{Nd^{2+}} \sqrt{D_{Nd^{2+}}} \quad (32)$$

Fig. 49 shows the linear relationship between the cathodic peak current of peak B and the square root of the potential scan rate.

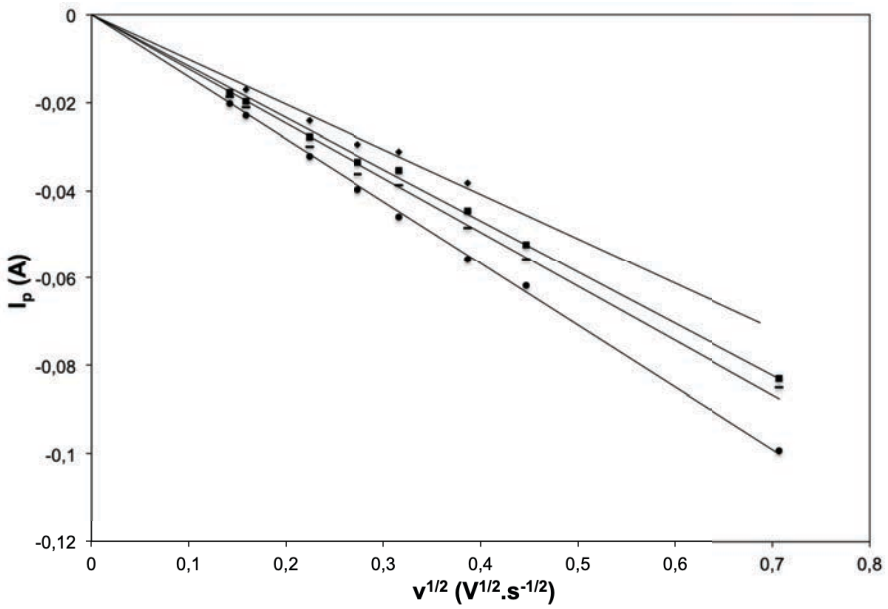

Fig. 49: Dependence of the cathodic current of the peak B versus $\nu^{1/2}$ for different temperatures. Working electrode: tungsten, counter electrode: molybdenum, reference electrode: Ag/AgCl; at (◆) 723 K, (■) 773 K, (-) 823 K, (●) 873 K

The influence of the temperature on the diffusion coefficient has been studied by the investigation of the cathodic current of the peak B. The number of electrons is assumed to correspond to a two-electron redox process.

The slope of the current versus the square root of the potential scan rate (Fig. 49) permits the calculation of the diffusion coefficient using Eq. (33). The values of the diffusion coefficient $D_{Nd^{2+}}$ are summarised in Tab. 13.

$$D_{Nd^{2+}} = \left[\frac{I_{p,B}}{\nu^{1/2}} * \frac{1}{-0.61 * (zF)^{3/2} * (RT)^{-1/2} * A * C_{Nd^{2+}}}\right]^2 \quad (33)$$

T (K)	$D_{Nd2+/Nd0}$ ($cm^2.s^{-1}$) x 10^5
723	0.48
773	0.67
823	0.78
873	1.07

Tab. 13: Diffusion coefficient D_{Nd^{2+}/Nd^0} depending on the absolute temperature, as determined by cyclic voltammetry analysis.

The linear relationship, which is shown on Fig. 50, proves that the variation of the diffusion coefficient depending on the absolute temperature is compatible to the Arrhenius law (Eq. (16)).

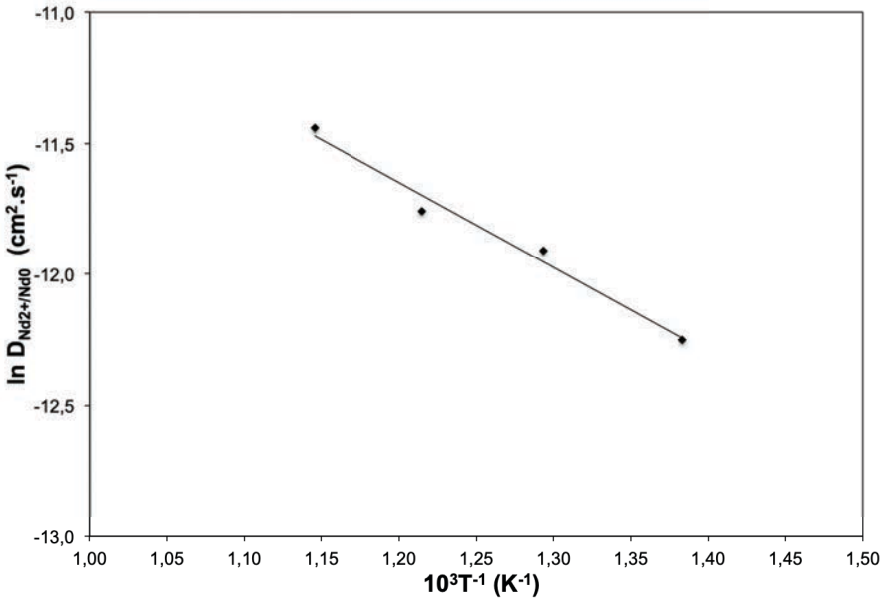

Fig. 50: Linear relationship between the logarithm of Nd^{2+} diffusion coefficient and the inverse of the absolute temperature

II.1.2. Study of the neodymium using the chronopotentiometry

The chronopotentiometry is the second technique to determine the apparent standard potential and the diffusion coefficient of the neodymium ions, which are presented in the electrolyte. Fig. 51 shows typical chronopotentiograms of an eutectic LiCl-KCl electrolyte containing 0.5 mol% of $NdCl_3$. The curve should exhibit two plateaus, but due to the narrow values of the reduction potential of Nd^{3+} and Nd^{2+} only one plateau can be identified on Fig. 51. For the analysis, the hypothesis of a single reduction step from Nd^{3+} to Nd^0 has been selected.

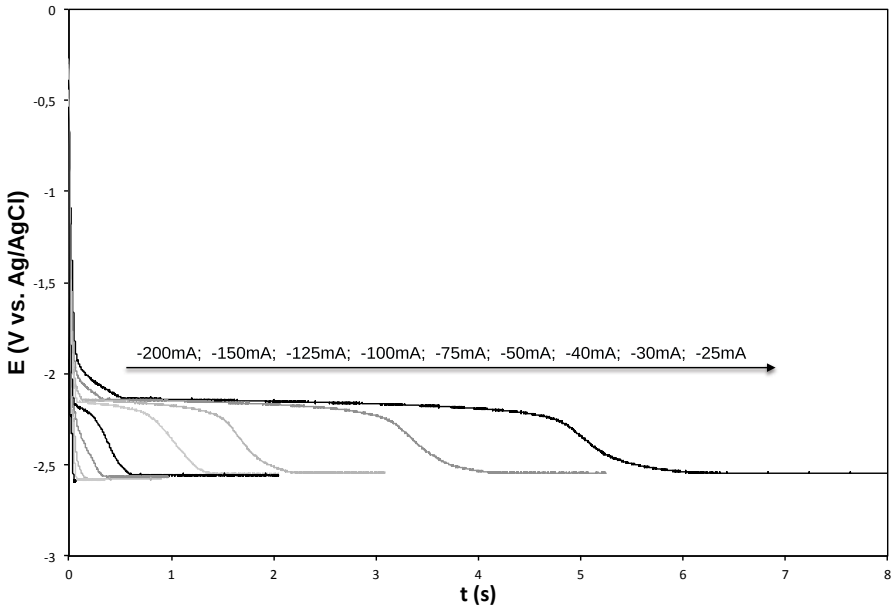

Fig. 51: Chronopotentiogram of the eutectic LiCl-KCl containing 0.5 mol% of $NdCl_3$ at 723 K. Working electrode: tungsten, counter electrode: molybdenum, reference electrode: Ag/AgCl.

II.1.2.1. Determination of the diffusion coefficients $D_{Nd^{3+}/Nd^{2+}}$ and $D_{Nd^{2+}/Nd^{0}}$

According to the previous cyclic voltammetry experiments, chronopotentiometry measurements show a double reduction step of the neodymium ions. Fig. 52 represents a chronopotentiogram of 0.5 mol% of $NdCl_3$ in the eutectic LiCl-KCl salt, where the two reduction steps can be observed. Two transition times τ_1 and τ_2 are identified and correspond to both reduction steps respectively of Nd^{3+} to Nd^{2+} and then of Nd^{2+} to Nd^0.

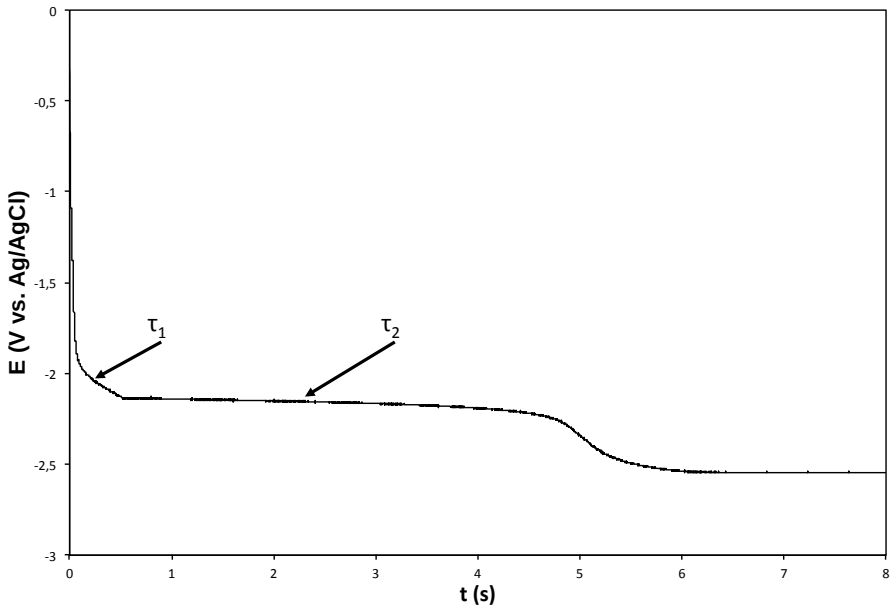

Fig. 52: Chronopotentiogram of 0.5 mol% of $NdCl_3$ in the eutectic LiCl-KCl electrolyte at 723 K, i: -25 mA ; Working electrode: tungsten, counter electrode: molybdenum, reference electrode: Ag/AgCl

According to the work of Berzins and Delahay[124], it is possible to determine the number of exchanged electrons during both reaction using the following Eq. (34):

$$\frac{\tau_2}{\tau_1} = 2\frac{z_2}{z_1} + \left(\frac{z_2}{z_1}\right)^2 \quad (34)$$

where

τ_1 and z_1 represent the transition time and the number of exchanged electrons for the Nd^{3+}/Nd^{2+} system.

τ_2 and z_2 represent the transition time and the number of exchanged electrons for the Nd^{2+}/Nd^{0} system.

The ratio $\frac{\tau_2}{\tau_1}$ is equal to 8, corresponding to a value of $\frac{z_2}{z_1}$ = 2. This result confirms that the reduction process of the Nd^{3+} ions in neodymium metal involves two steps: the first one engages only one electron whereas the second implies two electrons as described as follow:

$$Nd^{3+} + e^- \rightarrow Nd^{2+}$$
$$Nd^{2+} + 2e^- \rightarrow Nd^0$$

This conclusion has recently been confirmed by the work of Tang and co-corkers in which they also obtained a ratio $\frac{z_2}{z_1}$ equal to 2.[89]

The chronopotentiometry allows the determination of the diffusion coefficient of the different species, which is contained in the electrolyte. The Sand's relationship[125] (Eq. (35)) gives the relationship between the current density i and the transition time τ.[132]

$$i\tau^{1/2} = 0.5 * z * F * C_{Nd^{n+}} * A * \pi^{1/2} * D_{Nd^{n+}}^{1/2} \quad (35)$$

Fig. 53 and Fig. 54 represent the linear relationship between the applied current i and $\tau_1^{-1/2}$ in the temperature range between 723 and 873 K respectively for the Nd^{3+}/Nd^{2+} and Nd^{2+}/Nd^0 system. The linearity between the current density and the inverse of the transition time shows that the reduction process is reversible.

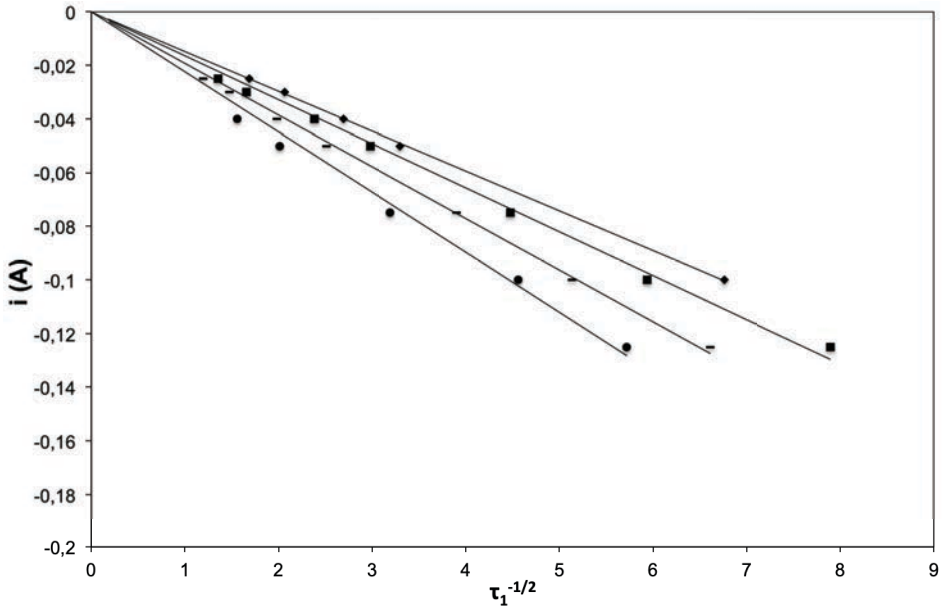

Fig. 53 : Dependence of the applied current versus $\tau_1^{-1/2}$ for different temperatures. Working electrode: tungsten, counter electrode: molybdenum, (◆) 723 K, (■) 773 K, (-) 823 K, (●) 873 K

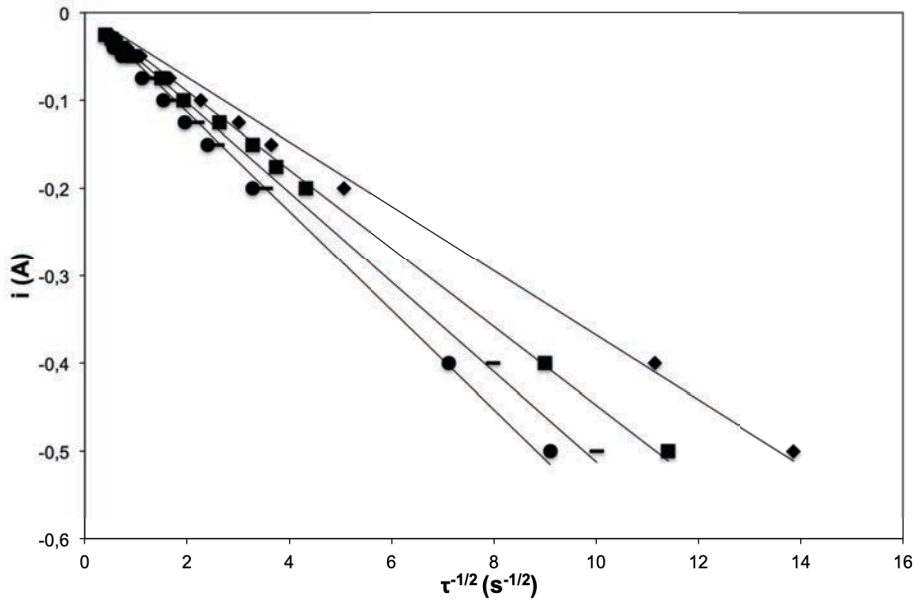

Fig. 54: Dependence of the applied current versus $\tau_2^{-1/2}$ for different temperatures. Working electrode: tungsten, counter electrode: molybdenum, (◆) 723 K, (■) 773 K, (-) 823 K, (●) 873 K

The slope of the curve corresponds to the value of the product $i\tau^{1/2}$. Using Eq. (35) and the slope of each curve, it is possible to determine the diffusion coefficients of Nd^{3+}/Nd^{2+} and Nd^{2+}/Nd^{0} systems at each temperature. The results are summarised in Tab. 14.

T (K)	$D_{Nd3+/Nd2+}$ ($cm^2.s^{-1}$) x 10^5	$D_{Nd2+/Nd0}$ ($cm^2.s^{-1}$) x 10^5
723	0.81	0.42
773	1.03	0.62
823	1.37	0.80
873	1.58	0.96

Tab. 14: Diffusion coefficients $D_{Nd^{3+}/Nd^{2+}}$ and $D_{Nd^{2+}/Nd^{0}}$ depending on the absolute temperature, as determined by chronopotentiometry analysis

The diffusion coefficents calculated through the analysis of the chronopotentiometric experiments are in accordance with the values previously determined by the analysis of the cyclic voltammogram.

The variations of the diffusion coefficients depending on the absolute temperature is represented on Fig. 55 and obeys to the Arrhenius' law.

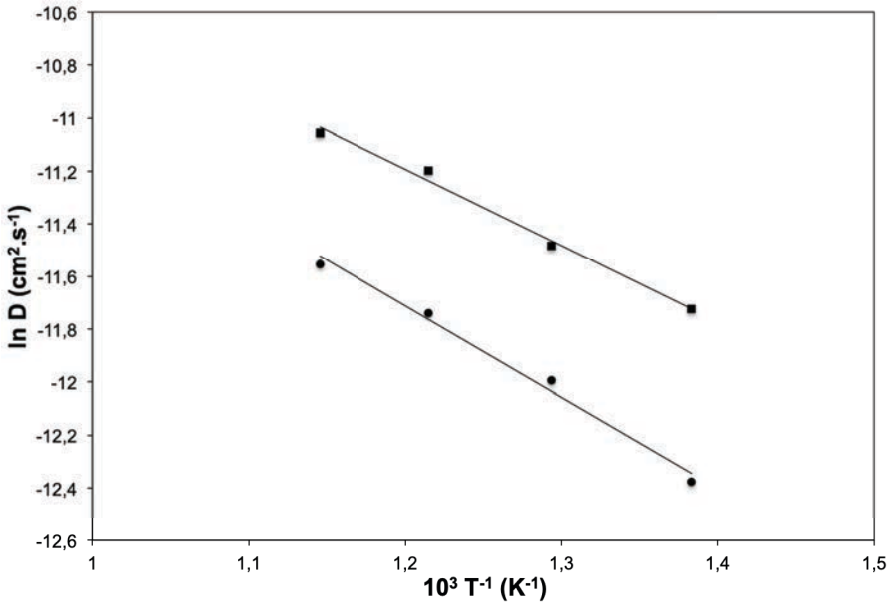

Fig. 55: Graphic representation of the logarithm of diffusion coefficients $D_{Nd^{3+}/Nd^{2+}}$ (■) and $D_{Nd^{2+}/Nd^{0}}$ (●) versus the inverse of the absolute temperature issue from the chronopotentiometry experiments

Tab. 15 summarises the values of the diffusion coefficients of neodymium ions. The values obtained during this study are in the same range as the values from the literature. We can see that the range of values is relatively broad. The accuracy of the various experiments and analysis methods is likely to explain this large scattering effect.

	$D_{Nd3+/Nd2+}$ ($cm^2.s^{-1}$) x 10^5			$D_{Nd2+/Nd0}$ ($cm^2.s^{-1}$) x 10^5		
T / K	**CV**	**CP**	**Literature**	**CV**	**CP**	**Literature**
723	1.12	0.81	1.1* / 0.28**	0.48	0.42	0.98**
733			0.95***			1.25***
748			0.45**			1.38**
773		1.03	0.54**/ 0.71****	0.67	0.62	1.69**/1.98****
798			0.76**			2.03**
823	1.30	1.37		0.78	0.80	
873	1.57	1.58		1.07	0.96	

Tab. 15: Comparison of the diffusion coefficients of this study and the literature, (*)[78]; (**)[90]; (***)[133]; (****)[134]

II.1.2.2. Determination of the apparent standard potential $E^{0*}_{Nd^{3+}/Nd^{0}}$

As described previously in section II.1.2.1. the analysis of the chronopotentiometric curves shows two reduction steps corresponding to the Nd^{3+}/Nd^{2+} and Nd^{2+}/Nd^{0} transitions.

The reduction potential is expressed as a function of the elapsed time t and the transition time τ, Eq. (36).[135]

$$E = E^{0}_{Nd^{p+}/Nd^{q+}} + \frac{RT}{zF}\ln\left(\frac{a_{Nd^{p+}}}{a_{Nd^{q+}}}\right) + \frac{RT}{zF}\ln\left(\frac{\tau^{1/2} - t^{1/2}}{\tau^{1/2}}\right) \quad (36)$$

Assuming that the activity of the pure neodymium metal is equal to one and using the combination of Eq. (25) and (36), the potential can be expressed as follow (Eq. (37)):

$$E = E^{0*}_{Nd^{p+}/Nd^{q+}} + \frac{RT}{zF}\ln(X_{Nd^{p+}}) + \frac{RT}{zF}\ln\left(\frac{\tau^{1/2} - t^{1/2}}{\tau^{1/2}}\right) \quad (37)$$

Representing of E versus $\ln\left(\frac{\tau^{1/2}-t^{1/2}}{\tau^{1/2}}\right)$ a straight line is obtained. The slope of this line allows to determine the number of exchanged electrons by using Eq. (38).

$$slope = \frac{RT}{zF} \quad (38)$$

The apparent standard potential can be calculated by the extrapolation of the straight line. The potential at the origin is expressed by Eq. (39).

$$E^{0*}_{Nd^{p+}/Nd^{q+}} + \frac{RT}{zF}\ln(X_{Nd^{p+}}) \quad (39)$$

Using Eq. (39) it is possible to determine the values of the apparent standard potential for the Nd^{3+}/Nd^{2+} and Nd^{2+}/Nd^{0} systems. Eq. (29) allows the calculation of the apparent standard potential $E^{0*}_{Nd^{3+}/Nd^{0}}$.

Tab. 16 summarises these values in the temperature range from 723 to 873 K.

T (K)	$E^{0*}_{Nd3+/Nd0}$ (V vs. Cl_2/Cl^-)
723	-3.091
773	-3.053
823	-3.009
873	-2.970

Tab. 16: Apparent standard potential $E^{0*}_{Nd^{3+}/Nd^{0}}$ determined by the analysis of the chronopotentiometry measurements

The values of this potential increase linearly with the increase of the temperature. The evolution of the apparent standard potential is described on Fig. 56. The values of $E^{0*}_{Nd^{3+}/Nd^{0}}$ fall along the line of equation:

$$E^{0*}_{Nd^{3+}/Nd^{0}} = -3.683 + (8.17 * 10^{-4}) * T \text{ in V vs. } Cl_2/Cl^- \quad (40)$$

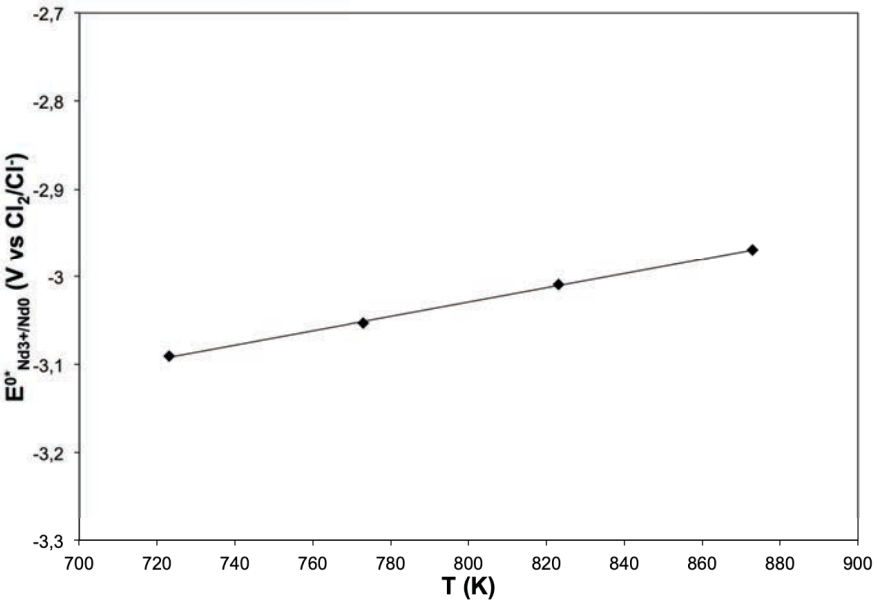

Fig. 56: Evolution of the apparent standard potential $E^{0*}_{Nd^{3+}/Nd^0}$ versus the absolute temperature issues from the chronoamperometry analysis

The evolution of the apparent standard potential is in accordance with the different studies already published in the literature where the evolution of the potential is represented by Eq. (41) to (43).[129,136,137]

$$E^{0*}_{Nd^{3+}/Nd^0} = -3.750 + (8.82 * 10^{-4}) * T \text{ in V vs. } Cl_2/Cl^- \quad (41)[136]$$

$$E^{0*}_{Nd^{3+}/Nd^0} = -3.554 + (6.40 * 10^{-4}) * T \text{ in V vs. } Cl_2/Cl^- \quad (42)[129]$$

$$E^{0*}_{Nd^{3+}/Nd^0} = -3.772 + (9.10 * 10^{-4}) * T \text{ in V vs. } Cl_2/Cl^- \quad (43)[137]$$

The previous results show that the values of the apparent standard potentials $\mathrm{E}^{0*}_{\mathrm{Nd^{3+}/Nd^0}}$ and the diffusion coefficients, determined from the analysis of the chronopotentiometric experiments, are similar to the values obtained by the experiments of cyclic voltammetry. These converging values seem to validate the analysis of the behaviour of neodymium ions in the eutectic LiCl-KCl.

All the electrochemical properties of the neodymium ions in the LiCl-KCl electrolyte are summarised in Tab. 17 and are in accordance with the literature.

T (K)		$E^{0*}_{Nd3+/Nd2+}$ (V vs. Cl_2/Cl^-)	$E^{0*}_{Nd2+/Nd0}$ (V vs. Cl_2/Cl^-)	$E^{0*}_{Nd3+/Nd0}$ (V vs. Cl_2/Cl^-)	$D_{Nd3+/Nd2+}$ ($cm^2.s^{-1}$) x 10^5	$D_{Nd2+/Nd0}$ ($cm^2.s^{-1}$) x 10^5
723	CV	-3.050 (*) -3.058[90]	-3.078 (*) -3.11[90]	-3.068 (*) -3.0927[90]	1.12 (*)	0.48 (*)
	CP			-3.091 (*)	0.81 (*)	0.42 (*)
	Mean			-3.080 (*)		0.45 (*)
773	CV	-3.016 (*) / -3.039[90]	-3.052 (*) -3.078[90]	-3.040 (*) -3.065[90]		0.67 (*)
	CP			-3.053 (*)	1.03 (*)	0.62 (*)
	Mean			-3.047 (*)		0.65 (*)
823	CV	-2.981 (*)	-3.011 (*)	-3.001 (*)	1.30 (*)	0,78 (*)
	CP			-3.009 (*)	1.37 (*)	0.80 (*)
	Mean			-3.005 (*)		0.79 (*)
873	CV				1.57 (*)	1.07 (*)
	CP			-2.970 (*)	1.58 (*)	0.96 (*)
	Mean				1.58 (*)	1.02 (*)

Tab. 17: Summary of the electrochemical properties of neodymium in the eutectic LiCl-KCl electrolyte, (*) : this study

II.1.3. Thermodynamic determination

The standard Gibbs energy of formation of $NdCl_3$ at an infinite dilution $\Delta G^{\infty}_{NdCl_3}$ can be calculated with the following Eq. (44).

$$\Delta G^{\infty}_{NdCl_3} = 3 * F * E^{0*}_{Nd^{3+}/Nd^0} \quad (44)$$

The difference between the Gibbs energy of formation at infinite dilution $\Delta G^{\infty}_{NdCl_p}$ and the Gibbs energy of formation at the supercooled state $\Delta G^{0}_{NdCl_{p,sc}}$ taken as the reference state, allows to calculate the activity coefficient of $NdCl_p$ using Eq. (45):

$$\Delta G^{\infty}_{NdCl_3} - \Delta G^{0}_{NdCl_{3,sc}} = RTln(\gamma_{NdCl_3}) \quad (45)$$

The Gibbs energy of formation at the supercooled state of $NdCl_3$ was calculated from the thermodynamic crystal data of MCl_x, the enthalpy of fusion data and the heat capacity of the liquid phase. This Gibbs energy is given by the Eq. (46) [138]:

$$\Delta G^{o}_{NdCl_{3,sc}} = -985.21 + 0{,}1867 * T \quad (46)$$

T (K)	$\Delta G^{\infty}_{NdCl_3}$ (kJ.mol^{-1})	$\Delta G^{o}_{NdCl_{3,sc}}$ (kJ.mol^{-1})	$Log(\gamma_{NdCl_3})$	$\gamma_{NdCl_3} x\ 10^3$
723	-891.42	-850.23	-2.976	1.056
773	-881.84	-840.89	-2.767	1.709
823	-869.84	-831.56	-2.430	3.716
873	-859.59	-822.22	-2.236	5.804

Tab. 18: Determination of the Gibbs energy of formation at an infinite dilution $\Delta G^{\infty}_{NdCl_3}$, the Gibbs energy of formation at the supercooled state $\Delta G^{0}_{NdCl_{p,sc}}$ and the activity coefficient γ_{NdCl_3} depending on the absolute temperature.

Tab. 18 presents the values of the apparent standard potential used to determine the Gibbs energy of formation at infinite dilution by using Eq. (46) and the Gibbs energy of formation at the supercooled state.

From Eq. (45), it is possible to obtain Eq. (47), which allows the determination of the activity coefficients $NdCl_3$ in the eutectic LiCl-KCl.

$$\gamma_{NdCl_3} = exp\left(\frac{\Delta G^{\infty}_{NdCl_3} - \Delta G^{0}_{NdCl_{3,sc}}}{RT}\right) \quad (47)$$

The values of the logarithm of the activity coefficients, which are summarised in Tab. 18, are in accordance with the literature.[129]

II.2. Electrochemical behaviour of neodymium ions in the eutectic LiF-CaF_2 electrolyte

The behaviour of neodymium in fluoride-based electrolytes has already been studied for its extraction from nuclear fuel.[97,107,139]

Compared to the chloride-based salts, the fluoride-based salts have a higher melting point. A comparison of different fluoride salts has already been done by Hamel and co-workers.[97] It was proved that the LiF-NaF and LiF-KF salts, which have a lower melting point, are not suitable for the electrochemical study of neodymium properties. These salts undergo a reduction of their cations, respectively Na^+ and K^+, before the reduction of the Nd^{3+} ions. Therefore the neodymium reduction step is inhibited. That's why it is not possible to determine its properties.[97]

There are two other salts having a reduction potential of their cations above the reduction potential of Nd^{3+}. These salts are LiF and LiF-CaF_2. The binary salt has two advantages in comparison to LiF, i.e. a lower melting point and a broader electrochemical window.

This is the reason why the eutectic LiF-CaF_2 has been selected for our study.

II.2.1. Study of the neodymium properties using the cyclic voltammetry

The cyclic voltammetry experiments have been carried out in the LiF-CaF_2 electrolyte in a temperature range between 1073 K and 1148 K. The binary salt has a melting point of 1040 K.

In fluoride-based electrolytes the neodymium is present in the electrolyte in the NdF_6^{3-} complex form.[99] This complex is formed by the addition of NdF_3 in a fluoride-based electrolyte according to the the reaction :

$$NdF_3 + 3F^- \rightarrow [NdF_6]^{3-}$$

Fig. 57 shows a typical cyclic voltammogram of the eutectic LiF-CaF_2 electrolyte containing 0.5 mol% of NdF_3. During the cathodic scan two reduction peaks are observed. The peak A represents the reduction of Nd^{3+} ions whereas peak B represents the reduction of the Li^+ ions. Moreover, there are two peaks A' and B' which are observed and which correspond respectively to the oxidation of lithium and neodymium.

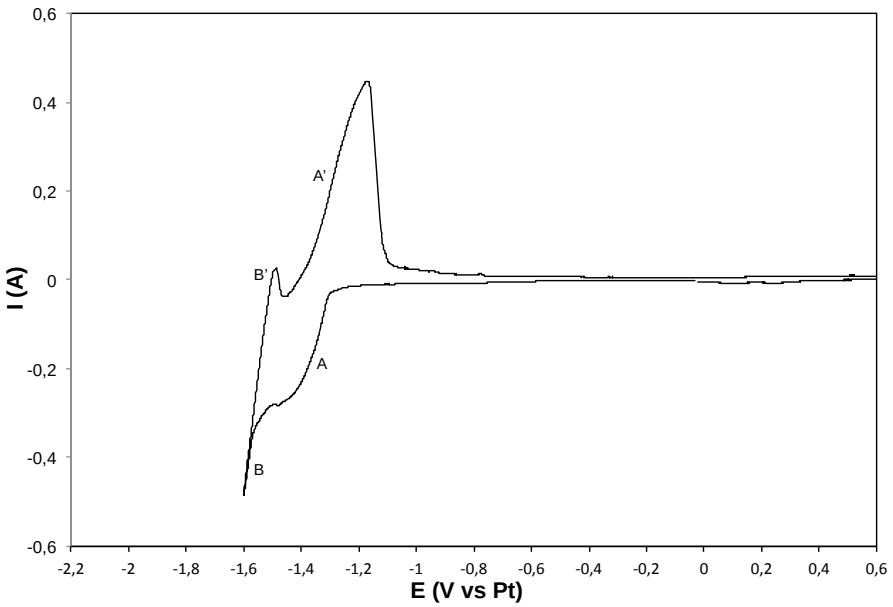

Fig. 57: Typical cyclic voltammogram of the eutectic LiF-CaF_2 electrolyte containing 0.5 mol% NdF_3 at 1148 K, scan rate 100 mV.s^{-1}. Working electrode: tantalum, counter electrode: glassy carbon, reference electrode: platinum

The single reduction and oxidation peak, which correspond to neodymium, shows that the Nd^{3+} ions are reduced to neodymium metal in one step following the mechanism described by the equation :

$$\boldsymbol{Nd^{3+} + 3e^- \leftrightarrow Nd^0}$$

The small « bump », which is observed at around -0.8 V versus Pt is attributed to the presence of impurities, which can correspond to a small amount of oxygen, probably due to

a rest of humidity in the salt. The presence of this impurity has no influence on the reduction process of neodymium.

II.2.2. Definition of a reference system for the study of the neodymium behaviour in the eutectic LiF-CaF_2 electrolyte

The reference electrode (described in chapter II) was a platinum wire, which is a quasi-reference electrode ($Pt/PtO_x/O^{2-}$). The potential of the quasi reference electrode depends on the concentration of O^{2-} ions in the electrolyte. Before starting the experiment, the salt was preliminary dried to remove the humidity in the electrolyte due to the hygroscopic character of each of them. During the whole experiment, the atmosphere in the reaction chamber was controlled by an argon flow to reduce the risk of the presence of O^{2-} ions. Unfortunately, conditions of the experiments cannot be totally controlled. A residual concentration of oxide in the electrolyte may influence the potential of the platinum electrode.

This possible shift of potential leads to an inaccurate determination of the equilibrium potential of the Nd^{3+}/Nd^0 system. In order to avoid this drawback, the equilibrium potential was determined by the comparison to the reduction potential of the electrolyte. In our case it is the reduction of the lithium ions, which is described with the following reaction:

$$Li^+ + e^- \rightarrow Li^0$$

The values of the reduction potential of lithium ions have been calculated by using the Fact Sage FSALT Database. For molten salts the liquid state of the compounds is considered as reference condition in most of cases. The determination of the reduction potential of the Li^+/Li couple takes pure $LiF_{liq.}$ as reference and its activity is calculated in the molten LiF-$CaF_{2eut.}$ for the experiment temperature range from 1073 until 1148 K. The reduction potentials of the lithium ions are summarised in Tab. 19.

T (K)	E_{Li^+/Li^0} (V vs. F_2/F^-)
1073	-5.329
1098	-5.315
1123	-5.302
1148	-5.288

Tab. 19: Calculated reduction potential of E_{Li^+/Li^0} versus F_2/F^- using the database FSALT

Fig. 58 describes the evolution of the reduction potential of the couple Li^+/Li^0. The potential increases linearly with the increase of the temperature and follows Eq. (48).

$$E_{Li^+/Li^0} = -5{,}922 + (5{,}52 * 10^{-4}) * T \quad (48)$$

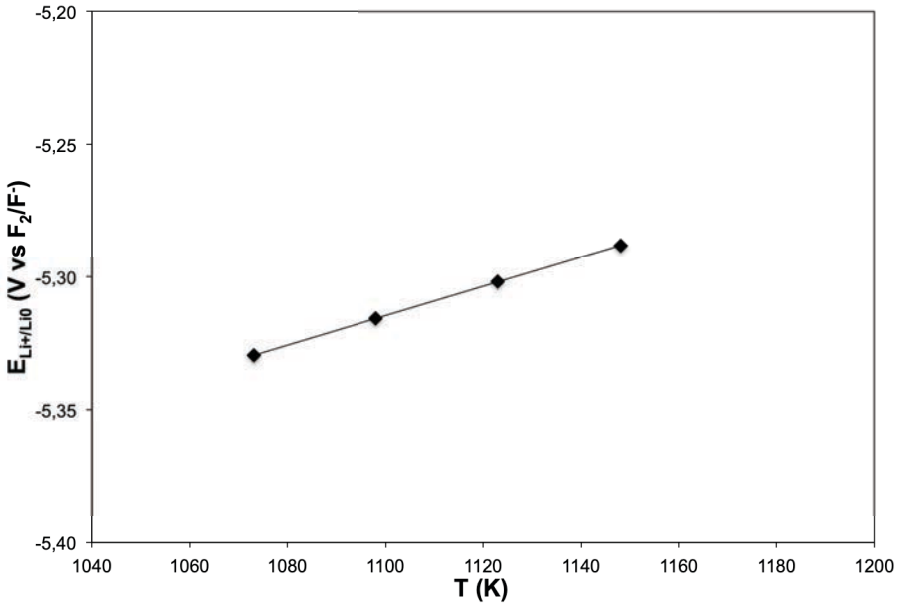

Fig. 58: Evolution of the reduction potential of the couple Li^+/Li^0 versus F_2/F^- depending on the absolute temperature

The difference between the reduction potentials of the lithium and the neodymium ions was denoted as ΔE and determined for each temperature as described on Fig. 59.

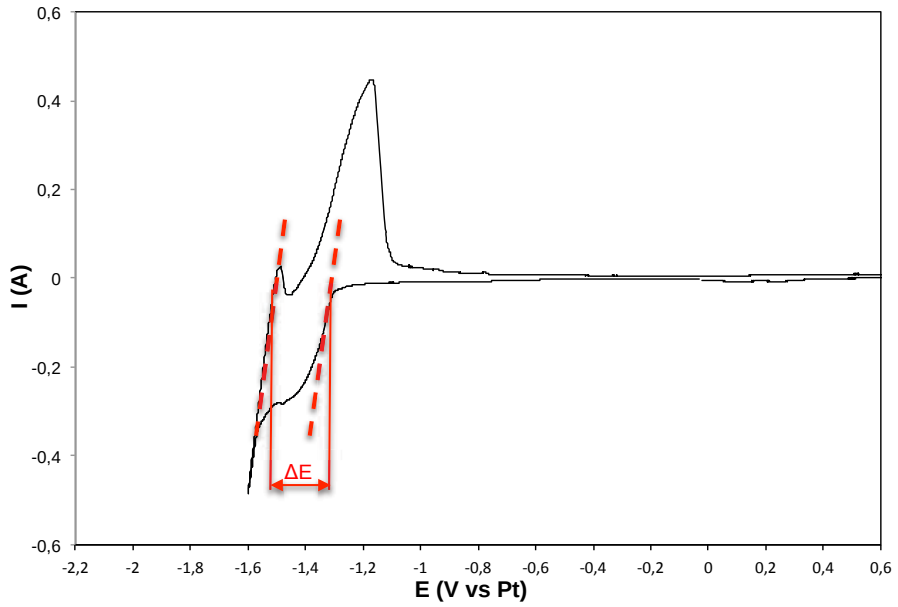

Fig. 59: Determination of ΔE on a cyclic voltammogram of the eutectic LiF-CaF_2 electrolyte containing 0.5 mol% NdF_3 at 1148 K, scan rate 100 $mV.s^{-1}$. Working electrode: tantalum, counter electrode: glassy carbon, reference electrode: platinum

II.2.3. Determination of the apparent standard potential from the cyclic voltammetry

Based on the new reference (F_2/F^- system) and by using the method previously described to determine ΔE corresponding to the potential value separating the reduction wave of

neodymium and of lithium, the reduction potential of the Nd^{3+}/Nd^0 system versus F_2/F^- can be calculated by Eq. (49) and (50).

$$E_{Nd^{3+}/Nd^0} = E_{Li^+/Li^0} + \Delta E \tag{49}$$

$$E_{Nd^{3+}/Nd^0} = E^0_{Nd^{3+}/Nd^0} + \frac{RT}{zF}\ln(a_{Nd^{3+}}) \tag{50}$$

Eq. (50) can be also expressed as Eq. (51) depending on the concentration $C_{Nd^{3+}}$ of the neodymium ions in the electrolyte and the activity coefficient of the same species $\gamma_{Nd^{3+}}$.

$$E_{Nd^{3+}/Nd^0} = E^0_{Nd^{3+}/Nd^0} + \frac{RT}{zF}\ln(C_{Nd^{3+}}) + \frac{RT}{zF}\ln(\gamma_{Nd^{3+}}) \tag{51}$$

The activity and the activity coefficient of the Nd^{3+} ions in the electrolyte are unknown. For this reason, the apparent standard potential $E^{0*}_{Nd^{3+}/Nd^0}$ was calculated by using Eq. (52).

$$E^{0*}_{Nd^{3+}/Nd^0} = E_{Nd^{3+}/Nd^0} - \frac{RT}{zF}\ln(C_{Nd^{3+}}) \tag{52}$$

The calculated values of the apparent standard potential of the Nd^{3+}/Nd^0 system are presented in Tab. 20.

T (K)	$E^{0*}_{Nd^{3+}/Nd^0}$ (V vs F_2/F^-)
1073	-4.907
1098	-4.890
1123	-4.875
1148	-4.853

Tab. 20: Apparent standard potential of the Nd^{3+}/Nd^0 system depending on the absolute temperature

The evolution of $E^{0*}_{Nd^{3+}/Nd^0}$ depending on the temperature is plotted in Fig. 60, which shows that the apparent standard potential increases with the increase of the temperature following Eq. (53).

$$E^{0*}_{Nd^{3+}/Nd^0} = -5.661 + (7.03 * 10^{-4})T \tag{53}$$

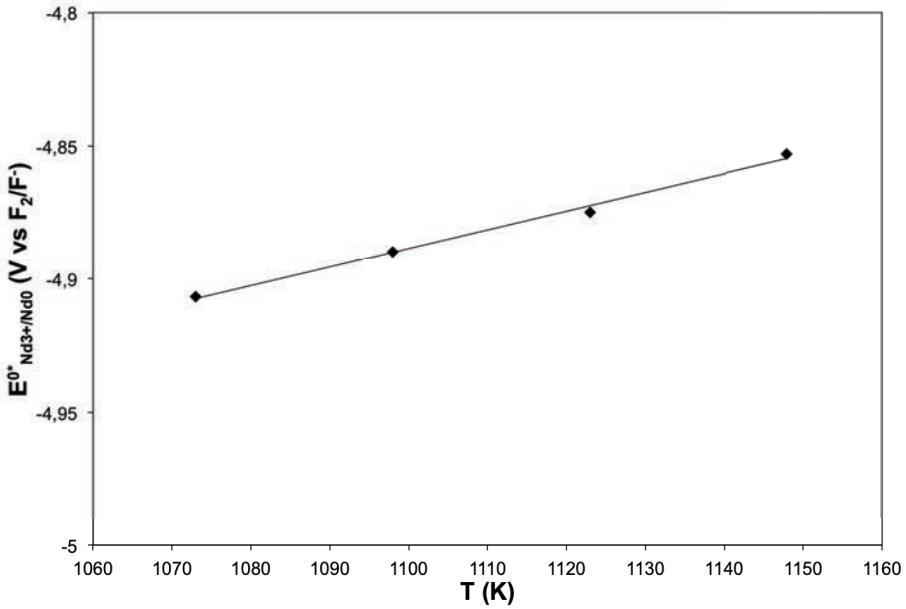

Fig. 60: Evolution of the apparent standard potential of the Nd^{3+}/Nd^{0} system versus F_2/F^- depending on the absolute temperature

II.2.4. Determination of the diffusion coefficient $D_{Nd^{3+}/Nd^{0}}$

The absolute values of the intensity of the cathodic and anodic peak are in the same range for each scan rate. The intensity of the cathodic peak increases with the increase of the scan rate velocity (Fig. 61). The quasi reversible system obeys the Randles-Sevcik's relationship for a soluble-insoluble transition (Eq. (17)).

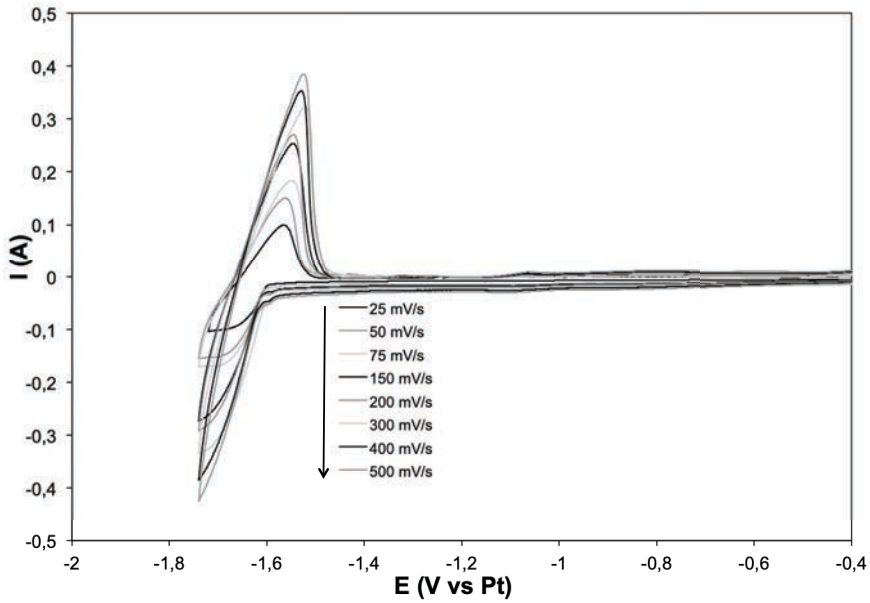

Fig. 61: Cyclic voltammogram of the eutectic LiF-CaF_2 electrolyte containing 0.5 mol% NdF_3 at 1073 K, scan rate : from 25 mV to 500 mV. Working electrode: tantalum, counter electrode: glassy carbon, reference electrode: platinum

The cyclic voltammograms, which are represented on Fig. 61, show a single reduction step related to the reduction of Nd^{3+} into Nd^0, which corresponds to a three-electrons redox process.

Fig. 62 shows the linear relationship between the cathodic peak current, which corresponds to the Nd^{3+}/Nd^0 system, and the square root of the potential scan rate. The slope of the current versus the square root of the potential scan rate enables the estimation of the calculation of the diffusion coefficient using Eq. (33). The values of the calculated diffusion coefficients are summarised in Tab. 21.

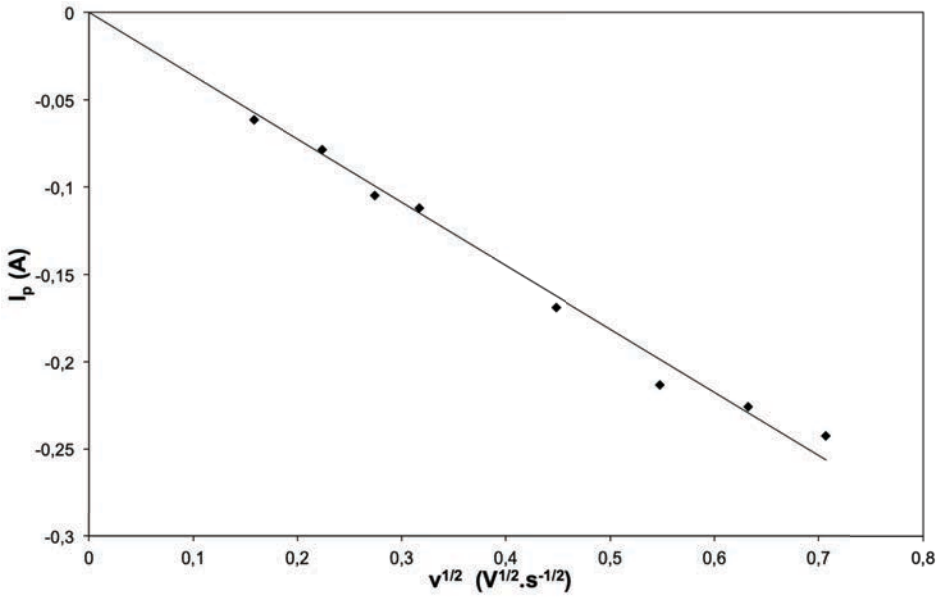

Fig. 62: Dependence of the cathodic current of the Nd^{3+} reduction step versus $\nu^{1/2}$ at 1073 K. Working electrode: tantalum, counter electrode: glassy carbon, reference electrode: platinum

T (K)	$D_{Nd3+/Nd0}$ ($cm^2.s^{-1}$) x 10^5
1073	1.42
1083	1.3[97]
1098	2.03
1123	2.22
1173	3.02

Tab. 21: Diffusion coefficient D_{Nd^{3+}/Nd^0} depending on the absolute temperature

The diffusion coefficient increases with the augmentation of the temperature and the evolution obeys the Arrhenius' law (Fig. 63).

The determined values of the diffusion coefficient of Nd^{3+} in the eutectic LiF-CaF_2 is in the same range than the values found in the literature.[97]

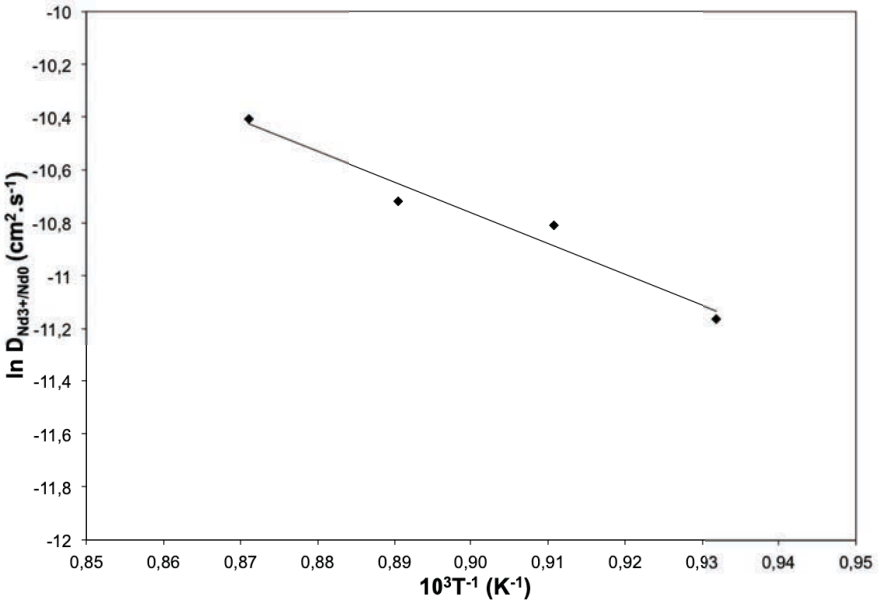

Fig. 63: Linear relationship between the logarithm of Nd^{3+} diffusion coefficient and the inverse of the absolute temperature

II.2.5. Determination of the thermodynamic properties of neodymium

Using the apparent standard potential, the determination of the standard Gibbs energy of formation at infinite dilution can be expressed with Eq. (54).

$$\Delta_f G^{\infty}_{NdF_3} = z * F * E^{0*}_{Nd^{3+}/Nd^0} \quad ((54)$$

The Gibbs energy of formation of NdF_3 at infinite dilution can also be expressed as a function of the standard enthalpy and standard entropy of formation by Eq. (55).

$$\Delta_f G^{\infty}_{NdF_3} = \Delta_f H^0 - \Delta_f S^0 * T \quad (55)$$

The Gibbs energy of formation of NdF_3 $\Delta_f G^0_{NdF_{3,sc}}$ in the supercooled state was determined

$$\Delta_f G^0_{NdF_{3,sc}} = -1602.73 + 0{,}193 * \mathrm{T} \quad (56)$$

For each temperature, the activity coefficients γ_{NdF_3} were determined by using Eq. (57).

$$\gamma_{NdF_3} = e^{\frac{\Delta_f G^{\infty}_{NdF_3} - \Delta_f G^0_{NdF_3}}{RT}} \quad (57)$$

The values of the Gibbs energy of formation at infinite dilution, the Gibbs energy of formation in the supercooled stated and the activity coefficient of NdF_3 in the eutectic LiF-CaF_2 electrolyte in the temperature range of 1073 to 1148 K are presented in Tab. 22.

T (K)	$E^{0*}_{Nd^{3+}/Nd^0}$ (V vs F_2/F^-)	$\Delta_f G^{\infty}_{NdF_3}$ (kJ.mol^{-1})	$\Delta_f G^{0}_{NdF_3}$ (kJ.mol^{-1})	$log(\gamma_{NdF_3})$	$\gamma_{NdF_3}\ x\ 10^2$
1073	-4.9067	-1420.47	-1396.07	-1.188	6.49
1098	-4.8897	-1415.38	-1391.26	-1.148	7.12
1123	-4.8749	-1410.3	-1386.44	-1.110	7.77
1148	-4.853	-1405.21	-1381.63	-1.073	8.45

Tab. 22: Summary of the apparent standard potential calculated by using the CVs abd CPs, Gibbs energy of formation at an infinite dilution $\Delta G^{\infty}_{NdF_3}$, the Gibbs energy of formation at the supercooled state $\Delta G^{0}_{NdF_{3,sc}}$ and the activity coefficient γ_{NdF_3} depending on the absolute temperature

The values of the activity coefficient give information about the complexation of Nd^{3+} in the electrolyte. By comparing the acitivity coefficients in the LiCl-KCl and LiF-CaF_2, we can notify that in the fluoride-based electrolyte the Nd^{3+} ions are less complexed than in the LiCl-KCl.

II.3. Electrochemical behaviour of neodymium ions in the LiCl-KCl-LiF electrolyte

The two previous sections explained the reduction mechanisms of the neodymium ions in the eutectic LiCl-KCl and LiF-CaF_2 electrolytes.

In the LiCl-KCl electrolyte, the analysis shows that the reduction process takes place in two steps:

$$Nd^{3+} + e^- \rightarrow Nd^{2+}$$
$$Nd^{2+} + 2e^- \rightarrow Nd^0$$

In the LiF-CaF_2, the reduction process is achieved in only one single step, the Nd^{3+} ions are directly reduced to neodymium metal.

$$Nd^{3+} + 3e^- \rightarrow Nd^0$$

The presence of fluoride ions in the electrolyte can influence the reduction process of the neodymium ions. In order to confirm or deny this hypothesis, the ternary mixture LiCl-KCl-LiF has been selected as electrolyte. Using the quaternary phase diagram LiCl-KCl-LiF-KF as described in section I.2.2. of chapter II, the eutectic composition of the LiCl-KCl-LiF has been determined to be:

- 58 mol% of LiCl
- 38 mol% of KCl
- 4 mol% of LiF.

Knowing the melting temperature of this ternary salt, which reaches 618 K, the behaviour of neodymium ions has been studied in the range of temperature of 773 to 873 K.

II.3.1. Determination of the electrochemical behaviour of neodymium by the analysis of the cyclic voltammetric measurements

Fig. 64 shows the cyclic voltammogram of 0.5 mol% of $NdCl_3$, which is mixed to the ternary LiCl-KCl-LiF electrolyte. During the cathodic run, two reduction peaks can be observed at around -2.15 V and -2.27 V. The peak A and B correspond respectively to the reduction of Nd^{3+} and Nd^{2+}. The corresponding peak B' can be observed at around -2.15 V during the anodic scan, whereas the oxidation peak A' cannot be identified. Either this peak is hidden below the peak B' or the intensity of the signal is too low to be observed.

For the same parameters (concentration of $NdCl_3$, scan rate and temperature) the signal observed in the LiCl-KCl-LiF electrolyte has a lower intensity than in the LiCl-KCl electrolyte.

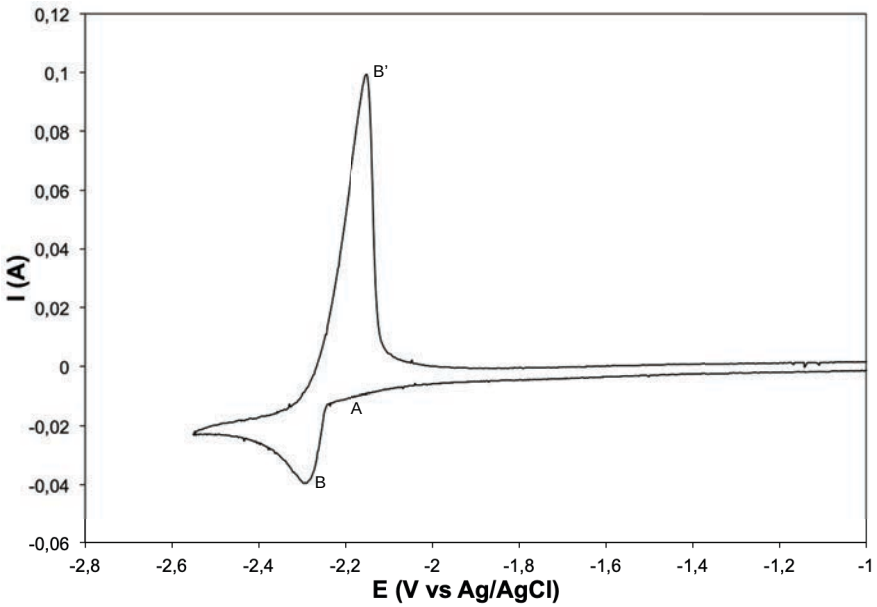

Fig. 64: Cyclic voltammograms of 0.5 mol % of $NdCl_3$ in LiCl-KCl-LiF salt mixture on a molybdenum electrode at 776 K, scan rate: 100 $mV.s^{-1}$

Fig. 65 shows the evolution of the cathodic and anodic peak potentials of the Nd^{2+}/Nd^0 system with the increase of scan rate. This system is considered as a quasi-reversible system due to the shift of the cathodic peak potential towards a more negative potential, whereas the anodic peak potential is shifted towards a more positive potential with the increase of the scan rate.

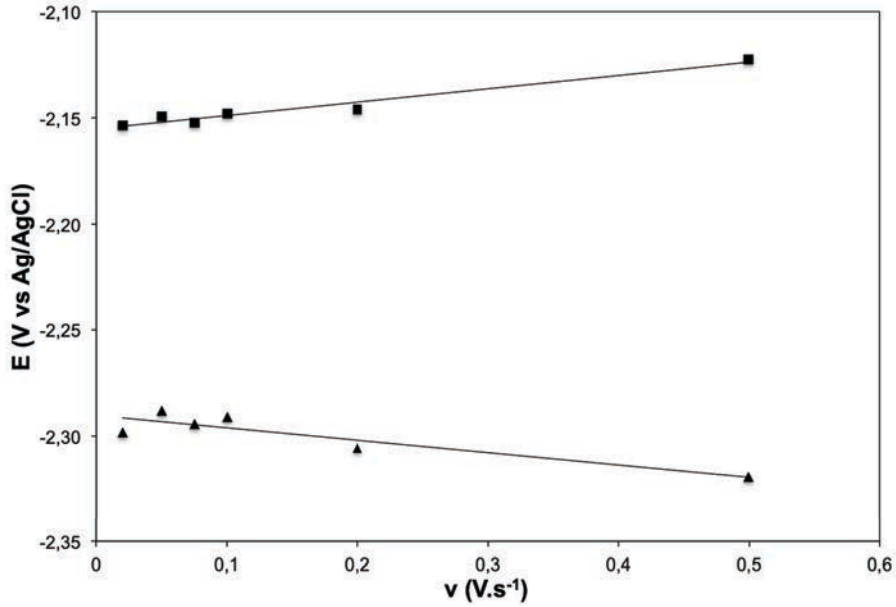

Fig. 65: Evolution of the cathodic and anodic peak potential corresponding to the Nd^{2+}/Nd^{0} redox system with the scan rate at 776 K

II.3.1.1. Determination of the apparent standard potential

Due to the too low intensity of the peaks A and A' the determination of the apparent standard potential $E^{0*}_{Nd(III)/Nd(II)}$ cannot be achieved by the analysis of the cyclic voltammograms.

The process to determine the apparent standard potential $\mathrm{E}^{0*}_{\mathrm{Nd^{2+}/Nd^{0}}}$ is similar to the process used for the eutectic LiCl-KCl electrolyte. The apparent standard potential is calculated from the value of the reduction peak potential $E_{p,B}$ using Eq. (24).

The values of the apparent standard potential have been calculated at 776, 823 and 872 K and are presented in Tab. 23.

T (K)	$E^{0*}_{Nd2+/Nd0}$ (V vs. Cl_2/Cl^-)
776	-3.212
823	-3.150
872	-3.105

Tab. 23: Apparent standard potential $E^{0*}_{Nd^{2+}/Nd^{0}}$

If the temperature increases the apparent standard potential increases linearly as well (Fig. 66) according to equation (Eq. (58)):

$$E^{0*}_{Nd^{2+}/Nd^{0}} = -4.041 + (1.08 * 10^{-3}) * T \text{ in V vs. } Cl_2/Cl^- \quad (58)$$

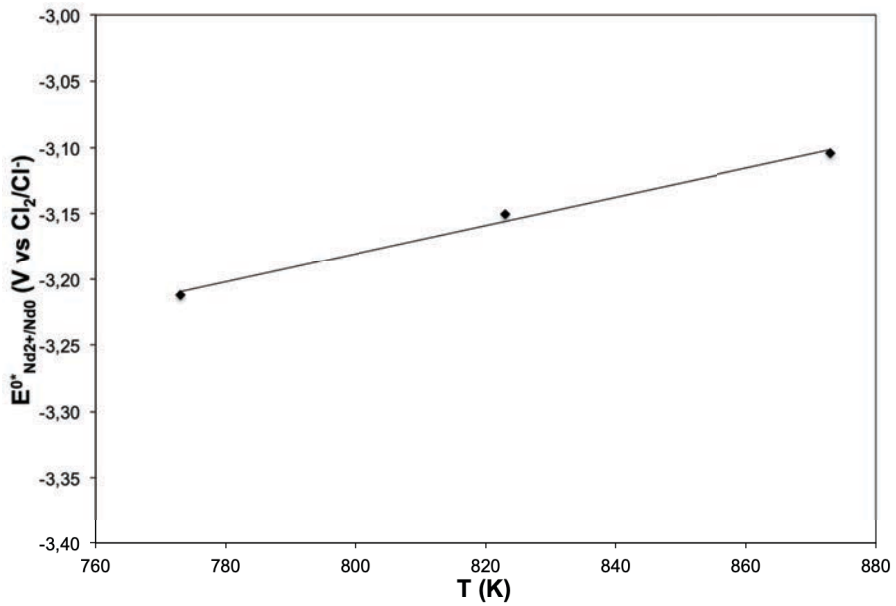

Fig. 66: Evolution of the apparent standard potential $E^{0*}_{Nd^{2+}/Nd^0}$ depending on the absolute temperature

II.3.1.2. Determination of the diffusion coefficient D_{Nd^{2+}/Nd^0}

As previously described, the analysis of the soluble-soluble transition is not accessible. For this reason, the diffusion coefficient has been only determined for the soluble-insoluble system.

As explained during the analysis of the behaviour of neodymium in the eutectic LiCl-KCl, the diffusion coefficient D_{Nd^{2+}/Nd^0} is calculated using the Berzins-Delahay's relationship for a soluble-insoluble transition (Eq. (32)).

Fig. 67 represents the evolution of the cathodic peak current versus the square root of the scan rate. The slope of the straight line increases with the increase of the temperature and allows the estimation of the diffusion coefficient of the Nd^{2+}/Nd^0 system using Eq. (33).

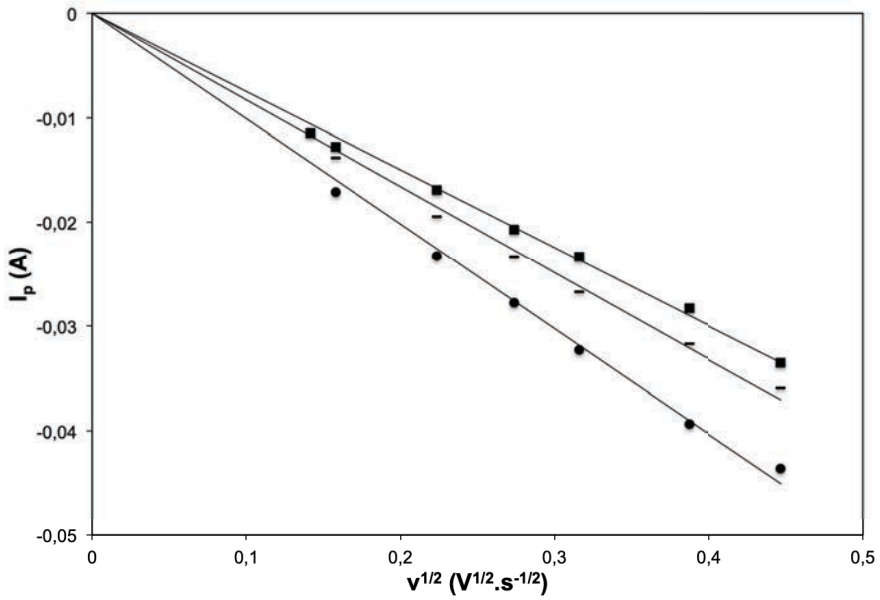

Fig. 67: Dependence of the cathodic current versus $\nu^{1/2}$ at different temperatures. Working electrode: tungsten, counter electrode: molybdenum, (■) 776 K, (-) 823 K, (●) 872 K

In the range of 773 to 872 K the diffusion coefficient D_{Nd^{2+}/Nd^0} is between 2.60*10^{-6} and 5.16*10^{-6} cm^2.s^{-1}. Each values of the diffusion coefficient are summarised in Tab. 24.

T (K)	$D_{Nd2+/Nd0}$ ($cm^2.s^{-1}$) x 10^5
776	0.26
823	0.33
872	0.52

Tab. 24: Diffusion coefficient D_{Nd^{2+}/Nd^0} depending on the absolute temperature which is determined by the analysis of cyclic voltammetry experiments.

The variation of the diffusion coefficient depends on the absolute temperature and obeys to the Arrhenius law (Fig. 68).

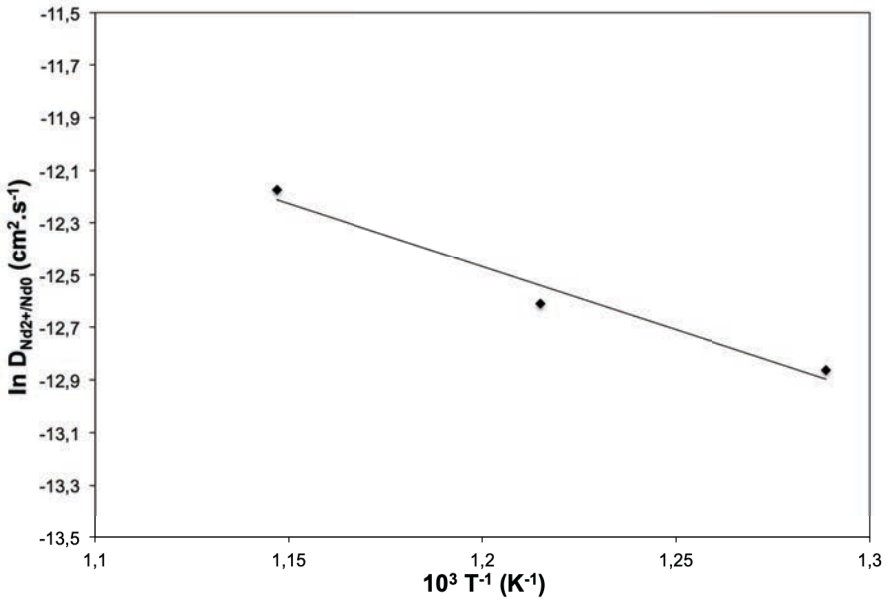

Fig. 68: Linear relationship between the logarithm of Nd^{2+} diffusion coefficient and the inverse of the absolute temperature issue from the cyclic voltammetry experiments

In comparison to the eutectic LiCl-KCl electrolyte the apparent standard potentials for the reduction of Nd^{3+} into Nd^0 are going towards more negative potentials. Concerning the diffusion coefficient, D_{Nd^{2+}/Nd^0} is lower in the eutectic LiC-KCl-LiF electrolyte than in the eutectic LiCl-KCl. This result can influence the efficiency of the extraction process during the electrolysis.

II.3.2. Determination of the electrochemical behaviour of neodymium by the analysis of the chronopotentiometric measurements

Fig. 69 shows a typical chronopotentiogram of the LiCl-KCl-LiF electrolyte containing 0.5 mol% of $NdCl_3$ at 776 K. The transition time τ increases with the decrease of the applied current. The analysis of the chronopotentiogram allows the determination of the diffusion coefficient and the apparent standard potential of the neodymium ions, which are contained in the electrolyte.

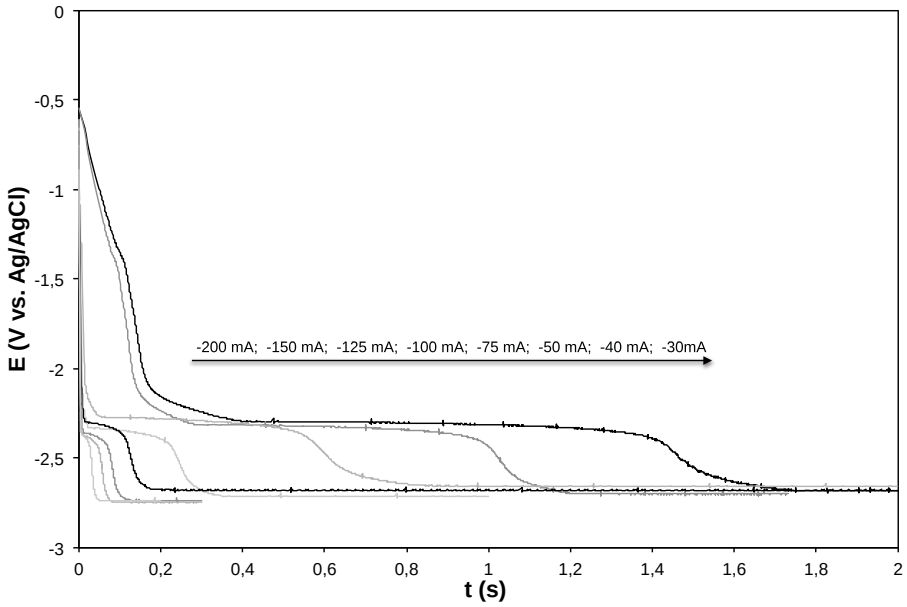

Fig. 69: Typical chronopotentiogram of the LiCl-KCl-LiF electrolyte containing 0.5 mol% of $NdCl_3$ at 778 K

II.3.2.1. Determination of the diffusion coefficients

The chronopotentiometry allows also the determination of the diffusion coefficient and the standard potential of the species contained in the LiCl-KCl-LiF electrotyte. The Sand's equation (Eq. (35)) gives the relationship between the current density i and the transition time τ and allows the determination of the value of the diffusion coefficient.

Determination of the diffusion coefficient $D_{Nd^{3+}/Nd^{2+}}$

Fig. 70 shows the evolution of the transition time $\tau_1^{-1/2}$, which depends on the applied current in a temperature range of 776 to 873 K. The linearity shown in Fig. 70, confirms the reversible property of the soluble-soluble transition.

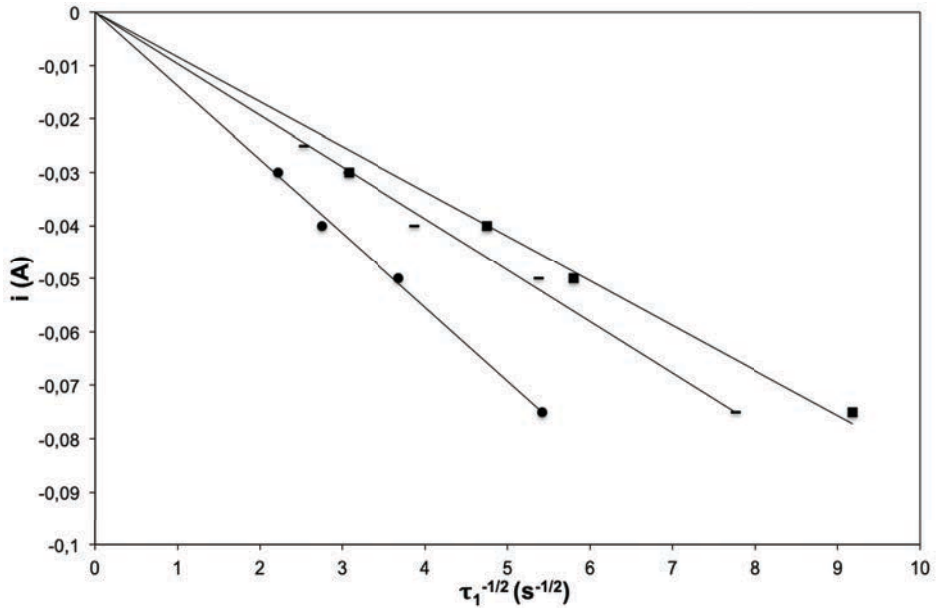

Fig. 70: Dependence of the applied current versus $\tau_1^{-1/2}$ for different temperatures. Working electrode: tungsten, counter electrode: molybdenum, (■) 776 K, (-) 823 K, (●) 872 K

Using the slope of the line represented in Fig. 70, which corresponds to factor $\boldsymbol{i\tau^{1/2}}$, and the Eq. (35), the diffusion coefficient of the Nd^{3+}/Nd^{2+} system is calculated. These values are summarised in Tab. 25.

T / K	$D_{Nd3+/\ Nd2+}$ ($cm^2.s^{-1}$) x 10^5
776	0.14
823	0.24
872	0.48

Tab. 25: Diffusion coefficient $D_{Nd^{3+}/Nd^{2+}}$ depending on the absolute temperature determine by chronopotentiometry analysis

Determination of the diffusion coefficient D_{Nd^{2+}/Nd^0}

Fig. 71 demonstrates the linear relationship between the applied current i and $\tau_2^{-1/2}$ in the temperature range between 723 and 873 K. The linearity between the current density and the inverse of the transition time shows that the reduction process is reversible.

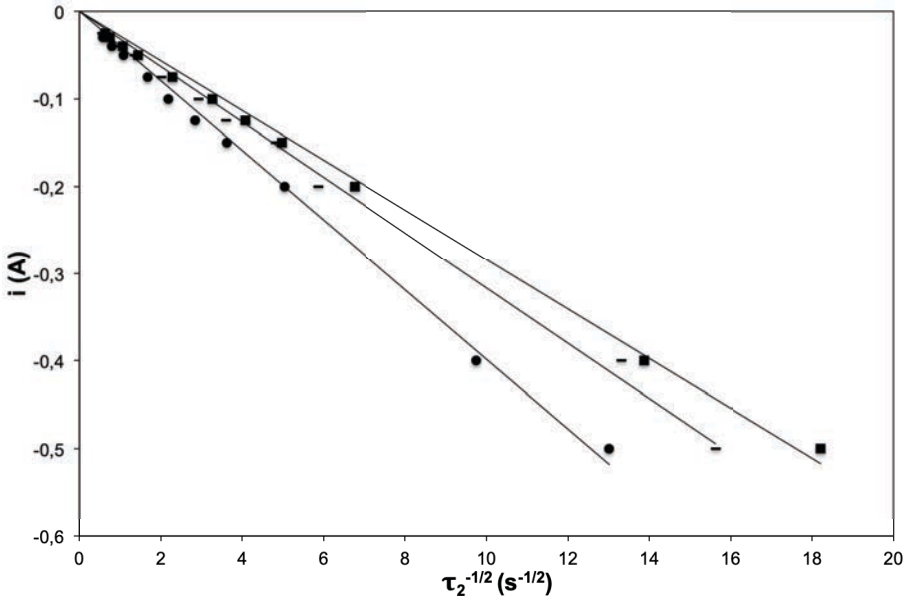

Fig. 71: Dependence of the applied current versus $\tau_2^{-1/2}$ for different temperatures. Working electrode: tungsten, counter electrode: molybdenum, (■) 776 K, (-) 823 K, (●) 872 K

The slope of each curve corresponds to the value of the product $i\tau^{1/2}$. By the correlation of this product and Eq. (35) it is possible to calculate the value of the diffusion coefficients of the system Nd^{3+}/Nd^0, which are summarised in Tab. 26.

T / K	$D_{Nd2+/Nd0}$ ($cm^2.s^{-1}$) x 10^5
776	0.24
823	0.32
872	0.49

Tab. 26: Diffusion coefficient D_{Nd^{2+}/Nd^0} depending on the absolute temperature, which is determined by chronopotentiometry analysis

The variation of the logarithm of the diffusion coefficient D_{Nd^{2+}/Nd^0} (Fig. 72) depends on the absolute temperature and obeys to the Arrhenius law.

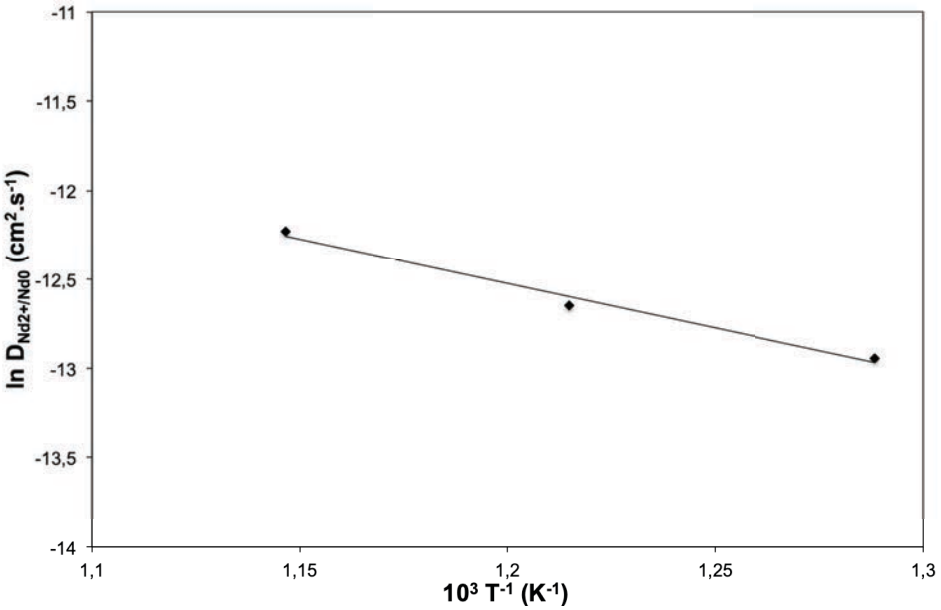

Fig. 72: Linear relationship between the logarithm of Nd^{2+} diffusion coefficient and the inverse of the absolute temperature issue from the chronopotentiometry experiments

The values of D_{Nd2+} confirm the results obtained by the analysis of the cyclic voltammetry.

II.3.2.2. Determination of the standard potential

By using the chronopotentiometry experiments the values of the standard potential of the Nd^{3+}/Nd^{2+} and Nd^{2+}/Nd^{0} systems can be determined. In the previous section we have estimated the transition time τ for each system. By using these values and the Eq. (36) it is possible to calculate each standard potential.

The activity of neodymium ions in the LiCl-KCl-LiF electrolyte is unknown, so the apparent standard potential has to be calculated with Eq. (39). The values of the apparent standard potential are presented in Tab. 27 and their evolution are displayed in Fig. 73.

T (K)	$E^{0*}_{Nd^{3+}/Nd^{2+}}(V\ vs.\ Cl_2/Cl^-)$	$E^{0*}_{Nd^{2+}/Nd^{0}}(V\ vs.\ Cl_2/Cl^-)$
773	-3.106	-3.233
823	-3.053	-3.186
873	-3.019	-3.113

Tab. 27: Apparent standard potential $E^{0*}_{Nd^{3+}/Nd^{2+}}$ and $E^{0*}_{Nd^{2+}/Nd^{0}}$ determined by chronopotentiometry analysis

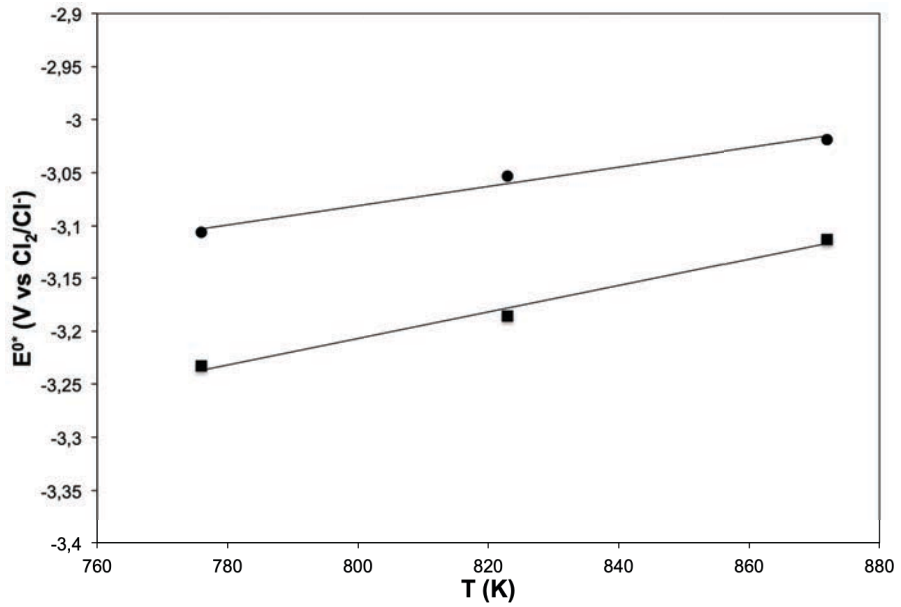

Fig. 73: Evolution of the apparent standard potentials (●) $E^{0*}_{Nd^{3+}/Nd^{2+}}$ and (■) and $E^{0*}_{Nd^{2+}/Nd^{0}}$ versus the absolute temperature issues from the chronoamperometry analysis

The apparent standard potential increases linearly with the increase of the temperature and follows Eq. (59) and (60).

$$E^{0*}_{Nd^{3+}/Nd^{2+}} = -3.810 + 9.11 * 10^{-4} \text{ in V vs. } Cl_2/Cl^- \quad (59)$$

$$E^{0*}_{Nd^{2+}/Nd^{0}} = -4.209 + 1.25 * 10^{-3} \text{ in V vs. } Cl_2/Cl^- \quad (60)$$

Tab. 28 summarises the values of the Gibbs energy of formation at the supercooled state, the activity coefficients of $NdCl_3$ in the eutectic LiCl-KCl-LiF and the apparent standard potential, which have been used to determine the Gibbs energy of formation at infinite dilution by using Eq. (44).

T (K)		$E^{0*}_{Nd^{3+}/Nd^{2+}}$ (V vs. Cl_2/Cl^-)	$E^{0*}_{Nd^{2+}/Nd^0}$ (V vs. Cl_2/Cl^-)	$E^{0*}_{Nd^{3+}/Nd^0}$ (V vs. Cl_2/Cl^-)	$\Delta G^{\infty}_{NdCl_3}$ (kJ.mol^{-1})	$\Delta G^{o}_{NdCl_{3,sc}}$ (kJ.mol^{-1})	10^5 x γ_{NdCl_3}
	CV		-3.212				
776	CP	-3.106	-3.233				
	Mean	-3.106	-3.223	-3.184	-921.53	-840.89	0.373
	CV		-3.150				
823	CP	-3.053	-3.186				
	Mean	3.053	-3.168	-3.130	-905.90	-831.56	1.912
	CV		-3.105				
872	CP	-3.019	-3.113				
	Mean	-3.019	-3.109	-3.079	-891.23	-822.220	7.343

Tab. 28: Scheme of the apparent standard potentials calculated by using the CVs abd CPs, the Gibbs energy of formation at an infinite dilution $\Delta G^{\infty}_{NdCl_3}$, the Gibbs energy of formation at the supercooled state $\Delta G^{0}_{NdCl_{3,sc}}$ and the activity coefficient γ_{NdCl_3} depending on the absolute temperature

The activity cofficients increase with the augmentation of the temperature, which means that the activity of neodymium in LiCl-KCl-LiF increases with the increase of the temperature too.

This conclusion is in accordance with the fact that the diffusion coefficient increases with the temperature.

II.4. Electrochemical behaviour of neodymium ions in the eutectic LiF-SrF_2 electrolyte

In the previous sections, it was demonstrated that in chloride-based electrolytes, the reduction process of the Nd^{3+} ions into Nd^0 is a two steps mechanism as described in the following reactions:

$$Nd^{3+} + e^- \rightarrow Nd^{2+}$$
$$Nd^{2+} + 2e^- \rightarrow Nd^0$$

Afterwards, the behaviour of neodymium ions in fluoride-based electrolyte has been studied in LiF-CaF_2. In this electrolyte, it was demonstrated that in comparison to the chloride-based electrolytes the reduction process takes place in a single step according to the following reaction :

$$Nd^{3+} + 3e^- \rightarrow Nd^0$$

Moreover the diffusion coefficients of neodymium seems to be higher in fluoride-based electrolytes than in chloride-based electrolytes.

This hypothesis should be confirm with the study of the neodymium behaviour in the eutectic LiF-SrF_2 electrolyte.

The eutectic mixture of the LiF-SrF_2 is composed of 81.5 mol% of LiF and 18.5 mol% of SrF_2 and has a melting point of 1044 K as described in section I.2.4 of chapter II.

II.4.1. Determination of the apparent standard potential from the cyclic voltammetry measurement

Fig. 74 shows a cyclic voltammogram of 1 mol% of NdF_3, which is mixed in the eutectic LiF-SrF_2. In Fig. 74 two peaks A and B are represented during the cathodic scan, which correspond respectively to the Nd^{3+}/Nd^0 and Li^{+}/Li^0 sytems. During the anodic scan, the reverse peaks A' and B' are observed, which correspond to the oxidation process of the before reduced compounds. Some bumps are observed between -0.8 and -1.2 V, which corresponding to impurities, like the presence of a small amount of oxid in the electrolyte.

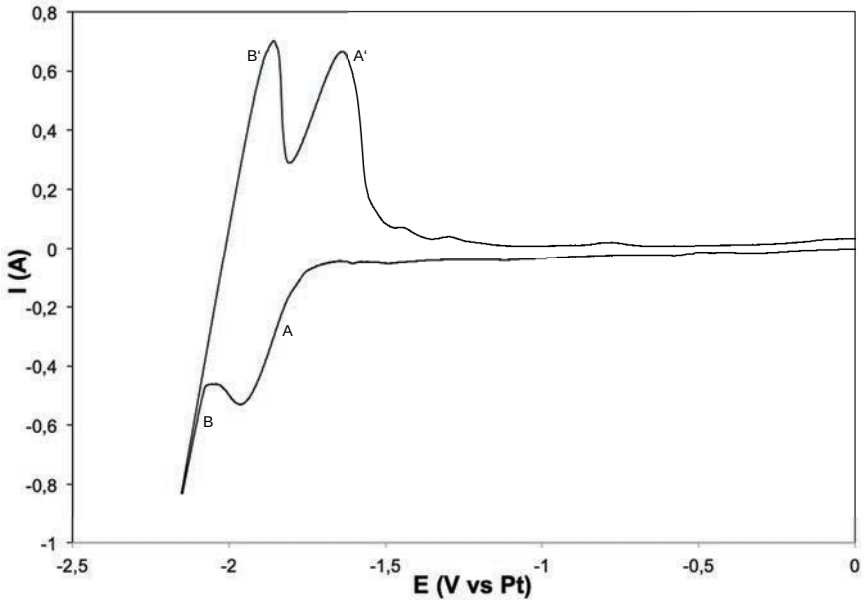

Fig. 74: Cyclic voltammogram of the eutectic LiF-SrF_2 electrolyte containing 1 mol% NdF_3 at 1098 K, scan rate 100 $mV.s^{-1}$. Working electrode: tantalum, counter electrode: glassy carbon, reference electrode: platinum

The reference electrode was a platinum wire, which is considered as a quasi electrode. For the description of the result, it was necessary to refer the measured potential to a fixed reference. In our case all potentials have to be refered versus the F_2/F^-. The calculation is described in section II.2.2 of this chapter.

By using Eq (49) and the value of ΔE which corresponds to the potential difference between the reduction step of the neodymium and the lithium ions, the redox potential of the Nd^{3+}/Nd^0 system versus F_2/F^- can be calculated.

After the determination of the redox potential E_{Nd^{3+}/Nd^0}, it is possible to calculate the values of the apparent standard potential $E^{0*}_{Nd^{3+}/Nd^0}$ with the Eq. (52).

The values of the apparent standard potential of the Nd^{3+}/Nd^0 system are summarised in Tab. 29.

T (K)	$E^{0*}_{Nd^{3+}/Nd^0}$ (V vs F_2/F^-)
1098	-4.900
1148	-4.861

Tab. 29: Apparent standard potential of the Nd^{3+}/Nd^0 system depending on the absolute temperature in the eutectic LiF-SrF_2 electrolyte

The evolution of the apparent standard potential increases with the increase of the temperature and follows the Eq. (61):

$$E^{0*}_{Nd^{3+}/Nd^0} = -5.752 + (7.76 * 10^{-4})T \quad (61)$$

The values of the apparent standard potential in the eutectic LiF-SrF_2 is in the same range that in the LiF-CaF_2 electrolyte. Moreover the evolution of the values of $E^{0*}_{Nd^{3+}/Nd^0}$ described with Eq. (61) is comparable to Eq. (53) corrresponding to the evolution of the potential in LiF-CaF_2.

II.4.2. Determination of the diffusion coefficient D_{Nd^{3+}/Nd^0}

The determination of the diffusion coefficient of the Nd^{3+} ions in the LiF-SrF_2 electrolyte follows the same procedure as described in section I.2.4. in this chapter. The values of the diffusion coefficients D_{Nd^{3+}/Nd^0} are summarised in Tab. 30.

T (K)	$D_{Nd3+/Nd0}$ ($cm^2.s^{-1}$) x 10^5
1098	4.74
1148	5.18

Tab. 30: Diffusion coefficient D_{Nd^{3+}/Nd^0} depending on the absolute temperature in the eutectic Lif-SrF_2 electrolyte

III. Conclusion of the chapter

In this chapter the electrochemical behaviour of neodymium has been analysed in four different electrolytes:

- LiCl-$KCl_{eut.}$
- LiF-CaF_{2eut}
- LiCl-KCl-$LiF_{eut.}$
- LiF-$SrF_{2eut.}$

It was demonstrated, that the neodymium ions in the LiCl-KCl- and LiCl-KCl-LiF are reduced to neodymium metal in a two-step process passing through the instable intermediate Nd^{2+}. However during the reduction process the Nd^{2+} ions disproportionate in Nd^0 and Nd^{3+} through the following reaction:

$$3Nd^{2+} \leftrightarrow 2Nd^{3+} + Nd^0$$

This disproportion reaction shows that the reduction of Nd^{3+} ions to neodymium metal can not be entirely completed. It will not be possible to achieve the extraction of neodymium from permanent magnet scraps in the eutectic LiCl-KCl and LiCl-KCl-LiF electrolyte.

However in the fluoride-based electrolytes like the eutectic LiF-CaF_2 and LiF-SrF_2 electrolytes the reduction process possesses only one step. The Nd^{3+} ions, which are contained in the electrolyte, are directly reduced to neodymium metal through the following reaction:

$$Nd^{3+} + 3e^- \rightarrow Nd^0$$

The eutectic LiCl-KCl-LiF electrolyte contains only 4 mol% of LiF. It can be possible that a higher amount of LiF in the LiCl-KCl-LiF electrolyte could avoid the drawback of the disproportion reaction, observed in chloride-based electrolytes and maybe allows a single reduction step like in fluoride-based electrolytes. This hypothesis has been not verified during this study.

The one step reduction process can allow the whole extraction of neodymium, which is contained in the Nd-based magnet. This hypothesis shows that the complete recovery of neodymium from permanent magnets can be achieved.
Moreover, it was demonstrated that the diffusion coefficients in fluoride-based electrolytes are higher than in chloride-based electrolytes.
The diffusion coefficient corresponds to the velocity of the neodymium ions in an electrolyte. A higher diffusion coefficient can accelerate the reduction process of Nd^{3+} ions.

The higher diffusion coefficients in fluoride-based eletrolytes compared to the chloride-based electrolytes show that for a-given period of time it is possible to reduce higher amounts of neodymium.
This evidence can be influenced by the size of the cations and anions, which are included in the electrolyte. This hypothesis will be discussed in the next chapter.

The next chapter will deal with the separation and the analysis of the electronic scraps, which have been collected in two recycling companies. This analysis will show the complexity of a separation process and the difficulty of the enrichment of the electronic scraps with neodymium compounds.

After the explanation of the separation processes, we will focus on the extraction of neodymium from permanent magnets based on the conclusion of this chapter.

Chapter V:
Experimental Part –
Extraction of neodymium on an inert electrode from Nd-based magnets

Table of contents

After the study of the electrochemical behaviour of neodymium in the previous chapter, this chapter deals with the extraction of neodymium from permanent magnets by an electrolysis process on an inert electrode.

Before starting the extraction process by electrolysis, samples which have been collected in two electronic scraps recycling companies were analysed. The first aim of these analyses is the determination of the amount of neodymium contained in the electronic scraps fraction. Moreover, the second aim is to confirm if an extraction by electrolysis is possible and realistic.

The first part of this chapter deals with the analysis of the electronic scraps samples, which were provided by two electronic scraps recycling companies.
The second part summarises the results of the neodymium recovery investigations by electrolysis in selected electrolytes and its corresponding process efficiency.

I. Analysis from electronic scraps

Simultaneously with the electrochemical study of the neodymium behaviour in molten salt for its extraction from the Nd-based magnets, which are contained in the electronic scraps, we studied various electronic scraps fractions provided by two electronic scraps recycling companies. These different fractions arose from distinct processing steps of the separation. They were assumed to be representative from real sourcing.

I.1. Analysis of the electronic scraps provided by the first recycling company

The resulting fractions were manually pre-sorted from a provided electronic scraps waste with a separation in three categories:

- a metallic fraction (Fig. 75 (a))
- a magnetic fraction (Fig. 75 (b))
- a RE-magnet fraction (Fig. 76)

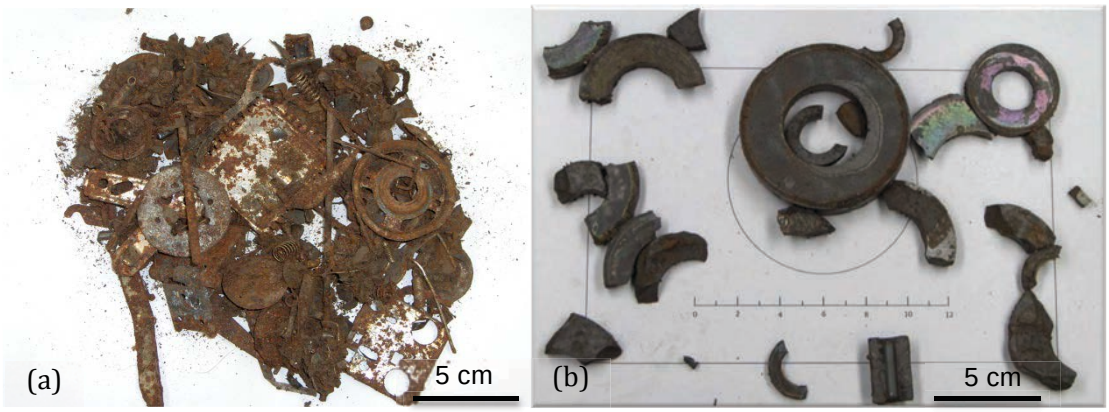

Fig. 75: Picture of the metallic fraction (a) and the magnetic fraction (b), which compose the electronic scraps fraction

After the manual separation process, the analysis of the magnet-containing fraction was carried out. Tab. 31 summarises the results of the magnet-fraction analysis.

	Mass (g)	(%)
Metallic fraction	2038.4	48.58
Magnetic fraction	2155.2	51.37
Nd-based Magnet	2.2	0.05

Tab. 31: Analysis of the electronic scraps waster

The analysis of the composition shows that Nd-based magnets represent a very small amount of the whole electronic scraps mass. That means that only 0.05 % of the total mass consists of Nd-based permanent magnets. This result shows that an effective enrichment of neodymium in the magnet fraction has to be developed prior to any further extraction by the electrolysis process. No industrial process for neodymium extraction could be economically acceptable using a so low initial neodymium amount. Each fraction was characterised by means of XRD and SEM / EDX.

Fig. 76 shows a picture of a permanent magnet, which has been extracted from the magnetic fraction.

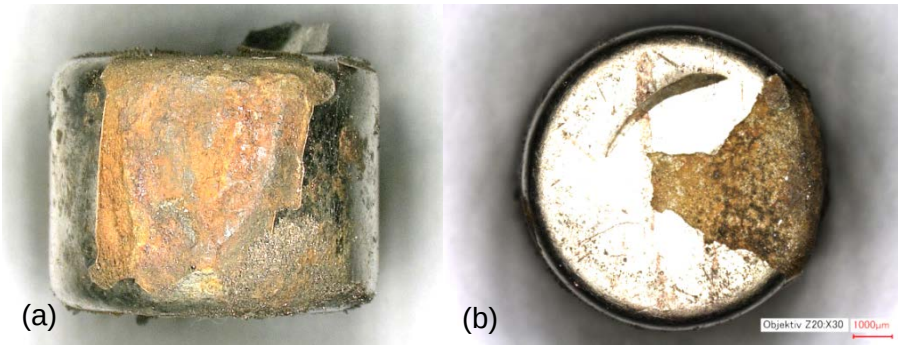

Fig. 76: Picture of RE-magnet, which was extracted from the magnetic fraction

The surface and the inside part of collected permanent magnets have been analysed, the results are summarised in Tab. 32.

	O	Al	Si	S	K	Ca	Fe	Ni	Cu	Mo	Sr	Nd	Sm	Dy	Er	Lu	Hg
RE-magnet inside	24.6	0.4	0.2				33.3	0.27	0.27	0.6		38	0.3	1.2	0.59		
RE-magnet surface	30.3		1,5	0.3	0.1	0.3	2.76	51.2	10.3		0.1	0.4			0.1	0.2	2.6

Tab. 32: EDX-analysis of the RE-magnet, which has been extracted from the magnet fraction (content in at%)

The surface of the permanent magnets is mostly composed of nickel and copper, which are used as a protection surface against corrosion. The inside part of the magnet is made of a mixture between iron and neodymium with some extra elements like samarium, dysprosium and europium. The presence of these lanthanides in the scraps can disturb the extraction of neodymium due to their narrow standard potential. Boron, which is also an essential component of the permanent magnets, cannot be detected during EDX-analysis.
The presence of dysprosium in the permanent magnets is related to the preparation process of these magnets, which leads to an increase of their strength.

I.2. Analysis of electronic scraps provided by the second recycling company

The second electronic scraps recycling company provided three different fractions, which were extracted from the whole recycling process.

- Magnetic waste fraction (1st fraction), which contains RE-based permanent magnets and ferrite permanent magnets as well as others iron based compounds (Fig. 77).
- Light fraction (2nd fraction), which contains non-ferrous metals and which is supposed to contain RE.
- Plastic fraction (3rd fraction), which is also supposed to contain RE.

Fig. 77: Picture of the magnetic waste fraction, which was analysed by EDX

The 1st fraction was analysed by the Energy Dispersive X-ray spectroscopy (EDX) method. The results are summarised in Tab. 33. Only the 1st fraction was analysed, because it was the fraction in which it was possible to find the highest amount of neodymium.

The elemental analysis of the magnetic fraction shows a really low amount of neodymium with an average of 0.1 %. The largest share is composed of iron and oxygen, which suggests that this fraction consists of components from ferrite magnets and others metals, which are attached to them.

	O	Mg	Al	Si	S	Cl	K	Ca	Ti	Mn	Fe	Ni	Cu	Zn	Sn	Nd	Tb	Dy	Pb
Average (%)	31.0	2.2	3.5	5.2	0.3	0.3	0.3	2.6	0.6	2.2	38.3	1.5	2.6	5.6	0.9	0.1	0.3	0.4	2.2
Max	32.3	2.6	5.2	7.1	0.3	0.3	0.4	3.2	0.8	2.7	42.2	2.2	3.4	6.7	1.0	0.2	0.6	0.7	2.8
Min	29.6	1.9	2.1	2.7	0.3	0.3	0.3	2.3	0.4	1.8	34.0	1.1	1.8	4.6	0.9	0	0	0.3	1.7

Tab. 33: EDX-Analysis of the 1st fraction (magnetic waste fraction)

A control analysis using a wet-chemical method at Fraunhofer UMSICHT Oberhausen yielded similar results.

The EDX-analysis was confirmed by an ICP-OES analysis of the 1st and the 3rd fraction. The ICP-OES analysis of the 1st fraction shows a mean amount of 1,700 ppm of neodymium per kilogram of electronic scraps. In comparison the 3rd fraction was also analysed and the concentration of neodymium represents only 200 ppm per kilogram of electronic scraps.

The 1st fraction was also analysed by XRD in order to determine the compounds and phases, presented in the sample (Fig. 78). The diffractogram contains mostly phases, which correspond to ferrite magnets and shows few peaks, which represent the expected $Nd_2Fe_{14}B$ composition.

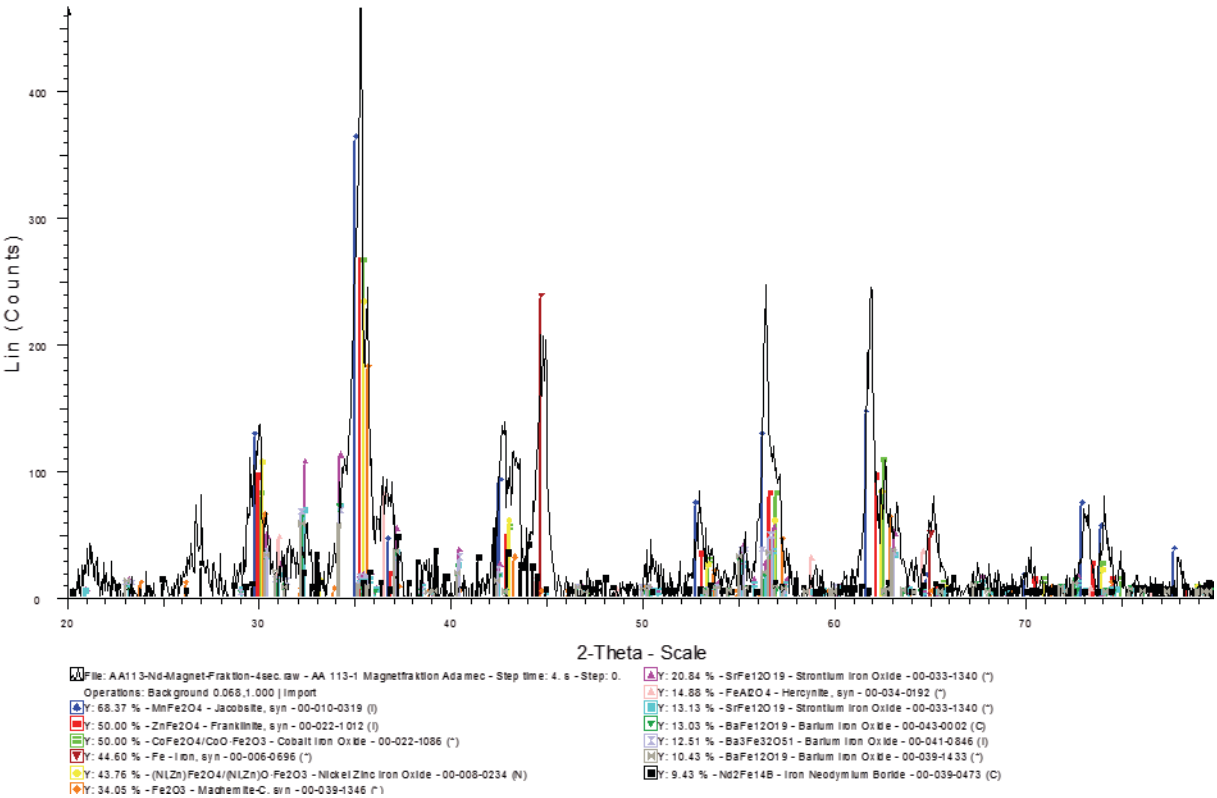

Fig. 78: XRD-analysis of the 1st fraction

The 1st fraction is the fraction, which should contain the highest amount of neodymium. After the previous mentioned analysis of this fraction, it was shown that they are only small amounts of neodymium. That's why we have decided that it is not necessary to analyse the 2nd and 3rd fractions.

I.3. Conclusions

The analyses of the magnetic fractions obtained from the two different electronic scraps recycling companies shows, that the recovery of RE compounds requires suitable sorting techniques. Therefore, a strategy still has to be developed, in order to increase the amount of neodymium in the magnetic fraction for an economical suitable extraction process.

Due to the complexity and variability of the magnetic fraction composition in scraps, it was decided to study the possibility to extract pure neodymium from clean permanent magnets.

II. Electrolysis process

The aim of this second part is to show if it is possible to extract neodymium from permanent magnets without extracting other compounds and modifying the concentration of neodymium in the electrolyte. As explained above, new "clean" magnets will be used for this feasibility study. However the extraction efficiency will also be estimated as well as the eventual

presence of extra elements in order to get some insights into a possible use on used scraps having a lower neodymium concentration or others alloying elements.

II.1. Electrolysis method

The electrolysis process can be controlled by using a fixed potential or a fixed current. The neodymium, which is contained at the anode, will be oxidised to obtain Nd^{3+} ions. These ions will be transported through the electrolyte to the cathode. Finally the Nd^{3+} ions will be reduced to their metallic form on the cathode surface. The simplified principle of the electrolysis is described in Fig. 79.

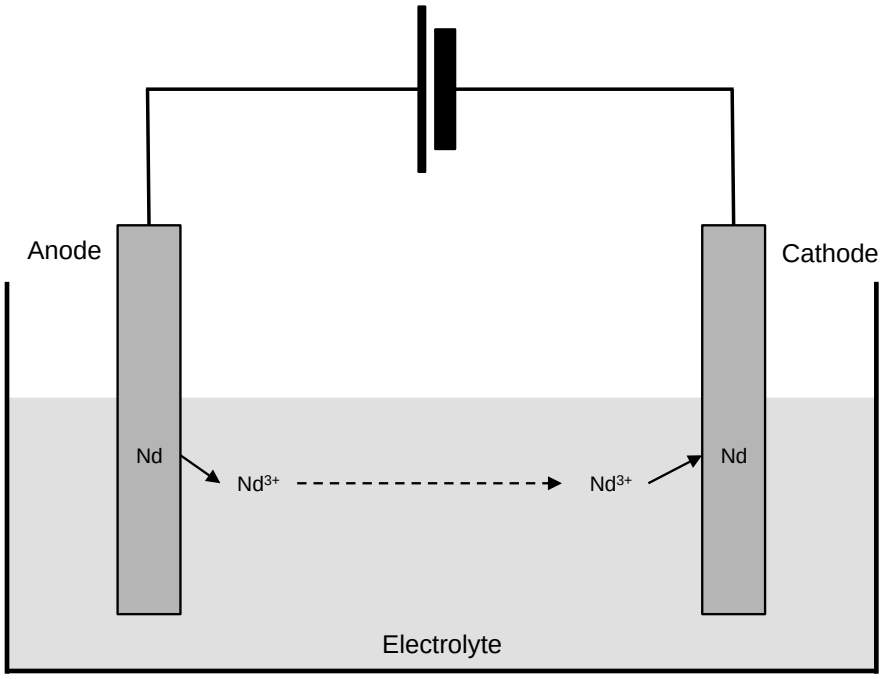

Fig. 79: Simplified principle of the electrolysis process

The electrolysis at fixed potential consists of applying a constant potential versus a reference or between two electrodes which are defined as anode and cathode. This method allows the control of the reduction of the desired compound. Compounds having a higher reduction potential will not be reduced until an ohmic voltage drop occurs. That is why the electrolysis experiments have been performed in eutectic LiCl-KCl, LiF-CaF_2 and LiF-SrF_2 electrolytes.

On the other hand the electrolysis at fixed current consists of applying a constant current and measuring the potential at the anode and cathode during the whole reaction. This method allows high kinetics due to the possibility to operate at a limit current. Unfortunately side reactions easily occur if the applied current becomes higher than the limit current. In our case, the reduction of lithium ions can be obtained.

In order to compare the extraction efficiency of neodymium in some electrolytes, the electrolysis was performed in selected salts, which were studied in the chapter IV. The electrolysis experiments were performed by applying a constant current because of the higher kinetic of this method.
For the neodymium extraction, an inert cathode was preferred to a reactive cathode. The inert electrode allows an extraction of pure neodymium without its consumption. Moreover, with an inert electrode the reduction process is limited by the diffusion of the neodymium ions whereas by using a reactive electrode the reaction is limited by the intermetallic diffusion, which is slower than the diffusion of the neodymium ions.

During the electrolysis process the reduction potential has to be maintained above the reduction potential of the lithium ions, contained in the electrolyte. By applying a constant current, the recorded reduction potential slowly shifts to more cathodic potentials with the neodymium depletion at the electrode interface. When the whole neodymium is extracted the recorded potential “drops down” corresponding to the reduction potential of the lithium cations from the electrolyte.

II.2. Electrolysis kinetics

As explained above, the electrolysis parameters have been fixed in order to optimised the reaction conditions and favour significant kinetics.
Under these conditions, the yield of the electrolysis was determined by using Eq. (62):

$$yield = \frac{n_i - n_f}{n_i} \quad (62)$$

where
n_i: mol of neodymium at the anode before the electrolysis
n_f: mol of neodymium at the anode after the electrolysis

By using the Faraday law (Eq. (63)), it is possible to estimate the mass “m” of the compound, which is liberated from the electrode.

$$m = \varepsilon \frac{Q}{F} * \frac{MM}{z} \quad (63)$$

where
m represents the mass of neodymium extracted from the electrode in grams
Q represents the electric charge in coulombs, which passes through the electrode
F represents the Faraday constant
MM represents the molar mass of the compound

z represents the number of exchanged electrons per ions
ε represents Faradaic efficiency

During the electrolysis process at constant current: Q=i*t, the rewriting of Eq. (63) leads to Eq. (64)

$$n = \frac{i * t}{z * F} \tag{64}$$

where
n represents the number of moles, which have been theoretically reduced during the electrolysis
t represents the time of the electrolysis in second
i represents the constant applied current in A

The theoretical time necessary to extract the whole neodymium can then be estimated by using Eq. (65).

$$t = \frac{n * z * F}{i} \tag{65}$$

The following experimental tests and analyses will lead to experimental values that will be compared to the results of the above theoretical equations.

III. Setting parameters for the electrolysis process

III.1. Selection and preparation of neodymium based magnets

Due to the complex composition of electronic scraps as described in section 1 of this chapter, it was decided to start the extraction of pure neodymium from clean permanent magnets.
As described in section I.3.4. of chapter II, the neodymium based permanent magnets were maintained at the anode in a basket made with a tantalum wire as showed in Fig. 80.

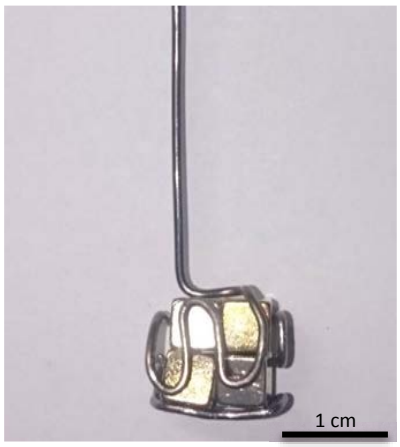

Fig. 80: Picture of the anode configuration before the electrolysis; four magnets are fixed together with a tantalum wire.

Before the construction of the anode, the permanent magnets were demagnetised through a thermal treatment. The demagnetisation of permanent magnets can be easily performed by heating the magnet above its Curie temperature.

The composition of the permanent magnets was determined before the experiment. The average values are reported in Tab. 34. The presence of nickel and copper in small amounts comes from the composition of the protective surface treatment of the magnets. The average amount of neodymium in a permanent magnet represents around 18.9 wt%.

Element	wt% (±0.05)
B	1.2
Cu	0.9
Fe	77.6
Nd	18.9
Ni	1.5

Tab. 34: Composition of a Nd-based permanent magnet, which was determined by a ICP-OES-analysis

The quantity of neodymium, which is contained in the permanent magnets fixed at the anode, as well as the quantity in the electrolyte before and after the electrolysis was determined by using the ICP-OES as described in section II.3.3 of chapter II.

III.2. Configuration of the electrolysis cell

Considering the results presented in the previous chapter, it was decided to select only three electrolytes for the recovery of neodymium from permanent magnets:

- $LiCl\text{-}KCl_{eut.}$: benchmark
- $LiF\text{-}CaF_{2eut.}$
- $LiF\text{-}SrF_{2eut.}$

For the electrolysis process in fluoride-based electrolytes an inert electrode was used to recover the pure neodymium and to avoid the formation of an alloy by the use of a reactive electrode.
During the electrolysis experiments the neodymium concentration was 1 mol% in 90 g of electrolyte. The electrolysis was conducted during four hours at a constant current of -50 mA. A higher value for the current would have been possible as well, but a high current value will lead to a too quick reduction of the neodymium. The neodymium contained in the electrolyte would have been consumed very rapidely and the reduction of the lithium ions would have been difficult to avoid. That is the reason why a constant current of -50 mA has been fixed, which corresponds to the start of the reduction step of Nd^{3+} as described in Fig. 81. The lower current allows the neodymium which is contained at the anode to be oxidised, carried until the cathode and be reduced without side reactions.

The theoretical quantity of extracted neodymium from the permanent magnets was estimated to $2.62*10^{-3}$ mol by using Eq. (64).
$2.62*10^{-3}$ mol represents the optimal quantity of neodymium, which can be extracted during the electrolysis and corresponds to 378.7 mg of pure neodymium.

IV. Extraction of neodymium from permanent magnets in fluoride-based electrolytes

IV.1. Electrolysis in $LiF-CaF_2$

The extraction of neodymium from the permanent magnets, which are fixed at the anode were performed at 1073 and 1123 K.
Fig. 81 represents a typical cyclic voltammogram of the $LiF-CaF_2$ electrolyte containing 1 mol% of neodymium, which has been recorded before the electrolysis.
The recorded cyclic voltammogram is in accordance with the results obtained in chapter IV (Fig. 57). In this cyclic voltammogram two reduction peaks can be identified during the cathodic scan. The first peak occurs at around -1.4 V versus Pt (A), which corresponds to the reduction of Nd^{3+} to Nd^0. The second reduction peak corresponds to the reduction of Li^+ ions to Li^0. During the anodic scan the reverse reactions can be identified (peak B´ and A´) respectively corresponding to the oxidation of lithium and neodymium.

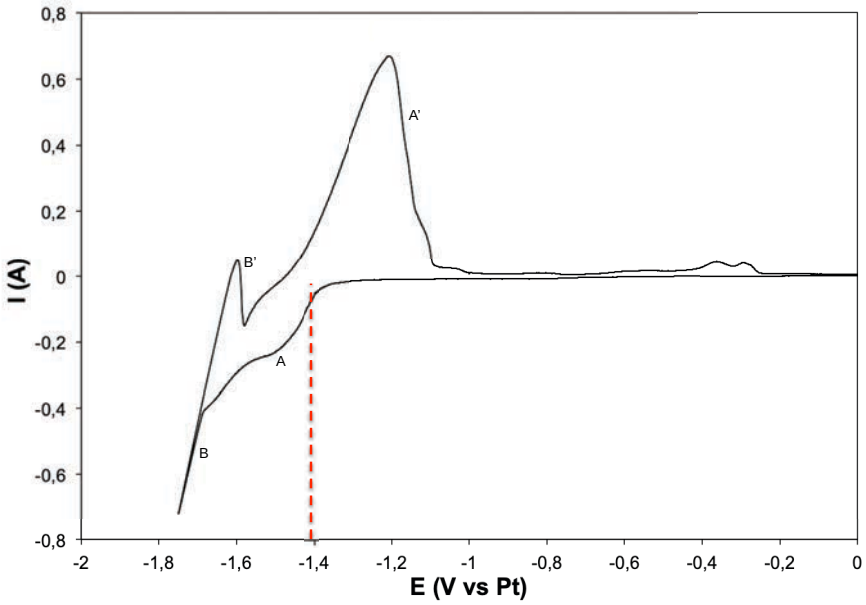

Fig. 81: Cyclic voltammogram before the electrolysis for the system LiF-CaF_2-NdF_3 (1 mol%) at 1073 K, scan rate: 0.1 $V.s^{-1}$. Working electrode: molybdenum, counter electrode: tantalum, reference electrode: platinum

By applying a constant current of -50 mA, the potential was recorded to be at around -1.4 V versus Pt (Fig. 82). According to Fig. 81, this potential corresponds to peak A, which characterises the reduction of the Nd^{3+} ions in Nd^0.

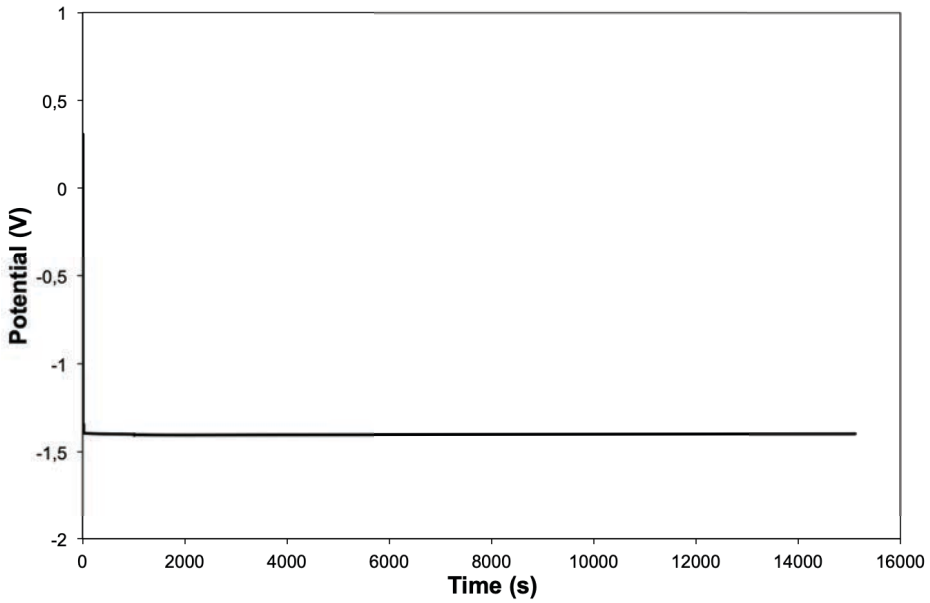

Fig. 82: Evolution of the potential during the electrolysis at a constant current of -50 mA in the eutectic LiF-CaF_2 electrolyte at 1073 K

During the whole test, the recorded potential remains stable, which confirms that only the Nd^{3+} ions have been reduced by the following reaction:

$$Nd^{3+} + 3e^- \rightarrow Nd^0$$

Fig. 83 represents the results of the electrolysis experiments. The graphic shows that the extraction efficiency is higher at 1123 K than at 1073 K. We can also see that in both cases the extraction efficiency is not perfect and remains lower than the theoretical one. A higher electrolysis temperature seems to improve the extraction efficiency. This point will be discussed in details in the following section.

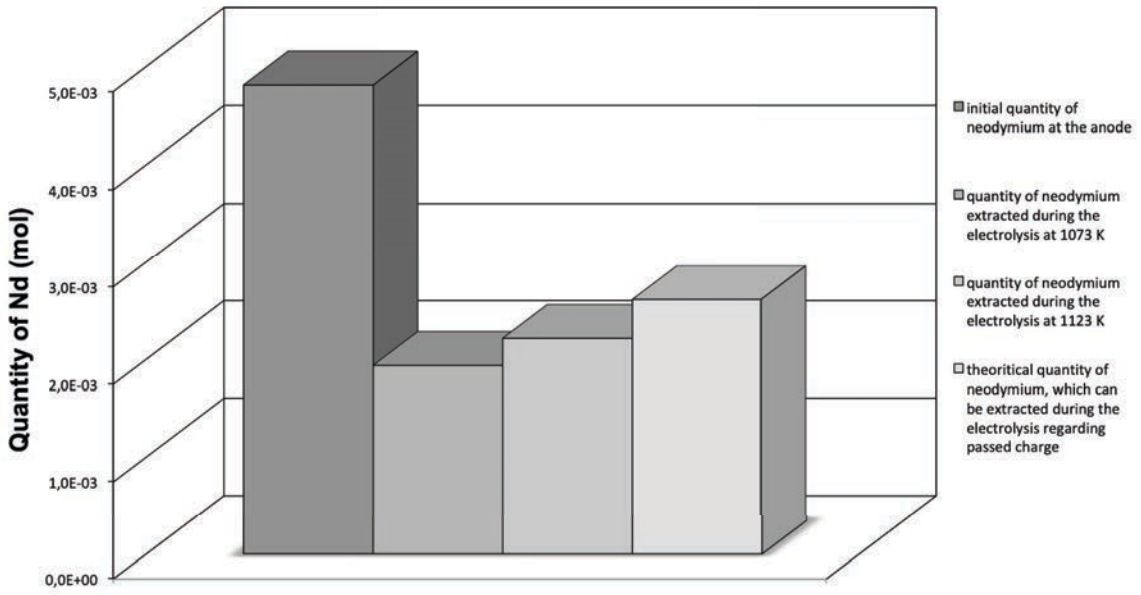

Fig. 83: Representation of the extracted quantity of neodymium compared to the initial quantity at the anode and the theoretical quantity of neodymium, that can be extracted during the electrolysis in LiF-CaF_2 electrolyte.

After the electrolysis process the neodymium concentration remaining in the permanent magnets (anode) and in the electrolyte were analysed by ICP-OES. The initial quantity of neodymium in the permanent magnets was also measured by ICP-OES for accurate comparison. The process for the preparation of ICP-OES samples described in chapter II was used.

After four hours of reaction, 40.2 % at 1073 K and 46.0 % at 1123 K of the quantity of neodymium contained in permanent magnets, which are fixed at the anode have been extracted. These values are in good agreement with the previous results. The faraday efficiency for both electrolyses is respectively 74.1 % and 84.7 % compared to the theoretical one. The results of the electrolysis in the eutectic LiF-CaF_2 are summarised in Tab. 35.

T (K)	n_i (mol)	n_f (mol)	n_{th} (mol)	efficiency (%)
1073	4.81E-03	1.94E-03	2.61E-03	74.1
1123	4.81E-03	2.21E-03	2.61E-03	84.7

Tab. 35: Summary of the electrolysis results in the eutectic LiF-CaF_2 at 1073 K and 1123 K; n_i represents the initial quantity of neodymium at the anode; n_f represents the extracted quantity of neodymium during the electrolysis; n_{th} represents the theoretical quantity of neodymium, which can be extracted during the electrolysis.

With the increase of the temperature we have seen a better extraction efficiency, which can be explained by the evolution of the diffusion coefficients. It was demonstrated in chapter IV, that the values of the diffusion coefficients of neodymium ions increase with the increase of the temperature.

Fig. 84 is a cross section of the cathode after the electrolysis process. The picture (a) shows a dendritic deposition of the metallic neodymium during the electrolysis around the molybdenum wire (cathode). The picture (b) details the dendritic deposition of neodymium (1) together with a eutectic mixture (2), which corresponds to the electrolyte LiF-CaF_2.

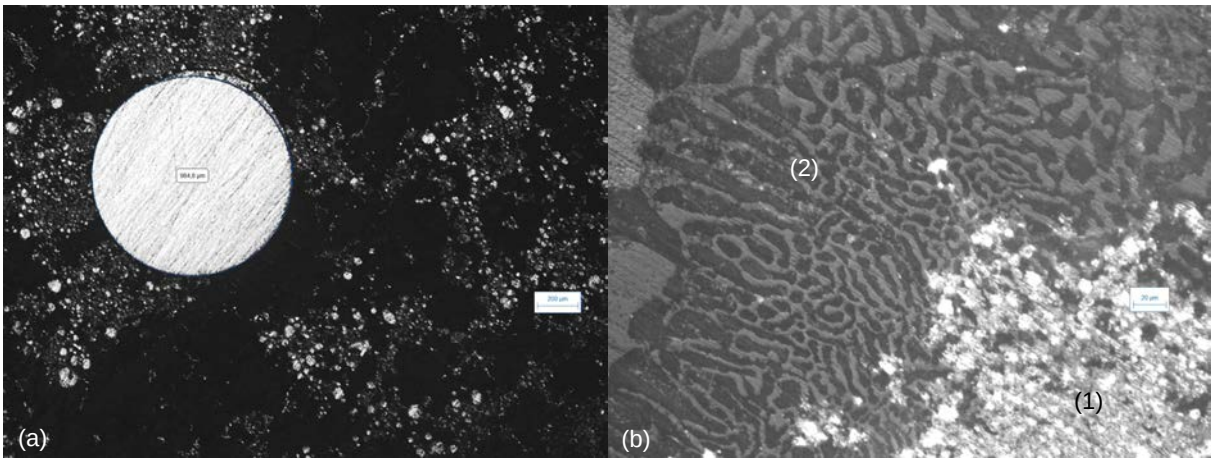

Fig. 84: Optical micrographs (x20) of the cathode cross-section after four hours of electrolysis in LiF-CaF_2 at 1123 K

SEM analyses have been performed to check the presence of the various elements in the different zones. Fig. 85 confirms the results obtained in Fig. 84. Around the molybdenum wire (Fig. 85(a)), the metallic neodymium deposition can clearly be distinguished (Fig. 85(b)). These various observations (optical and electronic microscopies) also show that the deposition of neodymium on the cathode is not dense and allows the penetration of the electrolyte.

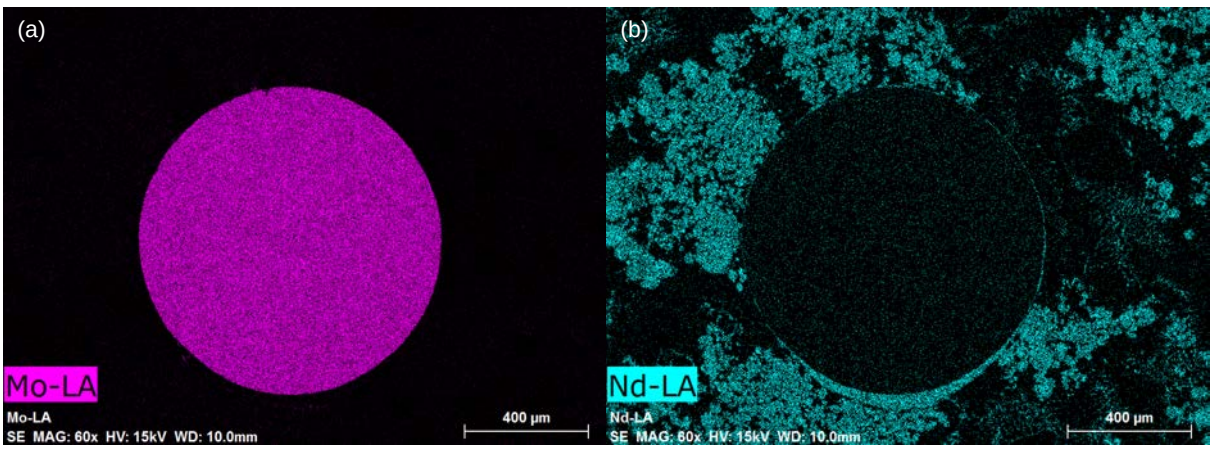

Fig. 85: SEM-analysis of a cross section of the cathode after four hours of electrolysis at 1123 K in LiF-CaF_2. (a): Map of molybdenum repartition in the sample showing that the anode remains unaffected during the electrolysis, (b): Map of the neodymium, which was deposed on the cathode.

The evolution of the neodymium concentration in the electrolyte has to be controlled before and after the electrolysis process. The concentration has changed for less than one percent. Such a small variation is not significant and due to a systematic error during the test. This result confirms that the neodymium deposited on the cathode is coming from the neodymium, which is contained in the permanent magnets fixed at the anode.

IV.2. Electrolysis in LiF-SrF_2

Fig. 86 represents a typical cyclic voltammogram as recorded at 1073 K as described in chapter IV. A single reduction step can be observed, which starts at around -1.4 V corresponding to the reduction of Nd^{3+} ions into neodymium metal. No other reaction including the reduction of extra ions can be detected in the range of operating conditions. Due to the degradation of the electrolyte, which leads to the production of an instable signal at higher temperatures, the electrolysis in the LiF-SrF_2 electrolyte was only done at 1073 K.

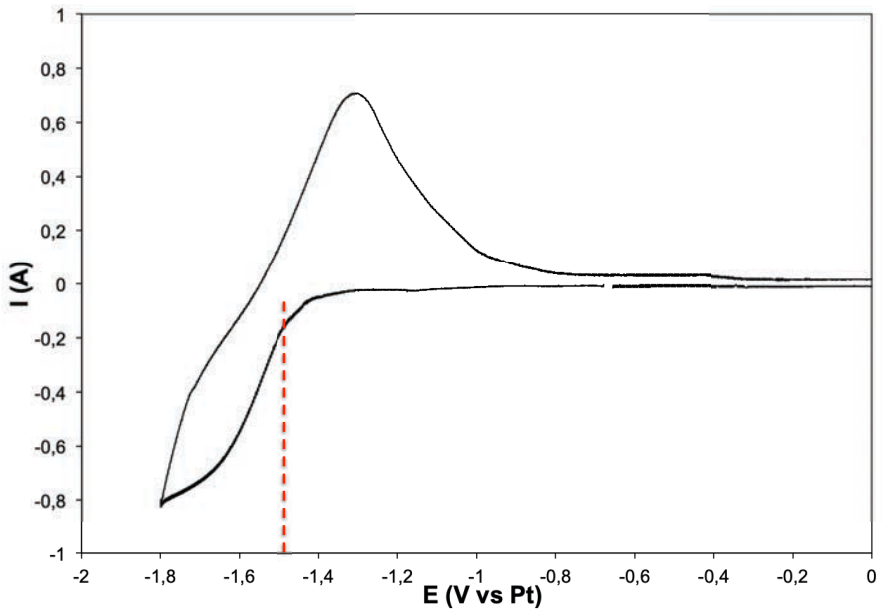

Fig. 86: Cyclic voltammogram before the electrolysis for the system LiF-SrF_2-NdF_3 (1 mol%) at 1073 K, scan rate: 0.1 $V.s^{-1}$. Working electrode: molybdenum, counter electrode: tantalum, reference electrode: platinum

By applying a constant current of -50 mA, the potential was recorded to be stable at around -1.5 V versus Pt (Fig 87). Just before the beginning of the experiment a short time is necessary to stabilise the potential. In comparison with Fig. 86, this potential corresponds to the peak, which characterises the reduction of the Nd^{3+} ions in Nd^0. During this electrolysis, the constant recorded potential also confirms that only the Nd^{3+} ions have been reduced without any side reaction.

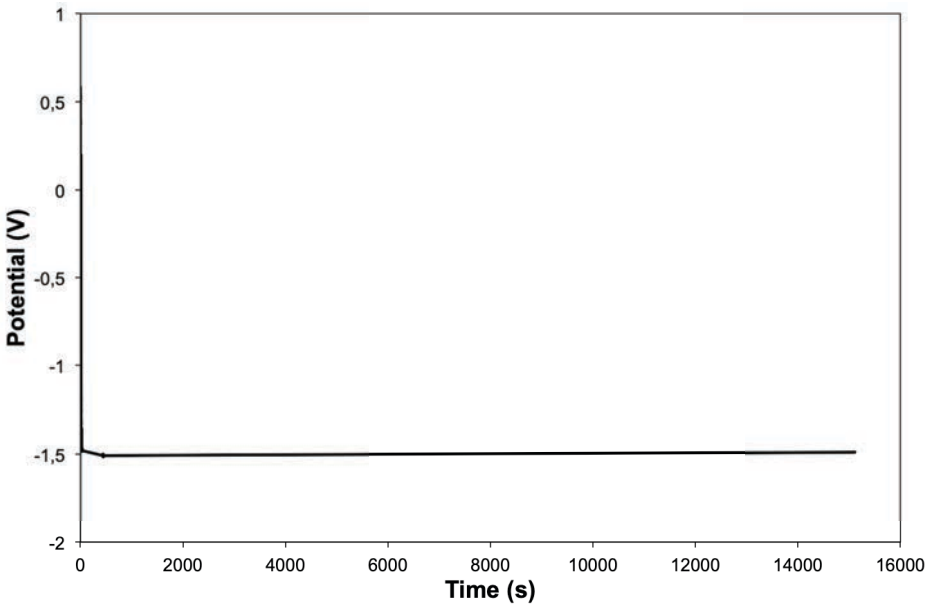

Fig. 87: Evolution of the potential during the electrolysis at a constant current of -50 mA in the eutectic LiF-SrF_2 electrolyte at 1073 K

Fig. 88 compares the quantity of neodymium fixed on the anode before the electrolysis, the quantity of neodymium, which can theoretically be extracted and the real amount of neodymium, which was extracted from the permanent magnets.

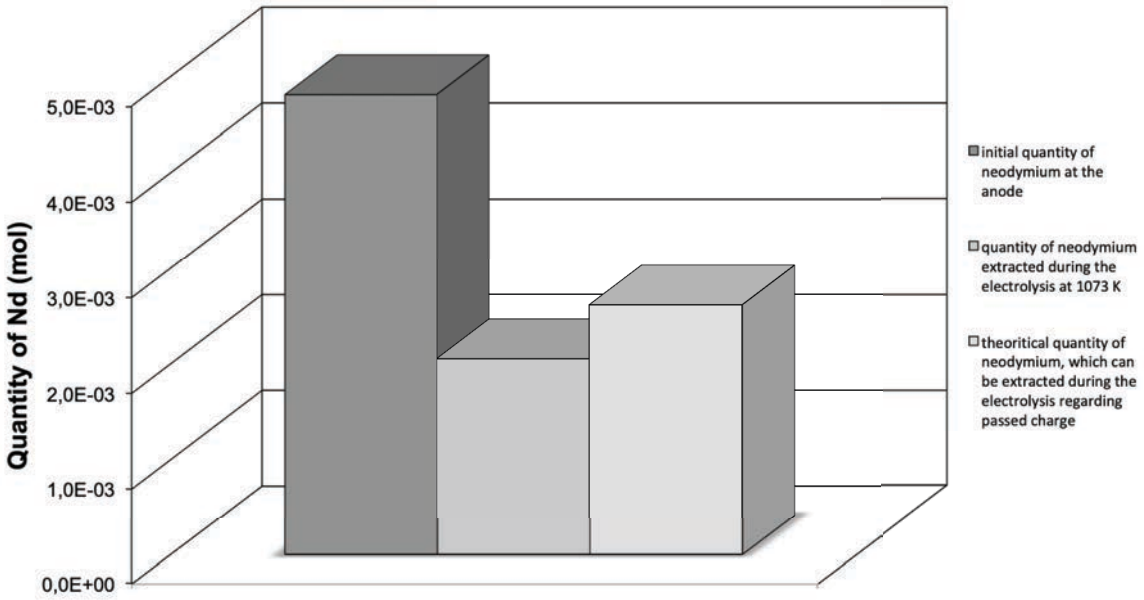

Fig. 88: Representation of the extracted quantity of neodymium compared to the initial quantity at the anode and the theoretical quantity of neodymium, which can be extracted during the electrolysis in LiF-SrF_2 electrolyte.

After a four hours electrolysis test, 42.6 % of the neodymium contained at the anode has been extracted leading to an efficiency of 78.4 % compared to the theoretical value.

In order to show if the duration of the electrolysis process has an influence on the efficiency, a test has been carried out at the same constant current of - 50 mA but lasting only two

hours. By using the above mentioned parameters, the efficiency of this shorter test was 92.3 %. The results of both electrolysis experiments are summarised in Tab. 36.

These results demonstrate that the efficiency of an electrolysis lasting two hours is higher than an electrolysis during four hours at a same constant current. An explanation is that during the test the neodymium concentration at the anode continuously decreases from 18.9 % to 14.4 % after two hours and to 10.9 % after four hours. It is always more difficult to extract the last neodymium atoms contained in the permanent magnets.

T (K)	Duration (h)	n_i (mol)	n_f (mol)	n_{th} (mol)	efficiency (%)
1073	2	4.81E-03	1.15E-03	1.24E-03	92.3%
	4		2.05E-03	2.61E-03	78.4%

Tab. 36: Summary of the electrolysis results in the eutectic LiF-SrF_2 at 1073 K during two hours and four hours; n_i represents the initial quantity of neodymium at the anode; n_f represents the extracted quantity of neodymium during the electrolysis; n_{th} represents the theoretical quantity of neodymium, which can be extracted during the electrolysis

Fig. 89 presents a SEM micrograph of a cross section of the cathode (Fig. 89a) as well as the corresponding EDS maps of molybdenum (Fig. 89b) and neodymium (Fig. 89c). The figures show a compact deposit of metallic neodymium on the molybdenum electrode. The observations are clearly different from the obtained results using the previous LiF-CaF_2 salt where deposits of neodymium and eutectic electrolyte were mixed around the molybdenum wire.

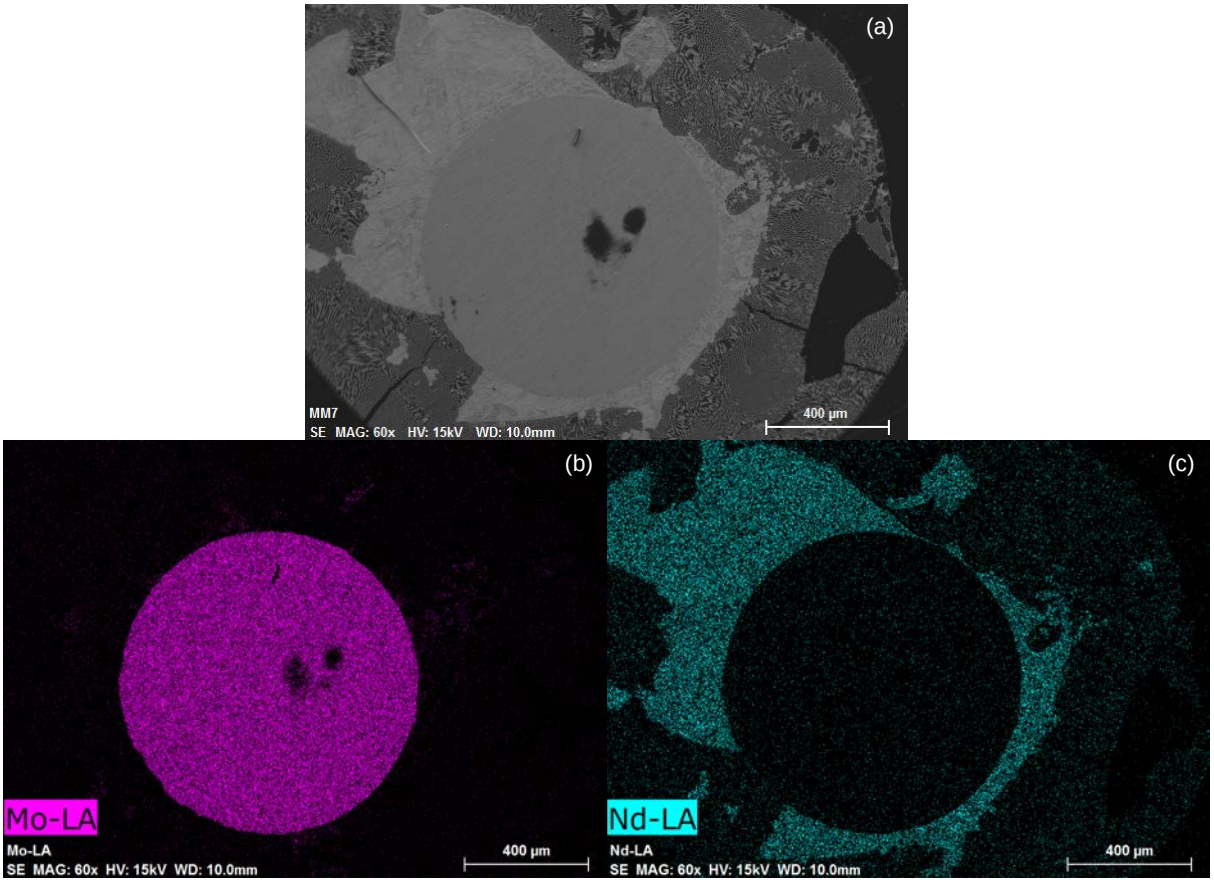

Fig. 89: SEM-analysis of a cross section of the cathode after a four hours electrolysis at 1073 K in LiF-SrF_2. (a) : overview of the cross section, (b) : EDS Map of molybdenum repartition in the sample showing that the anode remains unaffected during the electrolysis, (c) representation of the neodymium deposit on the cathode.

As previously described for the LiF-CaF_2 electrolyte, the neodymium concentration in the electrolyte has to be controlled before and after the electrolysis process. Once again, the concentration was changed by less than one percent due to a systematic error during the analysis. This result confirms that the neodymium, which is deposed on the cathode during the electrolysis in LiF-SrF_2 is coming from the permanent magnets fixed at the anode.

IV.3. Electrolysis in LiCl-KCl

Fig. 90 represents a cyclic voltammogram, which was recorded before the electrolysis. Two reduction steps can be identified (peak A and B), which correspond respectively to the reduction of Nd^{3+} and Nd^{2+} as previously described during the study of neodymium behaviour in chapter IV. The oxidation peaks A' and B' correspond respectively to the oxidation of Nd^{0} and Nd^{2+}.

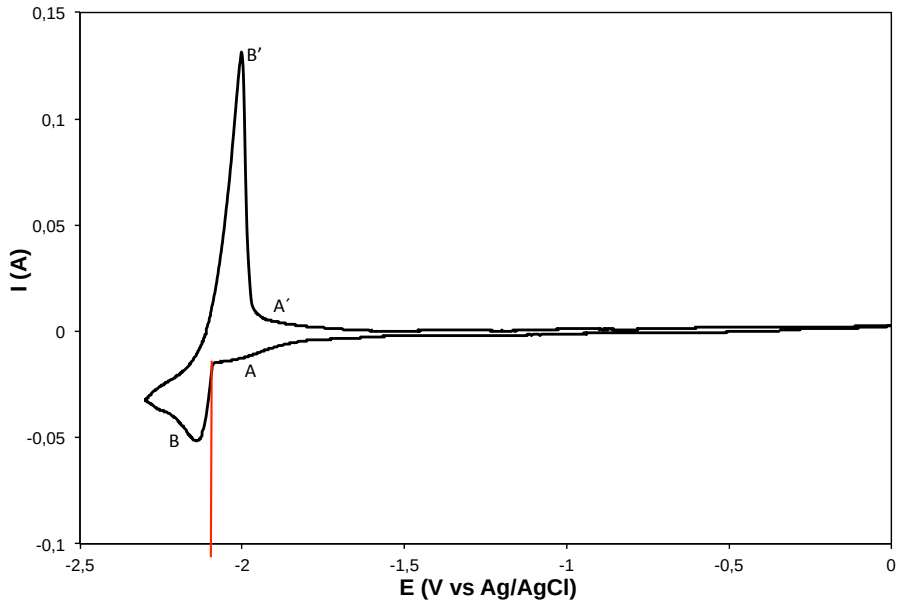

Fig. 90: Cyclic voltammogram before the electrolysis for the system LiCl-KCl-$NdCl_3$ (1 mol%) at 773 K, scan rate 0.1 $V.s^{-1}$. Working electrode: tungsten, counter electrode: molybdenum

The electrolysis in the eutectic LiCl-KCl has been made at 773 K with the same parameters as previously described. The constant current was fixed at -50 mA for four hours. The evolution of the potential is described in Fig. 91.

In comparison with Fig. 90, this potential corresponds to the peak, which characterises the production of Nd^0. During this electrolysis, the recorded potential remains stable confirming that only the Nd^{3+} ions have been reduced without any side reaction.

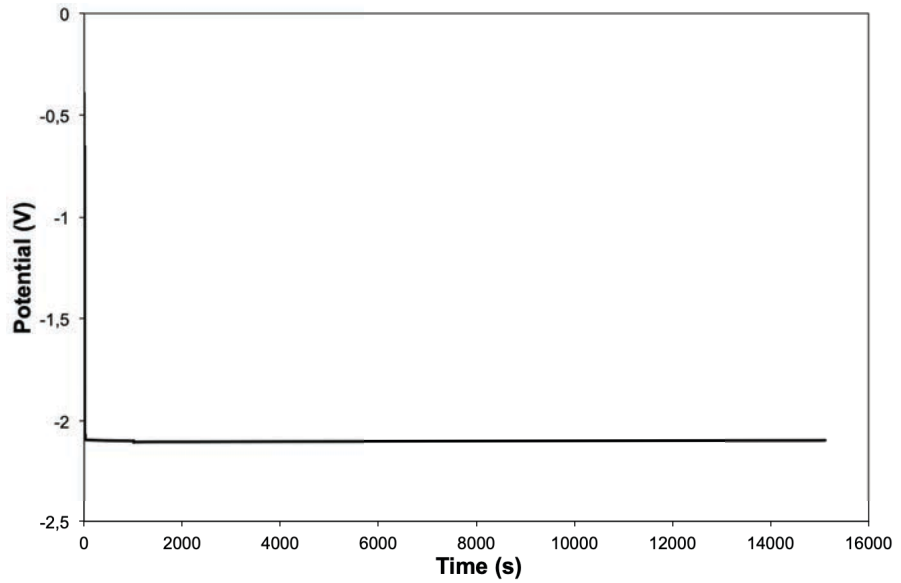

Fig. 91: Evolution of the potential during the electrolysis at a constant current of -50 mA in the eutectic LiCl-KCl electrolyte at 773 K

Fig. 92 compares the quantity of neodymium fixed on the anode before the electrolysis, the quantity of neodymium, which can theoretically be extracted and the real amount of

neodymium, which was extracted from the permanent magnets. After the electrolysis with a duration of four hours, 30.6 % of the neodymium contained at the anode has been extracted with an efficiency of 56.3 % compared to the theoretical one.

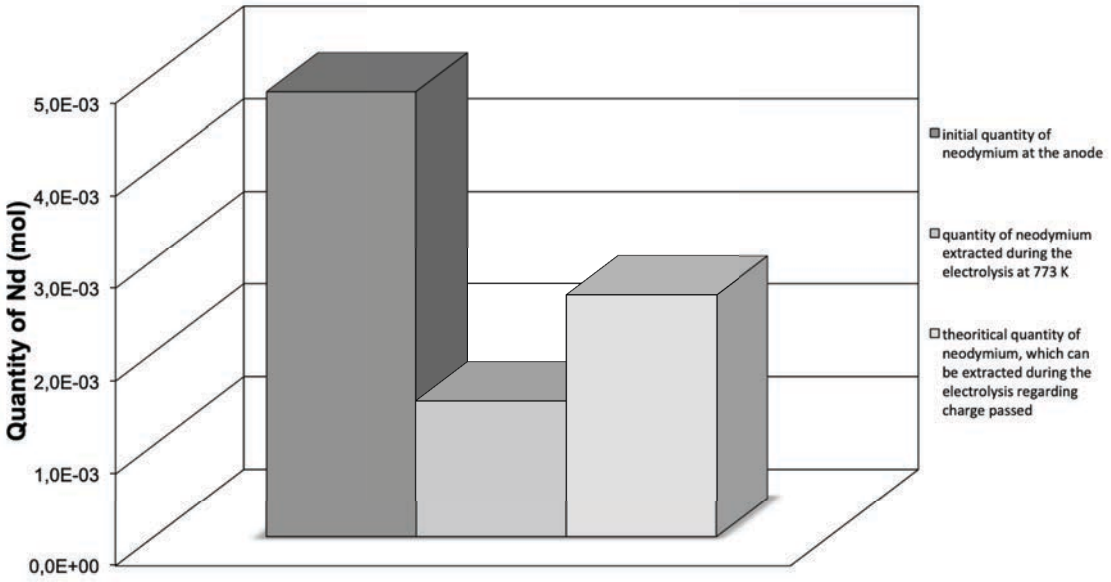

Fig. 92: Representation of the initial quantity, the extracted quantity and the theoretical quantity of neodyium, which can be extracted during the electrolysis in LiCl-KCl electrolyte.

The lower faradic efficiency could be explained by the reaction of disproportion of Nd^{2+}, which avoid the complete reduction of the neodymium ions to metallic neodymium. The second explanation could be the lower values of the diffusion coefficients of Nd^{3+} ions in LiCl-KCl compared to the diffusion coefficients in fluoride-based electrolytes as described in chapter IV.

V. Conclusion of the chapter

In the first part of this chapter it was demonstrated that the extraction of neodymium from permanent magnets including in electronic scraps has to be improved before any commercial use.

The two electronic scraps recycling companies, which have provided samples for our research, tried to extract a fraction with a high amount of permanent magnets from the electronic scraps. However the sorting processes are still not suitable. Further developments have to be done to increase the amount of neodymium and others RE in the metallic fraction obtained after the separation process. The low amount of neodymium in the sorted fraction prohibits any further recycling.

However, assuming that this progress will be achieved in a near future, the electrolysis process, which is used to recover neodymium from permanent magnets has been

successfully explored. The obtained results have demonstrated that the electrolysis has a better efficiency in fluoride-based electrolytes than in the chlorides-based.
This observation can be explained by the fact that in chloride electrolytes, neodymium ions are reduced in two steps passing through a intermediate Nd^{2+}, which disproportionates following the reaction:

$$3Nd^{2+} \rightarrow Nd^{0} + 2Nd^{3+}$$

At the same temperature, the electrolysis has a better efficiency in the LiF-SrF_2 electrolyte than in LiF-CaF_2 electrolyte. This observation is in accordance with the results, which have been obtained for the diffusion coefficients, which were higher in the LiF-SrF_2 electrolyte than in the LiF-CaF_2 electrolyte.

The temperature during the electrolysis influences the faradic efficiency. It has been demonstrated that an increase of 50 K leads to a higher efficiency of around 10 %. This observation is in a good agreement with the fact that the diffusion coefficients in the electrolyte increase with a higher temperature.

Moreover the faradic efficiency decreases with the increase of the duration of electrolysis. The decrease of the efficiency is explained by the depletion of the amount of neodymium at the anode and the difficulty to extract the last neodymium ions in the permanent magnets.

General conclusions and outlook

General conclusions

For some decades the demand in neodymium and others RE has increased drastically and the production of electronic scraps containing neodymium still increases too. Due to the geopolitical considerations the price of pure neodymium is unstable and more than 90 % of the global production is coming from China.

The aim of the thesis was to develop a process for the recycling of neodymium contained in the permanent magnets presented in electronic scraps.

First of all, a literature review has shown that no efficient process for the extraction of neodymium has been upscaled into an industrial process.

Each process has disadvantages. For example, there are processes with many extraction steps before obtaining the final product. Other processes using toxic chemical compounds are clearly environmentally unfriendly. That’s why an alternative process is needed. Along several possible methods, we decided to follow the pyrochemical process. Chapter I also explains the reasons of this choice.
The foreseen extraction uses molten salts as electrolyte and reduces selectively the required compounds, which is neodymium in our case. The selected salts and other used materials and chemical compounds are presented in chapter II. This part also detailed the various electrochemical tests and methods used during this work.

For the pyrochemical process a special reactor had to be developed. It had to be resistant to temperatures up to 1273 K and to corrosive media like chloride- and fluoride-based molten salts. This reactor was used as an electrochemical cell, which was composed of a three-electrode-system, a thermocouple in order to control the temperature of the melt and a gas input and output to control the atmosphere of the reaction chamber.
The electrochemical cell was made of Inconel 625, which is one of the only material who can resist to corrosive electrolyte based on fluorides and simultaneously to a temperature around 1273 K.

To validate the cell design, a first batch of tests has been performed on known systems. The obtained results lead coherent values that allow us to validate the whole cell design. This device represents one of the main achievements of this PhD work. The severe service conditions, which had to be fulfilled, have shown a very challenging aspect but the chosen options appear to be pertinent and respond correctly to the objectives.

In chapter IV, the newly developed cell has been used to test the molten salts selected in chapter one. Electrochemical properties such as the apparent standard potentials and the diffusion coefficients have been determined for the following electrolytes:

- LiCl-KCl
- LiCl-KCl-LiF
- LiF-CaF_2
- LiF-SrF_2

These experiments have shown that in the electrolytes containing chloride ions the mechanism of Nd^{3+} ions follows a two step reaction:

$$Nd^{3+} + e^- \rightarrow Nd^{2+}$$
$$Nd^{3+} + 2e^- \rightarrow Nd^0$$

During the reduction process, an instable intermediate Nd^{2+} is obtained, which disproportionates following the reaction described below:

$$3Nd^{2+} \rightarrow Nd^0 + 2Nd^{3+}$$

On the contrary, it was demonstrated that in the fluoride-based electrolytes the Nd^{3+} ions were directly reduced in neodymium metal without passing through any intermediate state.

The diffusion coefficients of the neodymium ions were determined in the above-mentioned electrolyte at different temperatures. It was shown that these coefficients increase with an increase of temperature. Simultaneously it was also demonstrated that the values of the diffusion coefficients are higher in fluoride-based electrolytes than in the chloride-based electrolytes.
These different results seem to indicate that a fluoride-based molten salt could be a better candidate for the neodymium recovery.

This point has been tested in the last chapter. For this, we analysed samples from electronic scrap recycling companies, which separate high value materials from other materials like plastic. In our case the aim was the separation of neodymium-based magnets from other wastes. It was shown that the neodymium concentration in the magnetic fraction was in fact very low, too low to enable any efficient recycling process. This study clearly shows that progress in sorting has to be done prior to any further economical recycling development. In order to increase the neodymium concentration it is necessary to improve the separation processes. Due to a very low neodymium concentration in the samples from the electronic scraps companies, we have decided to extract the neodymium from clean permanent

magnets. Even if not realistic this configuration allows us to test the proposed recycling process and to evaluate its feasibility and efficiency.

A significant concentration of around 19 % of neodymium has been shown by the analysis of the permanent magnets. The extraction of the neodymium contained in the permanent magnets has been performed under a constant current in the following electrolytes :

- LiCl-KCl
- LiF-CaF_2
- LiF-SrF_2

It was demonstrated that the extraction efficiency was higher in the fluoride-based electrolytes than in the LiCl-KCl electrolytes. The results can be explained by the detrimental effect of the reaction of the disproportion of the Nd^{2+} ions.

Moreover we have shown that the temperature has an influence on the efficiency of the extraction. An increase of the reaction temperature favours the extraction process during the electrolysis. This result is confirmed by the evolution of the diffusion coefficient as a function of the temperature.

The faradic efficiency declines with the increase of the electrolysis duration, which is due to the depletion of the neodymium concentration at the anode. This result shows finally that it will be difficult to extract the whole neodymium amount from the permanent magnets.

Outlook

Due to the new electrochemical cell developed during this study and the first encouraging results obtained, it would be interesting to study further the most promising system. It was demonstrated that the temperature has an influence on the extraction efficiency, further temperatures could be studied in order to define the optimal experimental conditions. The influence of the current during the electrolysis could be also studied to show if it has an effect on the extraction efficiency.

A further research topic could be the study of the interaction between neodymium in the electrolytes using simulation tools. Molecular modelling could for example be of great interest to better understand the neodymium and electrolyte behaviour.

However the results presented in chapter V clearly show that all progresses in recycling efficiency will be annihilated by the poor neodymium content of the sorted fraction. It is therefore essential to improve the separation processes that are used in the electronic scraps recycling companies in order to increase the neodymium ratio, which is contained in the metallic fraction.

After the above-mentioned step, the developed method for the extraction of neodymium from clean permanents magnets might be able to be used to extract the neodymium from the future metallic fractions provided by the electronic scraps companies. A new study would probably be necessary to adjust the operating parameters and estimate the process efficiency in presence of possible unexpected polluting elements.

References

References

1 NDR, Neodym: Das schmutzige Geheimnis sauberer Windräder, http://www.ndr.de/unternehhmen/presse/pressemitteillungen/pressemeldungndr8137.html.

2 European Commission, *Critical raw materials for the EU Report of the Ad-hoc Working Group on defining critical raw materials*, report, 2010.

3 U.S. Department of Energy, *Critical materials strategy*, report, 2011.

4 K. Binnemans, P. T. Jones, B. Blanpain, T. Van Gerven, Y. Yang, A. Walton and M. Buchert, *J. Clean. Prod.*, 2013, **51**, 1–22.

5 T. G. Goonan, *Rare Earth Elements — End Use and Recyclability Scientific Investigations Report 2011 – 5094*, 2011.

6 JOGMEC, *Mater. Flow Miner. Resour.*, 2010, 383–403.

7 W. M. Hubbard, E. Adams and J. V Gilfrich, *J. Appl. Phys.*, 1960, **31**, 368S–369S.

8 Y. Tawara and K. J. Strnat, *IEEE Trans. Magn.*, 1976, **12**, 954–958.

9 J. J. Croat, J. F. Herbst, R. W. Lee and F. E. Pinkerton, *J. Appl. Phys.*, 1984, **55**, 2078.

10 M. Sagawa, S. Fujimura, N. Togawa, H. Yamamoto and Y. Matsuura, *J. Appl. Phys.*, 1984, **55**, 2083–2087.

11 C. Auer von Welsbach, *Monatshefte für Chemie und verwandte Teile anderer Wissenschaften*, 1885, **6**, 477–491.

12 UNEP, *Metal Recycling: Opportunities, Limits; Infrastructure*, report, 2013.

13 E. Alonso, A. M. Sherman, T. J. Wallington, M. P. Everson, F. R. Field, R. Roth and R. E. Kirchain, *Environ. Sci. Technol.*, 2012, **46**, 3406–3414.

14 https://www.magnethandel.de, Neodymium Preisentwicklung. (accessed 13 June 2015)

15 J. H. Rademaker, R. Kleijn and Y. Yang, *Environ. Sci. Technol.*, 2013, **47**, 10129–10136.

16 J. H. Rademaker, R. Kleijn and Y. Yang, *Environ. Sci. Technol.*, 2013, **47**, 10129–10136.

17 H. M. D. Bandara, J. W. Darcy, D. Apelian and M. H. Emmert, *Environ. Sci. Technol.*, 2014, **48**, 6553–6560.

18 K. Habib, K. Parajuly and H. Wenzel, *Environ. Sci. Technol.*, 2015, **49**, 12441–12449.

19 Y. Yang, S. Abrahami and Y. Xiao, in *3rd international slag valorisation symposium*, Leuven, 2013, 249–252.

20 A. Walton, H. Yi, N. A. Rowson, J. D. Speight, V. S. J. Mann, R. S. Sheridan, A. Bradshaw, I. R. Harris and A. J. Williams, *J. Clean. Prod.*, 2015, **104**, 236–241.

21 J. P. Meakin, J. D. Speight, R. S. Sheridan, A. Bradshaw, I. R. Harris, A. J. Williams and A. Walton, *Appl. Surf. Sci.*, 2016, **378**, 540–544.

22 M. Zakotnik and C. O. Tudor, *Waste Manag.*, 2015, **44**, 48–54.

23 C. O. Bounds, *The recycle of sintered magnet swarf*, in Symposium on Metals and Materials Waste Reduction, Recovery and Remediation, October 3-6, 1994 in Rosemont, Illinois (U.S.), 173–186.

24 T. W. Ellis, F. A. Schmidt and L. L. Jones, *Methods and Opportunities in The Recycling of Rare Earth Based Materials*, Metallurgy and Ceramics Division, AMES Laboratory, internal report,1994.

25 J. W. Lyman and G. R. Palmer, *Scrap treatment method for rare earth transition metal alloys, P*atent no. US5129945, 1992.

26 J. W. Lyman and G. R. Palmer, *Recycling of Neodymium Iron Boron Magnet Scrap*, Bureau au Mines, 1993, Report of Investigations 9481, 28 p.

27 H.-S. Yoon, K. Chul-Joo, L. Jin-Young, K. Sung-Don, K. Joon-Soo and L. Jae-Chun, *J. Korean Inst. Resour. Recycl.*, 2003, **12**, 57–63.

28 H. S. Yoon, C.-J. Kim and J.-S. Kim, *J. Korean Inst. Resour. Recycl.*, 2004, **13**, 43–48.

29 S. T. Abrahami, Y. Xiao and Y. Yang, *Miner. Process. Extr. Metall.*, 2015, **124**, 106–115.

30 H. M. D. Bandara, K. D. Field and M. H. Emmert, *Green Chem.*, 2016, 753–759.

31 C. Lee, Y. Chen, C. Liao, S. R. Popuri, S.-L. Tsai and C.-E. Hung, *Metall. Mater. Trans. A*, 2013, **44A**, 5825–5833.

32 K. Koyama, A. Kitajima and M. Tanaka, *Kidorui (Rare Earths)*, 3009, **54**, 36–37.

33 Y. Wei, N. Sato and M. Nanjo, *Shigen-to-Sozai*, 1989, **2**, 965–970.

34 N. Sato, Y. Wei, M. Nanjo and M. Tokuda, *Shigen-to-Sozai*, 1997, **113**, 1082–1086.

35 T. Itakura, R. Sasai and H. Itoh, *J. Alloys Compd.*, 2006, **408**–**412**, 1382–1385.

36 M. Mohammadi, K. Forsberg, L. Kloo, J. Martinez De La Cruz and Ake Rasmuson, *Hydrometallurgy*, 2015, **156**, 215–224.

37 J. Kraikaew, W. Srinuttrakul and C. Chayavadhanakur, *J. Met. Mater. Miner.*, 2005, **15**, 89–95.

38 Y. Liu, H. S. Jeon and M. S. Lee, *Hydrometallurgy*, 2014, **150**, 61–67.

39 R. D. Abreu and C. A. Morais, *Miner. Eng.*, 2014, **61**, 82–87.

40 Z. X. Zhu, Y. Sasaki, H. Suzuki, S. Suzuki and T. Kimura, *Anal. Chim. Acta*, 2004, **527**, 163–168.

41 M. S. Lee, J. Y. Lee, J. S. Kim and G. S. Lee, *Sep. Purif. Technol.*, 2005, **46**, 72–78.

42 D. Kim, L. E. Powell, L. H. Delmau, E. S. Peterson, J. Herchenroeder and R. R. Bhave, *Environ. Sci. Technol.*, 2015, **49**, 9452–9459.

43 Y. Baba, F. Kubota, N. Kamiya and M. Goto, *J. Chem. Eng. Japan*, 2011, **44**, 679–685.

44 K. Shimojo, H. Naganawa, J. Noro, F. Kubota and M. Goto, *Anal. Sci.*, 2007, **23**, 1427–30.

45 S. J. Yoon, J. G. Lee, H. Tajima, A. Yamasaki, F. Kiyono, T. Nakazato and H. Tao, *J. Ind. Eng. Chem.*, 2010, **16**, 350–354.

46 Y. Kikuchi, M. Matsumiya and S. Kawakami, *Solvent Extr. Res. Dev.*, 2014, **21**, 137–145.

47 Y. Baba, F. Kubota, N. Kamiya and M. Goto, *Solvent Extr. Res. Dev.*, 2011, **18**, 193–198.

48 T. Vander Hoogerstraete, S. Wellens, K. Verachtert and K. Binnemans, *Green Chem.*, 2013, **15**, 919.

49 T. Vander Hoogerstraete, B. Blanpain, T. Van Gerven, K. Binnemans, *RSC Adv.*, 2014, **4**, 64099–64111.

50 D. Dupont and K. Binnemans, *Green Chem.*, 2015, **17**, 2150–2163.

51 S. Riano and K. Binnemans, *Green Chem.*, 2015, **17**, 2931–2942.

52 Z. Hua, J. Wang, L. Wang, Z. Zhao, X. Li, Y. Xiao and Y. Yang, *ACS Sustain. Chem. Eng.*, 2014, **2**, 2536–2543.

53 Z. S. Hua, L. Wang, J. Wang, Y. P. Xiao, Y. X. Yang, Z. Zhao and M. J. Liu, *Mater. Sci. Technol.*, 2015, **31**, 1007–1010.

54 T. W. Ellis, F. A. Schmidt, *Recycling of rare earth metals from rare earth-transition metal alloy scrap by liquid metal extraction*, Patent no. US5437709, 1995.

55 Y. Xu, L. S. Chumbley and F. C. Laabs, *J. Mater. Res.*, 2000, **15**, 2296–2304.

56 H. Okamoto and T. B. Massalski, *J. Phase Equilibria*, 1991, **12**, 148–168.

57 A. A. Nayeb-Hashemi and J. B. Clark, *Bull. Alloy Phase Diagrams*, 1985, **6**, 235–238.

58 O. Takeda, T. H. Okabe and Y. Umetsu, *J. Alloys Compd.*, 2006, **408**–**412**, 387–390.

59 T. H. Okabe, O. Takeda, K. Fukuda and Y. Umetsu, *Mater. Trans.*, 2003, **44**, 798–801.

60 O. Takeda, T. H. Okabe and Y. Umetsu, *J. Alloys Compd.*, 2004, **379**, 305–313.

61 M. Moore, A. Gebert, M. Stoica, M. Uhlemann and W. Löser, *J. Alloys Compd.*, 2015, **647**, 997–1006.

62 T. Saito, H. Sato, S. Ozawa, J. Yu and T. Motegi, *J. Alloys Compd.*, 2003, **353**, 189–193.

63 T. Saito, H. Sato and T. Motegi, *J. Alloys Compd.*, 2006, **425**, 145–147.

64 F. Meyer, Recycling von Neodym aus NdFeB-Magneten in Wlektroaltgeräten, B. thesis, Hamburg University of Applied Sciences, 2012, 95 p.

65 K. Asabe, A. Saguchi, W. Takahashi, R. O. Suzuki and K. Ono, *Mater. Trans.*, 2001, **42**, 2487–2491.

66 A. Saguchi, K. Asabe, W. Takahashi, R. O. Suzuki and K. Ono, 2002, **43**, 256–260.

67 A. Saguchi, K. Asabe, T. Fukuda, W. Takahashi and R. O. Suzuki, *J. Alloys Compd.*, 2006, **408**–**412**, 1377–1381.

68 R. O. Suzuki, A. Saguchi, W. Takahashi, T. Yagura and K. Ono, *Mater. Trans.*, 2001, **42**, 2492–2498.

69 Y. Bian, S. Guo, L. Jiang, J. Liu, K. Tang and W. Ding, *ACS Sustain. Chem. Eng.*, 2016, **4**, 810–818.

70 K. Machida, M. Masuda, S. Suzuki, M. Itoh and T. Horikawa, *Chem. Lett.*, 2003, **32**, 628–629.

71 T. Uda, *Mater. Trans.*, 2002, **43**, 55–62.

72 M. Itoh, K. Miura and K. Machida, *J. Alloys Compd.*, 2009, **477**, 484–487.

73 K. Murase, K. Machida and G. Adachi, *J. Alloy. Compd.*, 1995, **217**, 218–225.

74 M. A. R. Onal, C. R. Borra, M. Guo, B. Blanpain and T. Van Gerven, *J. Sustain. Metall.*, 2015, **1**, 199–215.

75 T. Oishi, H. Konishi, T. Nohira, M. Tanaka and T. Usui, *KAGAKU KOGAKU RONBUNSHU*, 2010, **36**, 299–303.

76 S. Kobayashi, K. Kobayashi, T. Nohira, R. Hagiwara, T. Oishi and H. Konishi, *J. Electrochem. Soc.*, 2011, **158**, E142–E146.

77 A. M. Martinez, O. Kjos, E. Skybakmoen, A. Solheim and G. M. Haarberg, *ECS Trans.*, 2012, **50**, 453–461.

78 P. Masset, R. J. M. Konings, R. Malmbeck, J. Serp and J.-P. Glatz, *J. Nucl. Mater.*, 2005, **344**, 173–179.

79 K. Fukasawa, A. Uehara, T. Nagai, T. Fujii and H. Yamana, *J. Alloys Compd.*, 2011, **509**, 5112–5118.

80 K. Fukasawa, A. Uehara, T. Nagai, T. Fujii and H. Yamana, *Green Energy Technol.*, 2010, **44**, 108–112.

81 A. Uehara, K. Fukasawa, T. Nagai, T. Fujii and H. Yamana, *J. Nucl. Mater.*, 2011, **414**, 336–339.

82 K. Fukasawa, A. Uehara, T. Nagai, T. Fujii and H. Yamana, *J. Nucl. Mater.*, 2011, **414**, 265–269.

83 A. Novoselova and V. Smolenski, *Electrochim. Acta*, 2013, **87**, 657–662.

84 S. Vandarkuzhali, P. Venkatesh, S. Ghosh, G. Seenivasan, B. Prabhakara Reddy, T. Subramanian, N. Sivaraman and K. Nagarajan, *J. Electroanal. Chem.*, 2007, **611**, 181–191.

85 K. Sridharan, *Thermal Properties of LiCl-KCl Molten Salt for Nuclear Waste Separation Thermal Properties of LiCl KCl Molten Salt for Nuclear Waste Separation*, U.S. Department of Energy, 2012, Project No. 09-780, 107 p.

86 H. Yamana, B. G. Park, O. Shirai, T. Fujii, A. Uehara and H. Moriyama, *J. Alloys Compd.*, 2006, **408**–**412**, 66–70.

87 T. Yamamura, M. Mehmood, H. Maekawa and Y. Sato, *Chem. Sustain. Dev.*, 2004,

12, 105–111.

88 V. Smolenski, A. Novoselova, A. Osipenko, M. Kormilitsyn and Y. Luk'yanova, *Electrochim. Acta*, 2014, **133**, 354–358.

89 H. Tang and B. Pesic, *J. Nucl. Mater.*, 2015, **458**, 37–44.

90 S. Vandarkuzhali, M. Chandra, S. Ghosh, N. Samanta, S. Nedumaran, B. Prabhakara Reddy and K. Nagarajan, *Electrochim. Acta*, 2014, **145**, 86–98.

91 Y. De Yan, Y. L. Xu, M. L. Zhang, Y. Xue, W. Han, Y. Huang, Q. Chen and Z. J. Zhang, *J. Nucl. Mater.*, 2013, **433**, 152–159.

92 K. Yasuda, S. Kobayashi, T. Nohira and R. Hagiwara, *Electrochim. Acta*, 2013, **92**, 349–355.

93 G. De Córdoba, A. Laplace, O. Conocar, J. Lacquement and C. Caravaca, *Electrochim. Acta*, 2008, **54**, 280–288.

94 K. R. Kvam, D. Bratland and H. A. Øye, *J. Mol. Liq.*, 1999, **83**, 111–118.

95 I. Barin, *Thermochemical data of pure substances,* VCH Verlagsgesellschaft/VCH Publishers, New York, Part I, 1989, 1-816.

96 I. Barin, *Thermochemical data of pure substances,* VCH Verlagsgesellschaft/VCH Publishers, New York, Part II, 1989, 817-1739.

97 C. Hamel, P. Chamelot and P. Taxil, *Electrochim. Acta*, 2004, **49**, 4467–4476.

98 E. Stefanidaki, C. Hasiotis and C. Kontoyannis, *Electrochim. Acta*, 2001, **46**, 2665–2670.

99 E. Stefanidaki, G. M. Photiadis, C. G. Kontoyannis, A. F. Vik and T. Ostvold, *J. Chem. Soc.*, 2002, **3**, 2302–2307.

100 R. Thudum, A. Srivastava, S. Nandi, A. Nagaraj and R. Shekhar, *Miner. Process. Extr. Metall.*, 2010, **119**, 88–92.

101 D. K. Dysinger and J. E. Murphy, *Electrowinning of Neodymium From a Molten Oxide-Fluoride Elektrolyte*, Bureau au Mines, 1994, Report of Investigations 9504.

102 P. Taxil, L. Massot, C. Nourry, M. Gibilaro, P. Chamelot and L. Cassayre, *J. Fluor. Chem.*, 2009, **130**, 94–101.

103 P. Taxil, P. Chamelot, L. Massot and C. Hamel, *J. Min. Metall.*, 2003, **39**, 177–200.

104 P. Chamelot, L. Massot, C. Hamel, C. Nourry and P. Taxil, *J. Nucl. Mater.*, 2007, **360**, 64–74.

105 C. Nourry, *Extraction électrochimique des lanthanides des milieux de fluorures fondus par formation d'alliages,* Thèse de l'université Paul Sabatier - Toulouse III, 2007.

106 T. Nohira, S. Kobayashi, K. Kobayashi, R. Hagiwara, T. Oishi and H. Konishi, *ECS Trans.*, 2010, **33**, 205–212.

107 C. Nourry, L. Massot, P. Chamelot and P. Taxil, *J. Appl. Electrochem.*, 2009, **39**, 2359–2367.

108 M. Ciumag, M. Gibilaro, L. Massot, R. Laucournet and P. Chamelot, *J. Fluor. Chem.*, 2016, **184**, 1–7.

109 M. Gibilaro, L. Massot, P. Chamelot and P. Taxil, *J. Nucl. Mater.*, 2008, **382**, 39–45.

110 G. Mathieu, *Co-réduction électrochimique de l'aluminium et des lanthanides en milieu fluorures fondus: application au traitement pyrochimique des effluents nucléaires, ,* Thèse de l'université Paul Sabatier - Toulouse III, 2008.

111 J.-B. Shim, S.-C. Hwang, E.-H. Kim, Y.-H. Kang, B.-J. Lee and J.-H. Yoo, *Oecd-Nea.Org*, 347–354.

112 R. Zvejskova, F. Lisy and P. Soucek, *Development of electrochemical separations of uranium and RE elements from fluoride melts.* In Seventh Information Exchange Meeting on Actinide and Fission Product Partitioning and Transmutation, (October 14–16, 2002, Jeju. Republic of Korea): Nuclear Energy Agency, 2002, 371-381.

113 LiCl-KCl Diagram, http://www.crct.polymtl.ca/fact/phase_diagram.php?file=KCl-LiCl.jpg&dir=FTsalt, (accessed 15 February 2015).

114 P. Chartrand and A. D. Pelton, *Metall. Mater. Trans. A*, 2001, **32**, 1385–1396.

115 LIF-CaF_2 Diagram, http://www.crct.polymtl.ca/fact/phase_diagram.php?file=CaF2-LiF.jpg&dir=FTsalt, (accessed 14 February 2015).

116 E. Renaud, C. Robelin, M. Heyrman and P. Chartrand, *J. Chem. Thermodyn.*, 2009, **41**, 666–682.

117 S. P. Fusselman, *J. Electrochem. Soc.*, 1999, **146**, 2573–2580.

118 L. Yang and G. Hudson, *J. Electrochem. Soc.*, 1959, **106**, 986–990.

119 J. Serp, R. J. M. Konings, R. Malmbeck, J. Rebizant, C. Scheppler and J.-P. Glatz, *J. Electroanal. Chem.*, 2004, **561**, 143–148.

120 V. Ghetta, J. Fouletier and P. Taxil, *Sels fondus à haute température*, Presses polytechniques et universitaires romandes, 1st ed., Lausanne, 2009, 336p.

121 P. T. Kissinger and W. R. Heineman, *J. Chem. Educ.*, 1983, **60**, 9242–5.

122 D. H. Evans, K. M. O'Connell, R. A. Petersen, M. J. Kelly, K. M. O'Connel, R. A. Petersen and M. J. Kelly, *J. Chem. Educ.*, 1983, **60**, 290.

123 G. A. Mabbott, *J. Chem. Educ.*, 1983, **60**, 697–702.

124 T. Berzins and P. Delahay, *J. Am. Chem. Soc.*, 1953, **75**, 555–559.

125 H. J. S. Sand, *Philos. Mag. Ser. 6*, 1901, **1**, 45–79.

126 S. M. A. P. Company, *Inconel Alloy 625*, 2013.

127 P. Masset, D. Bottomley, R. Konings, R. Malmbeck, A. Rodrigues, J. Serp and J.-P. Glatz, *J. Electrochem. Soc.*, 2005, **152**, A1109–A1115.

128 C. Caravaca, G. Córdoba, Y. Castrillejo, R. Bermejo, E. Barrado, R. Pardo and M. Vega, *Separation by electrolysis in chloride media*, 2003.

129 Y. Castrillejo, M. R. Bermejo, E. Barrado, A. M. Martínez and P. Díaz Arocas, *J.*

Electroanal. Chem., 2003, **545**, 141–157.

130 S. A. Kuznetsov and M. Gaune-Escard, *Electrochim. Acta*, 2001, **46**, 1101–1111.

131 M. Goto and K. B. Oldham, *Anal. Chem*, 1973, **45**, 2043–2050.

132 H. L. Lord, W. Zhan and J. Pawliszyn, in *Comprehensive Sampling and Sample Preparation*, Elsevier, Academic Press, 2012, pp. 677–697.

133 P. J. P. Glatz, R. Malmbeck, C. Pernel, C. Scheppler, J. Serp, *No TitleYROREP Contract No. FIKW- CT-2000-00049, Project No. FIS5-1999-00199*, .

134 J. Sim, Y. Kim, S. Paek, S. Kim and S. Lee, *Int. J. Electrochem. Sci.*, 2018, **13**, 2842–2859.

135 A. J. Bard and L. R. Faulkner, *Fundamentals and Applications*, Wiley, New York, 1980.

136 V. Smolenski, a. Novoselova, a. Osipenko, M. Kormilitsyn and Y. Luk'yanova, *Electrochim. Acta*, 2014, **133**, 354–358.

137 G. S. Picard, Y. E. Mottot and B. L. Tremillon, *Proc. Electrochem. Soc.*, 1986, **86**–**1**, 189–204.

138 J. Zhang, *J. Nucl. Mater.*, 2014, **447**, 271–284.

139 M. Gibilaro, L. Massot, P. Chamelot and P. Taxil, *J. Nucl. Mater.*, 2008, **382**, 39–45.

Titre : Développement d'un procédé électrochimique pour le recyclage du néodyme à partir de déchets électroniques

Mots clés : néodyme, électrochimie, aimants permanents, sels fondus, recyclage, déchets électroniques

Résumé : Le néodyme appartient à la série des lanthanides se trouvant dans le tableau périodique. Il est le composant clé des aimants permanents $Nd_2Fe_{14}B$ étant implantés dans différents appareils électroniques mais aussi dans appareils dits « écologiques » comme les éoliennes, les voitures ou vélos électriques. De nos jours seulement 1 % du néodyme présent dans les déchets électroniques est recyclé. Le prix du néodyme est très instable dû à de fortes tensions géopolitiques ainsi qu'à la croissance de la fabrication de ce type d'aimants ce qui réduit très rapidement les réserves en néodyme.
Depuis quelques décennies, plusieurs procédés de recyclage du néodyme ont été développés au niveau du laboratoire sans avoir été utilisés à l'échelle industrielle. Les procédés existants ont plusieurs désavantages comme un grandes nombre d'étapes avant d'obtenir le produit final ou encore l'utilisation de grandes quantités de produits chimiques. Le but de ces recherches est le développement d'un procédé pyrochimique pouvant être une alternative à ceux déjà existants. Ce procédé permettrait de récupérer le néodyme sous sa forme métallique en seulement une étape. Pour atteindre cet objet, il a fallu élaborer un réacteur pouvant résister à de hautes températures ainsi qu'aux sels fondus pouvant être corrosifs selon leur composition. Par la suite, les propriétés électrochimiques du néodyme ont été étudiées dans différents sels fondus à base de chlorures et de fluorures afin trouver la configuration optimale pour l'extraction du néodyme contenu dans les aimants permanents.
Nous avons ainsi prouvé qu'il était possible d'extraire le néodyme sous sa forme métallique renfermé dans de vieux aimants permanents en une seule étape durant une électrolyse.

Title : Development of an electrochemical process for the recycling of neodymium from electronic scraps

Keywords : neodymium, electrochemistry, permanent magnets, molten salts, recycling, electronic scraps

Abstract : Neodymium belongs to the lanthanide's serie of the period system and is the key component of the permanent magnets $Nd_2Fe_{14}B$, which are implemented in electronic devices and "green" technologies like wind turbines or electric cars and bicycles. Nowadays, only one percent of the neodymium in electronic scraps is recycled. Due to the geopolitical considerations and a strong increase of the use of permanent magnets, there is an impoverishment of the raw material resources, which leads to an instable market.
Since some decades, few recycling processes have been developed at the lab scale without an upscaling to the industrial scale. The existing processes have several disadvantages like multiple steps to obtain the final desired product. This means that these methods have a long process time or use a large amount of chemical products.
The aim of this research was the development of a pyrochemical process, which could be an alternative to the existing recycling processes, in order to extract neodymium from electronic scraps with less steps, a lower amount of chemical products and a higher recovery rate of the rare neodymium. For this purpose a special reaction chamber has been created, which resists to the strong experimental conditions due to the use of high temperatures and corrosive molten salts. Moreover the electrochemical behaviour of neodymium in different chloride- and fluoride-based molten salts was studied in order to find the most appropriated setup.
We could prove that the pyrochemical method could be the solution to recover neodymium from the old permanent magnets under its metallic form in just one single reaction step during an electrolysis.

UBFC UNIVERSITE BOURGOGNE FRANCHE-COMTE
Université Bourgogne Franche-Comté
32, avenue de l'Observatoire
25000 Besançon